Aus dem

Department für Frauengesundheit

Universitäts-Frauenklinik

Effects of non-invasive physical plasma (NIPP) on the ECM and cells responsible for postoperative intraabdominal adhesions

Inaugural-Dissertation
zur Erlangung des Doktorgrades
der Medizin

der Medizinischen Fakultät
der Eberhard Karls Universität
zu Tübingen

vorgelegt von

Rasch, Marie-Lena

2023

Dekan:	Professor Dr. B. Pichler
1. Berichterstatter:	Professor Dr. B. Krämer
2. Berichterstatter:	Professorin Dr. D. Alexander-Friedrich
Tag der Disputation:	21.03.2023

TABLE OF CONTENTS

ABBREVIATIONS 6

LIST OF FIGURES 9

LIST OF TABLES 11

1. INTRODUCTION 12

1.1 INTRAPERITONEAL ADHESIONS 12
1.2 PATHOPHYSIOLOGY 13
1.3 CONSEQUENCES 17
1.4 PREVENTION AND THERAPEUTICAL OPTIONS 18
1.5 NON-INVASIVE PHYSICAL PLASMA (NIPP) 18
1.6 AIM OF THIS STUDY 19

2. MATERIAL AND METHODS 22

2.1 CELL CULTURE 22
2.1.1 ISOLATION OF CELLS 23
2.1.2 PASSAGE 24
2.1.3 FREEZING AND THAWING OF CELLS 24
2.1.4 DETERMINATION OF CELL COUNT 25
2.1.5 SEEDING CELLS 25
2.2 ARGON PLASMA 26
2.2.1 PLASMA ACTIVATED MEDIUM (PAM) GENERATION 26
2.2.2 PLASMA TREATMENT 27
2.3 MICROSCOPY 29
2.3.1 BRIGHT FIELD MICROSCOPY 29
2.3.2 IMMUNOFLUORESCENCE MICROSCOPY 29
2.4 FIBRONECTIN ANALYSIS 29
2.4.1 IMMUNOFLUORESCENCE STAINING 29
2.5 COLLAGEN ANALYSIS 30
2.5.1 HYDROXYPROLINE ASSAY 30
2.5.2 COLLAGEN I ALPHA IF-STAINING 31
2.5.3 SIRCOL™ SOLUBLE COLLAGEN ASSAY 31
2.6 WESTERN BLOT 32
2.7 CYTOKINES MEASUREMENTS 34
2.8 RAMAN IMAGING 35
2.8.1 PRINCIPAL COMPONENT ANALYSIS (PCA) 36
2.9 ENZYME-LINKED IMMUNOSORBENT ASSAY (ELISA) 37
2.10 STATISTICAL ANALYSIS 38

3. RESULTS 40

3.1 DEFINITION OF PAM DOSAGES AND INFLUENCE ON ANTIPROLIFERATION 40
3.2 EFFECT OF PAM TREATMENT ON THE EXTRACELLULAR MATRIX 42
3.2.1 ECM WEIGHT DECREASES AFTER PAM TREATMENT 42
3.2.2 EFFECTS OF PAM TREATMENT ON COLLAGEN PRODUCTION 43
3.2.2.1 PAM TREATMENT LEADS TO ELEVATED SOLUBLE COLLAGEN LEVELS 43
3.2.2.2 INTRACELLULAR COLLAGEN CONTENT WAS NOT MODIFIED TROUGH PAM TREATMENT 44
3.2.2.3 TOTAL COLLAGEN CONTENT DECREASED THROUGH PAM TREATMENT 46
3.2.3 EFFECT OF PAM ON THE ECM COMPONENT FIBRONECTIN 49
3.2.3.1 FIBRONECTIN CONTENT DECREASES THROUGH PAM TREATMENT 49
3.3 PAM TREATMENT AFFECTS CYTOKINE PRODUCTION 53
3.3.1 SOME PRO INFLAMMATORY CYTOKINES INDICATE DECREASED LEVELS AFTER PAM 53
3.3.2 PAM TREATMENT DOES NOT CHANGE ANGIOGENESIS PROMOTING FACTORS 59
3.3.3 PAM TREATMENT DID NOT IMPACT ANTI-INFLAMMATORY CYTOKINES 61
3.3.4 SOME COLONY STIMULATING FACTORS CHANGE LEVELS AFTER PAM TREATMENT 62
3.4 INFLUENCE OF PAM ON MATRIX METALLOPROTEINASES 1 AND 2 64
3.5 INFLUENCE OF PAM ON CELLULAR COMPONENTS ANALYZED BY RAMAN MICROSPECTROSCOPY 68
3.5.1 TRUE COMPONENT ANALYSIS (TCA) 68
3.5.2 PRINCIPLE COMPONENT ANALYSIS (PCA) 69

4. DISCUSSION 76

4.1 PAM TREATMENT REDUCED CELL COUNT OF FIBROBLASTS 77
4.2 EXTRACELLULAR MATRIX FORMATION WAS REDUCED BY PAM TREATMENT 78
4.3 CYTOKINE LEVELS WERE DIFFERENTLY ALTERED BY PAM TREATMENT 83
4.4 CONCLUSION AND CLINICAL SIGNIFICANCE 85

5. SUMMARY 86

6. REFERENCES 88

7. ERKLÄRUNG ZUM EIGENANTEIL 95

8. VERÖFFENTLICHUNGEN 96

APPENIDX 97

DANKSAGUNG 103

Parts of this work were already published in
*Rasch, M.-L. and *Holl, M. *et al.*, *Cell type-specific anti-adhesion properties of peritoneal cell treatment with plasma-activated media (PAM)*, Biomedicines **2022**, 10, 927 [1].

*Authors contributed equally to this work.

ABBREVIATIONS

- BCA – Bicinchoninic acid
- BSA – Bovine serum albumin
- CAP – Cold atmospheric plasma
- DMSO – Dimethyl sulfoxide
- ECM – Extracellular Matrix
- ELISA – Enzyme-linked immunosorbent assay
- FCS – Fetal calve serum
- FGF – Fibrinogen growth factor
- FMOD – Fibromodulin
- GAPDH – Glyceraldehyde 3-phosphate dehydrogenase
- GM-CSF – Granulocyte-macrophage colony stimulating factor
- h – Hours
- HP – Hydroxyproline
- IF – Immunofluorescence
- IL – Interleukin(s)
- IL1-Ra – Interleukin1-receptor antagonist
- IFN – Interferon
- M-CSF – Macrophage colony stimulating factor
- MC – Mesothelial cell

- MD – Mean difference
- MEM – Minimal essential medium
- MIP-1 – Macrophage inflammatory protein-1
- MMP – Matrix metalloproteinase
- NIPP – Non-invasive physical plasma
- PAI – Plasminogen activator inhibitor
- PAM – Plasma activated medium
- PBS – Phosphate buffered saline
- PCA – Principal component analysis
- PFA – Paraformaldehyde
- PWC – Peritoneal wash cytology
- RNS – Reactive nitrogen species
- RONS – Reactive oxygen and nitrogen species
- ROS – Reactive oxygen species
- RT – Room temperature
- SEM – Standard error of the mean
- TBS – Tris-buffered saline
- TCA – True component analysis
- TGF-beta – Transforming growth factor beta
- TNF-alpha – Tumor necrosis factor alpha

- tPa – Tissue plasminogen activator
- TRIS-HCL – Tris(hydroxymethyl)aminomethane-hydrochloride
- VEGF – Vascular endothelial growth factor
- w/ – with

LIST OF FIGURES

Figure 1: Schematic Representation of the Peritoneal Anatomy. 13

Figure 2: Fibroblast isolation out of peritoneal tissue sample. 23

Figure 3: Generation of plasma activated media (PAM). 28

Figure 4: Scratch pattern used for Cytokine Assay. 34

Figure 5: Schematic representation of the Raman microscope. 37

Figure 6: Impact of PAM on cell confluency and ECM synthesis on fibroblasts 72 h after treatment. 41

Figure 7: PAM treatment affects soluble collagen levels in fibroblasts. 43

Figure 8: Effect of PAM on intracellular collagen in fibroblasts. 44

Figure 9: Effect on PAM on collagen expression in fibroblasts. 47

Figure 10: Modification of hydroxyproline in fibroblasts after PAM treatment. 48

Figure 11: Modification of fibronectin in fibroblasts after PAM treatment (western blot). 49

Figure 12: Modification of fibronectin in fibroblasts after PAM treatment (IF). 51

Figure 13: Analysis of pro-inflammatory cytokines IL-1b and TNF-alpha after PAM treatment. 54

Figure 14: Modification of INF gamma after PAM treatment. 55

Figure 15: PAM did not affect MIP-1 beta and MCP-1 levels in fibroblasts. 56

Figure 16: Analysis of TGF-beta 1 after PAM treatment. 57

Figure 17: Analysis of IL-1Ra after PAM treatment. 58

Figure 18: Angiogenesis promoting factors did not significantly change levels after PAM treatment. 60

Figure 19: PAM treatment did not change levels of anti-inflammatory acting cytokines. 61

Figure 20: CSF levels were partly altered by PAM treatment. 62

Figure 21: Impact of PAM-treatment on MMP-1 in fibroblasts and mesothelial cells. 65

Figure 22: Impact of PAM-treatment on MMP-2 in fibroblasts and mesothelial cells. 66

Figure 23: Characteristic spectra of detected molecular structures by Raman spectroscopy. 68

Figure 24: Raman imaging reveals changes in nuclei spectra in fibroblasts. 69

Figure 25: Loadings plot corresponding to specific PCAs of each patient. 71

Figure 26: Raman imaging reveals changes in protein spectra in fibroblasts. 73

Figure 27: Predicted impact of PAM treatment on the peritoneal cavity. 79

Supplementary Figure 1: Extracted collagen spectra. 97

Supplementary Figure 2: Fingerprint spectrum of lipids. 98

Supplementary Figure 3: Raman imaging reveals changes in lipid spectra in fibroblasts. 98

LIST OF TABLES

Table 1: Splitting format of MEM and PAM for desired PAM dilutions. 26

Supplementary Table 1: Raman peaks and their molecular assignments after identification by PCAs. 100

1. INTRODUCTION

1.1 Intraperitoneal Adhesions

Up to date, postoperative intraperitoneal adhesions remain a serious problem and frequent postoperative complication in the field of abdominal and pelvic surgery. They affect the outcome of surgeries and in particular the patient's quality of life. Studies estimate the incidence of postoperative adhesions at 67-93 % [2].

Adhesions are a naturally occurring consequence of tissue trauma resulting from injury, radiation or infection [3]. Following the trauma, a cascade of events is triggered leading to the formation of fibrinous adhesions in which different kind of cell types are involved. In short, adhesion bands are the results of disproportionate extracellular matrix (ECM) synthesis and reduced ECM degradation. Therefore, adhesions mainly consist of collagen and fibronectin fibers [4].

Especially in the field of gynecologic surgery, intraperitoneal adhesions are still present and no satisfactory solution for prevention has been found so far. Studies have shown that about one third of all patients undergoing open abdominal surgery were readmitted to the hospital due to complications resulting from the formation of intraperitoneal adhesions [5]. For instance, women undergoing abdominal hysterectomy have a significant higher risk to develop adhesion related small bowel obstruction and therefore often require emergency surgery [3].

Besides the resulting health related complications, longer surgery and therefore higher risks for intraoperative complications, postoperative intraperitoneal adhesions also have a major impact on health care costs. In the United States (US), health costs of more than one billion dollars yearly can be attributed to intraperitoneal adhesions [3].

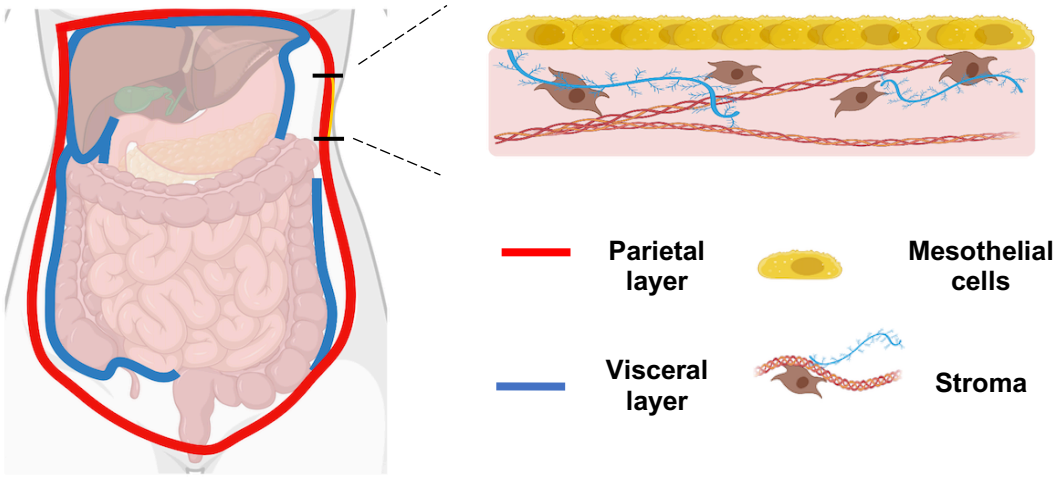

Figure 1. Schematic representation of the peritoneal anatomy. The abdominal cavity is lined by the peritoneum. The parietal layer (red) bounds the whole abdominal cavity, the visceral layer (blue) fits to selected internal organs such as parts of the colon and the liver. Histologically, mesothelial cells cover the surface of peritoneum. The underlying constructive tissue (stroma) consists of fibroblasts as well as of ECM forming structures such as collagen, fibronectin and proteoglycans. This figure was already published in Rasch, M.-L. and Holl, M. et al., *Cell Type-Specific Anti-Adhesion Properties of Peritoneal Cell Treatment with Plasma-Activated Media (PAM).* Biomedicines **2022**, 10, 927 [1]. Created with BioRender.com.

1.2 Pathophysiology

The peritoneum is a membrane lining the abdominal cavity while covering the intestinal organs and connecting them to each other or the abdominal wall. Consisting of a parietal and a visceral part, it creates the peritoneal cavity containing up to 100 ml peritoneal fluid *(Figure 1)*. Furthermore, it acts as a lubricant and allows the two walls to shift against each other without causing patient discomfort [4]. The abdominal cavity is lined with a monolayer of mesothelial cells also called mesothelium supported by another thin layer of connective tissue containing fibroblasts. These cells play a crucial part in the process of adhesion formation [6].

In case of tissue damage, e.g. caused by abdominal surgery, the mesothelial surface no longer protects the underlying tissue. This induces an inflammatory environment which subsequently results in a repair process. This process aims to restore the mesothelial cell layer and the injured connective tissue by synthesis of ECM components like collagen and fibronectin. Different modifications of the physiological wound healing process can lead to increased adhesion formation. An overstimulation of cells, an overproduction of collagen or fibronectin or an imbalance of cytokines represent examples for pathological wound healing processes leading to adhesion formation [4, 6].

Within 24 h after injury of the peritoneum, neutrophils and macrophages migrate into the wound. By secreting different cytokines, those cells initiate the repair process by promoting further transmesothelial migration of macrophages and neutrophils. On the other hand, the cytokines boost an inflammatory reaction of the tissue. By releasing vasoactive substances such as histamine, stromal mast cells promote the extravasation of leucocytes and plasma proteins into the tissue. Due to the injury, collagen of the connective tissue gets exposed to the blood platelets which results in thrombin generation [4].

The first cytokines being present after peritoneal injury are tumor necrosis factor alpha (TNF-alpha) and Interleukin-1 (IL-1). TNF-alpha is a cytokine which levels are rapidly increasing right after the event of peritoneal injury. It accelerates the wound healing process by stimulating the fibrin production of the fibroblasts and therefore the ECM synthesis [7]. Elevated levels of TNF-alpha in the peritoneal fluid correlate with the severeness of the adhesions and can therefore be considered as an indicator for adhesion formation [4]. Furthermore, TNF-alpha increases the release of other cytokines, such as IL-1 [7]. IL-1 itself leads to the activation of inflammatory cells and the release of other cytokines starting an inflammatory reaction as well. On the other hand, IL-1 stimulates the proliferation of fibroblasts which play a crucial role in the formation of peritoneal adhesions [8]. Transforming growth factor beta 1 (TGF-beta 1) is another cytokine being present in the injured peritoneal cavity. During the wound healing process, TGF-beta stimulates the wound contraction process as well as angiogenesis [4]. Since TGF-beta 1 leads to an increased expression of collagen type 1 and Plasminogen-activator-inhibitors (PAIs) - especially during a hypoxic state - elevated levels can be particularly found in

patients with intraperitoneal adhesions [4]. Besides TNF-alpha, TGF-beta 1 may therefore serve as another marker for adhesion formation.

An important component of the wound exudate is fibrin. After accumulating over the injured area, fibrin creates a stable matrix for migration of inflammatory and repair cells. In case of physiological wound healing, most of the fibrin is degraded during the process of fibrinolysis within 72-120 h [4]. This process is regulated through the enzyme plasmin by breaking down the fibrinous structures. Plasmin itself must be activated first by tissue thromboplastin activator (tPA). On the other hand, plasmin can be inactivated by PAIs which are upregulated by trauma, cancer, or infection. This leads to a decreased break down of fibrinous structures. It has been shown that the tPa/PAI ratio is up to 80 % higher in regular peritoneal fibroblast than in adhesion associated fibroblasts. The ratio therefore can be used as an indicator for adhesiogenic and fibrinolytic potential [4].

Besides different cytokines, hypoxia plays another crucial part in the process of increased adhesion formation. Due to the surgical procedure, the tissue no longer gets sufficient oxygen supply and nutrients. As a result of the hypoxic state, a series of molecular processes takes place, promoting inflammation and further leading to more fibrous tissue [9]. Furthermore, hypoxia effects the persistence of the fibrin matrix [10]. Hypoxia therefore leads to an increased expression of TGF-beta and collagen, but also to elevated PAI-I levels which result in decreased fibrinolysis, persistent fibrin matrices and therefore increased adhesion formation [4].

Apart of the affection of the collagen synthesis, hypoxia also promotes the expression of the glycoprotein dimer fibronectin, a major component of the ECM which is linking other matrix components [4]. Moreover, fibronectin is greatly involved in all stages of wound healing. Its interaction with fibroblasts enables them to migrate into the wound to synthesize further ECM components [11]. It has been shown that a fibronectin-rich ECM promotes further collagen type I and elastic fibers assembly and therefore matrix deposition [11]. Accordingly, an increased number of fibronectin molecules promotes additional ECM deposition and increased adhesion formation.

As stated, collagen represents a main part of the ECM and therefore of adhesion bands. 28 different types of collagen are known which can be further divided into categories like

fibril-forming, basement forming and network-forming collagens [12]. In the ECM and adhesion bands, collagen I - a fibril forming collagen - plays an essential role [4].

Collagen synthesis consists of different steps creating a stable triple-helix and strong ECM. A mutual characteristic feature of all collagen types is a right-handed triple-helix which contains three left-handed alpha-chains. The amino acid sequences of each alpha-chain feature a glycine molecule in every third place (Glycine-X-Y) which allows its left-handed turn [12, 13]. The other both positions often consist of lysin and proline as well as their hydroxylated forms hydroxyproline and hydroxylysine. Hydroxyproline is specific for collagen molecules which makes it an ideal marker for collagen detection [14]. The hydroxylation of proline and lysin is a posttranslational, intracellular modification of the procollagen molecule [13]. Another posttranslational modification is glycosylation. Furthermore, the three alpha-chains assemble to a triple helix [12]. For secretion of collagen, the triple helix molecules are packed into vesicles within the Golgi apparatus before the release out of the cell. Then, both ends of the triple helix - more specifically the N- and the C-propeptide - get cleaved off which allows an extracellular fibril assembly [13]. Finally, the fibrils get further stabilized by covalent cross-links leading to enhanced mechanical resistance of collagen fibrils [12].

Following the enhanced matrix deposition and the decreased fibrinolysis, vascularization and angiogenesis of the adhesion bands eventually occur. In this process vascular endothelial growth factor (VEGF), expressed by mesothelial, endothelial and mast cells, plays a major role. Due to the improved nutrition and oxygen supply trough new blood vessels, adhesions are strengthening [4].

Apart from components like fibronectin and collagen, the ECM also contains enzymes like matrix metalloproteinases (MMP) which are essential for ECM remodeling and wound healing. Especially any imbalance in the activities of MMP-2 and MMP-9 may enhance the severeness of peritoneal adhesions. Both of those enzymes are decisive during the wound healing process because they degrade several matrix components, preventing an excess of scar tissue. Moreover, they contribute to the formation of new blood vessels by activating cytokines like TNF-alpha and VEGF [15].

Over the time, maturation of the adhesions takes place. Patients may not feel any discomfort, since clinical manifestation can often take up to years, not to mention that some remain asymptomatic [4]. But since apoptotic and non-apoptotic cell death takes place in those fibrous adhesions, local inflammatory reaction increases and again leads to the formation of fibrous tissue. Additionally, levels of proinflammatory acting mediators such as TGF-beta, IL-1 and IL-6 may rise. Elevated levels of profibrotic factors such as fibrinogen growth factor 1 (FGF1) and fibromodulin (FMOD) have been shown to promote further adhesion formation and adhesion maturing [9].

To sum up, postoperative intraperitoneal adhesions are a result of various imbalanced components during the wound healing process. ECM main components fibronectin and collagen constitute a major part of the adhesion bands. Enhanced matrix deposition, impaired ECM degradation and cytokine imbalances all contribute to the establishment of postoperative adhesions.

1.3 Consequences

Even though the majority of postoperative intraperitoneal adhesions remain asymptomatic, adhesions can cause life threatening postoperative complications. With a mortality rate of 3 %, bowel obstructions are one of the most life-threatening complications resulting from postoperative adhesions [16]. 40 % of all intestinal obstructions result from postoperative adhesion formation [5]. Ranging between 13-16 % per 1000 patients, small bowel obstructions are a relatively common but dangerous complication when undergoing an abdominal hysterectomy [3]. Many patients also suffer from chronic pelvic and abdominal pain after surgery, even though the exact relation between adhesions and pain remains unknown [3].

Being the leading cause of secondary infertility in women, especially gynecological surgeons aim to prevent postoperative adhesions as much as possible since adhesions can cause peritoneal infertility in 15-20 % of women [17]. Infertility results from adhesions distorting adnexal anatomy as well as the interference of them to gamete and embryo transport [3, 17].

1.4 Prevention and therapeutical options

Different approaches have been made to prevent or reduce the formation of postoperative intraperitoneal adhesions. In particular, surgeons use minimal invasive surgical techniques, or employ absorbable suture material [4, 18]. Another approach is the application of anti-inflammatory drugs such as corticosteroids and non-steroidal anti-inflammatory drugs, or the use of anticoagulants [18]. Other attempts include surgical adhesion barriers including bioresorbable membranes (e.g. Seprafilm, Genzyme Corporation, Cambridge, MA), gels (e.g. SprayGel, Confluent Surgical Inc., Integra LifeSciences, Princeton, NJ, USA) or peritoneal instillates (e.g. Adept Adhesion Reduction Solution, Baxter Healthcare Corp) [3, 4]. Unfortunately, a method which sufficiently reduces or prevents adhesions is not available yet.

Up to date, no sufficient and long-lasting method treating postoperative intraperitoneal adhesions has been established. Accordingly, a second look surgery is the only treatment option in most cases.

1.5 Non-invasive physical plasma (NIPP)

Plasma, considered as the fourth physical state, is an ionized gas. It is composed of different charged molecules like electrons, ions as well as free radicals [19]. Plasma can be divided into three groups: low-, atmospheric- and high-pressure plasma [20]. Furthermore, it can be classified in high temperature plasma and low temperature plasma which can be distinguished by the different thermal equilibrium states of the ions, electrons and neutral species. High temperature plasma is also considered as equilibrium plasma because all containing species (e.g. ions, electrons) have the same temperature and therefore are in thermal equilibrium [20]. Other than high-temperature plasma, low temperature plasma can be further divided into two groups: Thermal plasma and non-thermal plasma. The species in thermal plasma are in a local thermal equilibrium state, also called quasi-equilibrium. Like in high-temperature plasma, cooling requirements limit the applicability due to the high temperature. On the opposite, non-thermal plasma is also referred as non-equilibrium-plasma or cold plasma. While the ions and neutrals almost remain at room temperature (RT), the electrons are the only species being thermalized [21]. Consequently, cold atmospheric plasma (CAP) can be applied to heat

sensitive surfaces. It is therefore also referred to as non-invasive physical plasma (NIPP). Since it is possible to synthesize non-thermal plasma at nearly RT and at atmospheric pressure, NIPP is suitable for clinical application.

In the past, NIPP has offered promising treatment options for improved wound healing and has shown selective antineoplastic effects on tumor cells [22-24]. Furthermore, plasma has been already established in dental medicine, for blood coagulation, and for the treatment of various dermatological diseases such as psoriasis or actinic keratosis [25-27]. Containing differently charged molecules and particles, free radicals, infrared and ultraviolet radiation, NIPP is capable of mediation of cell and tissue effects [19, 28]. Presumably, those effects are related to the generation of reactive nitrogen and oxygen species (RNS, ROS, RONS), resulting in antiproliferation and cell death [29]. Besides direct plasma treatment, it is also possible to generate plasma-activated medium (PAM) through indirect plasma treatment. By treating a medium such as a cell culture medium with NIPP, RONS and other species diffuse into the medium which can then be applied to the cells. In numerous studies, the same antiproliferative effects as during direct plasma treatment could be observed [30]. It has been shown that PAM is able to dose-dependently modify protein biosynthesis and proliferation in human fibroblasts [28].

1.6 Aim of this study

Up to date, there are no sufficient prevention methods for postoperative intraperitoneal adhesion formation. Options already available at the market did not show clear clinical benefit. As a prophylactic intraoperative treatment, plasma activated medium (PAM) could prevent or limit the formation of intraperitoneal adhesion. The aim of this study was to evaluate the effect of different PAM concentrations to fibroblasts and the ECM to study a possible treatment option for postoperative intraperitoneal adhesions.

In this purpose, effects of PAM on cell confluency were evaluated. ECM components collagen and fibronectin were both studied with western blot and immunofluorescence. Additionally, collagen was further evaluated by hydroxyproline and Sircol™ Soluble collagen assays. Raman spectroscopic imaging was used for further evaluation of protein but also for lipid and nuclei modifications. Matrix metalloproteinases were studied by

ELISA. Besides components of the ECM, cytokines increasing the adhesion formation were evaluated by Multiplex assays.

2. Material and Methods

2.1 Cell culture

All procedures were operated under sterile conditions under a laminar air flow hood. Cell culture medium and cell culture material were used in sterile conditions. Alpha-MEM was supplemented with 10 % fetal calve serum (FCS), 1 % glutamine and 1 % penicillin-streptomycin (all GIBCO, Waltham, MA, USA). DMEM / F-12 + GlutaMAX was supplemented with 10 % FCS, 1% L-glutamine, 1% penicillin-streptomycin (all GIBCO). The cell culture media, Dulbecco's phosphate buffered saline (PBS; GIBCO) and 0.05 % Trypsin (GIBCO) were stored at 4 °C and were pre-warmed using a 37 °C water bath before application on the cells.

Primary human fibroblasts were isolated from peritoneal tissue samples obtained from consenting patients that were undergoing a cesarean section. Mesothelial cells were isolated from peritoneal wash cytologies (PWC) which were obtained from laparoscopic surgeries. The Ethical Committee of the Medical Faculty of the Eberhard Karls University Tübingen approved the scientific use (649-2017BO2, approval: 12.01.2018; and 495/2018BO2, approval: 19.10.2018).

Right after sampling, peritoneal tissue samples were placed in 50 ml falcon tubes filled with precooled alpha-MEM. Culture medium was supplemented with 10 % FCS, 1 % glutamine and 1 % penicillin-streptomycin (all GIBCO). PWC and tissue samples were stored at 4 °C for up to 6 h until they were transported on ice to the laboratory. Isolation of cells was performed immediately after arrival.

Cells were incubated at 37 °C and 5% CO_2 at a humified atmosphere (incubator by Gottlieb Binder GmbH, Holzgerlingen, Germany). Cell culture medium change was performed every two to three days under a sterile laminar air flow hood. Therefore, the medium was aspirated and discarded. When cultivated in 75 cm^2 cell culture flasks, 12 ml of medium was added, in case of 25 cm^2 cell culture flasks 5 ml of medium was added.

Cells between passage 2 and 9 were used for all experiments.

2.1.1 Isolation of cells

The isolation of fibroblasts was performed as follows: Tissue samples were first washed with PBS (GIBCO) twice. After removing any fatty residue and greater blood vessels, the tissue was cut into pieces of approximately 1 cm using sterile scalpel and sterile forceps. Tissue pieces were then placed into 6-well plates with 1 ml MEM per well already added. Cells were incubated in an incubator at 37°C, 5 % CO_2 atmosphere for 3-4 days before the first medium change. After 2 weeks, 80 % cell layer confluence was reached (*Figure 2*), and cells were transferred into a 75 cm^2 cell culture flask.

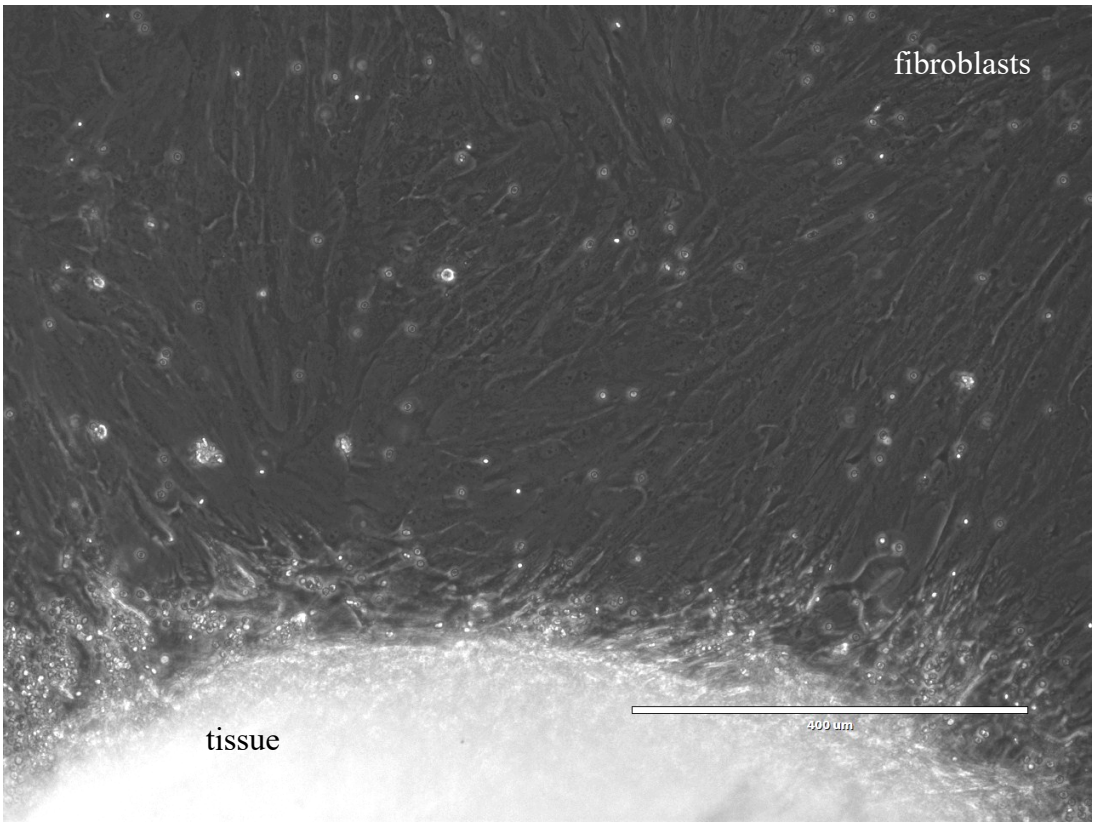

Figure 2. Fibroblast isolation out of peritoneal tissue sample. Peritoneum tissue sample was cut into pieces of 1 cm, placed into 6-well plates, and cultivated in MEM at 37° C, 5 % CO_2 atmosphere. Picture was taken 10 days after start of cultivation. Scale bar represents 400 µm.

Mesothelial cells were isolated from PWC according to Holl *et al*. [31]. PWC was centrifuged for 5 min at 300 g. Supernatant was aspirated and cells were resuspended in 10 ml of PBS. After another centrifugation for 5 min at 300 g, supernatant was aspirated and discarded again, cell pellet was resuspended in 5 ml cell culture medium (DMEM / F-12 + GlutaMAX, supplemented with 10 % FCS, 1 % L-glutamine, 1 % penicillin-streptomycin (all GIBCO)). Cells were seeded in 0,1 % gelatin coated 75 cm^2 flasks and cultured at 37°C at 5 % CO_2.

2.1.2 Passage

For cell passage, cell culture medium was aspirated, and cells were washed in PBS once. Cells in 25 cm^2 flasks were then trypsinized with 3 ml 0.05 % Trypsin-EDTA (GIBCO), for 75 cm^2 flasks 5 ml Trypsin-EDTA was used. Cells were incubated at 37 °C humified atmosphere, 5 % CO_2. After an incubation time of 5 to 8 min, cell culture medium containing 10 % FCS was added for trypsin inactivation. For 25 cm^2 flasks 5 ml medium was used, 8 ml medium was added to 75 cm^2 flasks.

The cell suspension was then transferred into a 15 ml falcon tube and centrifuged for 3 min at 300 g. Afterwards, the supernatant was aspirated and discarded. The cell pellet was resuspended in 2 ml cell culture medium and was then either transferred into a cell culture flask in the desired splitting format or cells were seeded at a specific cell density for further experiments.

2.1.3 Freezing and thawing of cells

Cells were trypsinized and collected as described above in the section *1.2 Passage*. Cell count was determined using the NucleoCounter® NC-200™ (ChemoMetec A/S, Allerod, Denmark). After determination of cell count, 200 µl FCS, 100 µl DMSO and 1000 µl of the cell suspension were added to a cryovial (Roth Selection, Carl Roth GmbH, Karlsruhe, Germany). The tube was then placed into an -80 °C freezer.

For thawing of cells, the cryovial was placed into a 37°C water bath just until there were no more ice crystals visible. Then, cell suspension was immediately transferred into a 15

ml falcon already containing 5 ml prewarmed cell culture medium. In the following, the tube was centrifuged for 3 min at 300 g. Afterwards, supernatant was aspirated and discarded, and the cell pellet was resuspended in 2 ml cell culture medium. Cells were then cultivated in 75 cm^2 cell culture flasks.

2.1.4 Determination of cell count

To be able to refer the measured analyte to a single cell, cells were seeded under the same conditions and cell seeding densities as for the respective experiments. At the time point of interest, cells were trypsinized using 0.05 % Trypsin-EDTA, were then collected and centrifuged for 3 min at 300 g. Cell count was determined using the Nucleo-Counter® NC-200™. Therefore 100 µl of the cell suspension was transferred into a 1.5 ml Eppendorf cup. The Via1-Casette™ was loaded with the suspension before placing the cassette into the NucleoCounter for cell counting.

2.1.5 Seeding cells

Before seeding out the cells, cell count had to be determined. After calculation of the amount of cell suspension needed, cells were seeded into the desired cell culture flask or well plate. For 6-well plates 1.5 ml medium was used per well, for 96-well plates 150 µl/well was used.

2.2 Argon Plasma

2.2.1 Plasma Activated Medium (PAM) generation

For the generation of PAM using argon gas a carrier gas, the kINPen MED (Neoplas GmbH, Greifswald, Germany) was used. The operating conditions were as follows: "*argon gas flow 4,0 l/min, frequency 1 MHz, line voltage 2-3 kV, power 1 W. The distance between the plasma source and the surface of medium was fixed at 7 mm*" [1]. Medium irradiation was performed for 120 s. For control treatment, pure argon gas was applied on 2 ml of MEM. PAM was freshly generated when needed for the experiments and not stored. The resulting medium was defined as 100 % PAM. In the following, a dilution series was set up using 100 % PAM and MEM as diluent. See Table 1 and Figure 3.

Table 1. Splitting format of MEM and PAM for desired PAM dilutions. Example for 2 ml volume. For other amounts, values were converted to desired volume.

PAM dilution	**Amount of MEM (ml)**	**Amount of PAM (ml)**
Argon (control)	1.6	0.4 non ionized argon gas was used
PAM 1:10	1.82	0.18
PAM 1:9	1.80	0.20
PAM 1:8	1.778	0.222
PAM 1:7	1.75	0.25
PAM 1:6	1.714	0.286

PAM 1:5	1.667	0.333
PAM 1:4	1.60	0.40
PAM 1:3	1.50	0.50
PAM 1:2	1.334	0.666
PAM 1:1	1.0	1.0
PAM 100 %	2.00	0.00

2.2.2 Plasma treatment

For determination of the values used for this study's experiments, fibroblasts were seeded into 96-well plates with 2 x 10^3 cells/well. Plasma treatment was performed 24 h after seeding with different PAM dilutions ranging from 1:1 to 1:10 (*Figure 3*). Cells were monitored constantly with the IncuCyte S3 (Essen BioScience, Göttingen, Germany) and pictures were taken every 4 h. After 72 h and 120 h post PAM treatment, analysis of confluency of cells was performed using the IncuCyte software program. The calculated confluency (%) was then normalized to the argon mean value.

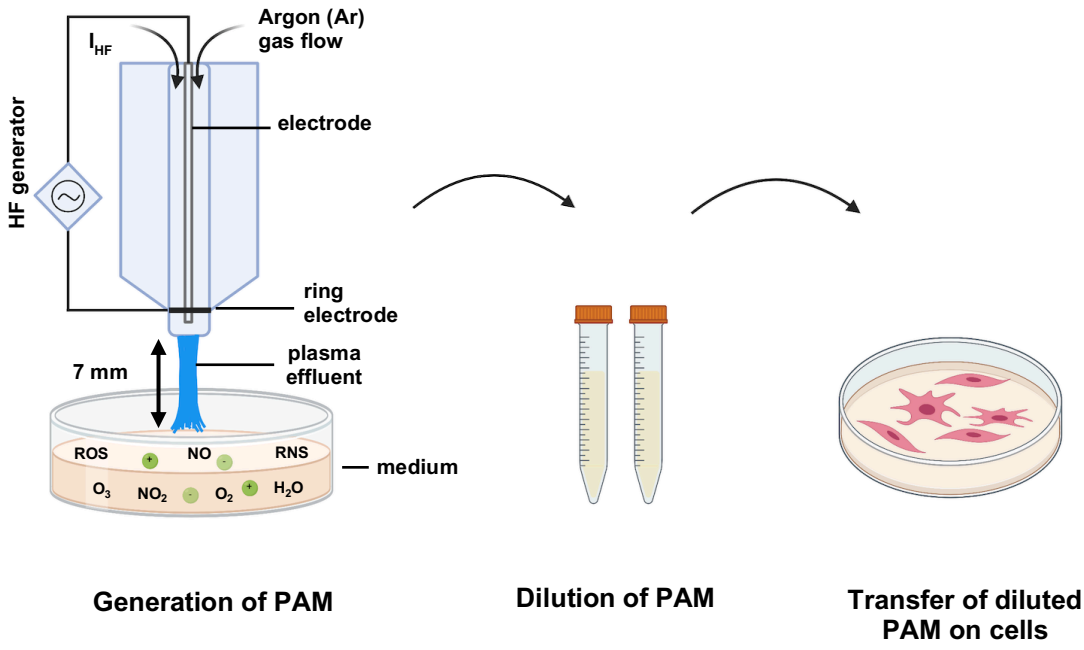

Figure 3. Generation of Plasma activated media (PAM). 2 ml of MEM was treated with argon plasma for 2 min for PAM generation with an exposure distance of 7 mm between plasma head and the medium surface. Argon gas flow was 4.0 l/min, frequency was 1 MHz, power was 1 W and line voltage 2-3 kV. Next, PAM was diluted with MEM for desired PAM to MEM ratio. Dilution ratios are indicated above in Table 1. Diluted PAM was then transferred on cells. After an incubation time of 4 h, PAM was removed, cells were washed with PBS and were then covered with cell culture medium. Parts of this figure were already published in Rasch, M.-L. and Holl, M. *et al*., *Cell Type-Specific Anti-Adhesion Properties of Peritoneal Cell Treatment with Plasma-Activated Media (PAM)*. Biomedicines **2022,** 10, 927 [1]. Created with BioRender.com.

2.3 Microscopy

2.3.1 Bright Field Microscopy

The bright field microscope Olympus CKX4 (Olympus, Hamburg, Germany) was used for observation of cells maintained in cell culture flasks as well as for PAM treated cells in well plates and petri dishes.

For taking microscopic pictures the EVOS microscope (Thermo Fisher Scientific, Waltham, MA, USA) and its associated software was used.

2.3.2 Immunofluorescence Microscopy

For fluorescence microscopy, a LSM 710 confocal microscope (Carl Zeiss AG, Oberkochen, Germany) was employed. Imaging was performed with 10x and 63x objectives and wavelengths of 405 nm and 488 nm. All samples of the respective antibody staining were imaged with identical settings.

2.4 Fibronectin Analysis

2.4.1 Immunofluorescence staining

The primary antibody for fibronectin was obtained from Abcam (Abcam, Cambridge, UK; 1:200 in 0.1 % BSA in PBS) the secondary antibody AlexaFluor 488 was obtained from Thermo Fisher Scientific (1:1000 in 0.1 % BSA in PBS).

One day prior to Plasma treatment, isolated fibroblasts were seeded into 12 well chambers (ibidi GmbH, Gräfelfing, Germany) with 6.25 x 10^3 cells/cm^2. Working volume was 250 µl per well. PAM treatment was performed after 24 h incubation. For the generation of 100 % PAM the same protocol was used as described above in the section '*2.1 Plasma activated medium (PAM) generation*'. In the following, 100 % PAM was diluted with MEM as diluent for the generation of PAM 1:2, PAM 1:5 and argon as control.

Cells were washed three times with PBS at 120 h after PAM treatment. Fixing of cells was performed with 4 % PFA in 1X PBS for 10 min at 37°C. After incubation, wells were

washed three times with PBS before adding 0.1 % Triton-X-100 in 1X PBS for permeabilization. After 15 min incubation at RT, cells were washed three times again. Blocking was performed with 2 % BSA in 1X PBS for 60 min at RT. Immunostaining with primary antibody fibronectin in 0.1 % BSA in 1X PBS was performed over night at 4 °C. Fibronectin antibody was diluted in a 1:200 ratio. One well served as control and 0.1 % BSA instead of primary antibody was added. The next day, cell layers were rinsed three times with PBS and incubated in secondary antibody solution. AlexaFluor 488 antibody was diluted in a 1:1000 ratio with 0.1 % BSA in 1X PBS. Cells were counterstained with NucBlue (#R37165 by Thermo Fisher Scientific, 2 drops/ml diluted in 0.1 % BSA in 1X PBS). After an incubation time of 45 min at RT, cells were washed three times with PBS before imaging using a confocal LSM 710 microscope (Carl Zeiss).

2.5 Collagen Analysis

2.5.1 Hydroxyproline Assay

Detection of the insoluble collagen amount of the ECM was performed according to Capella-Monsonís *et al*. and Keller *et al.* [32, 33] using Sigma Aldrich's Hydroxyproline-Assay (Merck KGaA, Darmstadt, Germany) [1].

Fibroblasts were seeded into 100 mm petri dishes with 2,4 x 10^4 cells/cm^2. Cells were treated with PAM 1:2, PAM 1:5 and argon as control 24 h after seeding. Plasma procedure was followed as described above. 120 h after plasma treatment, cell culture medium was discarded. For the hydroxyproline assay, 2 ml of MiliQ H_2O supplemented with phosphatase and inhibitor tablets (Pierce, ThermoScientific) were added before collection of cells using a cell scraper. Suspension was transferred into a 2 ml Eppendorf cup. Aliquots were taken and frozen at -80°C.

The cell suspension of seven cell culture dishes of fibroblasts of the same patient were pooled and centrifuged using Amicon Ultra-15 spin filter tubes, 10 kDa (Merck KGaA) for 90 min at 4000 g [34]. The ECM was then collected and lyophilized overnight using the Alpha 1-4 LSCbasic (Martin Christ Gefriertrocknungsanlagen GmbH, Osterode am Harz, Germany).

7 mg of the lyophilized ECM was transferred into 1.5 ml screw cap microtubes (Starlab International GmbH, Hamburg, Germany) and diluted with 500 µl of 37 % HCl (Carl Roth). Hydrolysis was then performed at 110°C overnight. Manufactures instructions were followed. Collagen concentration was calculated using the standard curve. Absorbance was measured at 560 nm using the Spark Microplate Reader (Tecan Group AG, Männedorf, Switzerland). Collagen content was then normalized to cell count and respective control.

2.5.2 Collagen I alpha IF-Staining

Cells were seeded at a density of 6.25 x 10^3 cells/cm^2 in 12 well chambers (ibidi GmbH) at 24 h before PAM treatment. After 120 h, cell culture medium was discarded and cells were washed with PBS before continuing with the fixation, permeabilization and blocking. The same immunostaining procedure as described above was followed. Cells were stained with collagen 1 alpha antibody (Novus Biologicals, Littleton, CO, USA; 1:1.000 in 0.1 % BSA in 1X PBS) and incubated overnight. The next day, cells were incubated with the secondary antibody AlexaFluor 488 (ThermoScientific; 1:1.000 in 0.1 % BSA in 1X PBS). Counterstaining of cells was performed by use of NucBlue (Hoechst Invitrogen, #R37165 by Thermo Fisher Scientific, USA). A LSM 710 confocal microscope (Carl Zeiss) was used for imaging of cells.

2.5.3 Sircol™ Soluble Collagen Assay

For determination of the total soluble collagen amount of the ECM, the Sircol™ Soluble Collagen Assay (Biocolor, County Antrim, UK) was used. For every assay, samples and standards were run in duplicates.

24 h prior to PAM treatment, fibroblasts with a confluency of 6 x 10^3 cells/cm^2 were seeded into 75 cm^2 flasks. PAM treatment was then performed as described above for the argon control group, and treatment groups PAM 1:2, PAM 1:5. 120 h after PAM treatment, cell culture medium was collected and frozen at -80 °C for further analysis.

For determination of the cell count, five pictures per flask were taken using an Evos microscope (ThermoScientific).

Cells were washed with PBS. Since cell culture extended five days, acid-pepsin extraction was performed at a pepsin concentration of 0.1 mg/ml 0.5 M acetic acid, as recommended in the manufacture's manual (Pepsin porcine obtained from Serva Electrophoresis GmbH, Heidelberg, Germany). After adding 7 ml of the pepsin/acid solution, petri dishes were placed into a 4 °C refrigerator on a plate shaker (90 mots/min) for overnight incubation. The extracts were then harvested and either frozen at -20 °C or used right away for collagen concentration determination.

The manufacture's Isolation and Concentration Protocol was followed before moving on to the collagen staining protocol. The Spark Microplate Reader (Tecan) was used at 555 nm for measuring the samples' absorbance for soluble collagen content. Collagen concentrations were obtained from the standard curve. Collagen concentration was then normalized to respective cell count and control.

2.6 Western Blot

For both fibronectin and collagen I alpha detection, western blot analysis was performed. Membranes were first stained for fibronectin, then stored at -20° C, thawed and restained for collagen I alpha detection.

Cells were seeded into 10 cm petri dishes at a confluency of 3.4×10^5 cells/dish 24 h prior to PAM treatment. PAM treatment was performed as described above with PAM 1:2, PAM 1:5 and argon as a control. Five days after treatment, cell culture medium was discarded. After triple washing of cells with PBS, dishes were placed into a -80 °C refrigerator for 60 min minimum or overnight. Low protein binding tubes (Eppendorf, Hamburg, Germany) were pre-cooled on ice before use. After incubation at -80 °C, petri dishes were placed on ice and 1 ml ice cold TRIS-HCl cell lysis buffer was added. Cells were harvested from the bottom of the dish using a cell scraper. Lysate was then resuspended several times before the transfer into a new pre-cooled 1,5 ml tube. Tubes were incubated on ice for 30 min but got vortexed for 5 s every 5 min. After incubation,

samples were centrifuged for 15 min at 13.000 rpm at 4 °C and supernatant was transferred into a new pre-cooled 1,5 ml tube afterwards. Pierce BCA Assay Kit (ThermoScientific) was used for protein quantification. An aliquot was taken for BCA-Protein Assay following manufactures instructions. For analysis, the Spark microplate reader (Tecan) was used. Rest of sample was frozen at -20°C or was used right away.

For western blot, denaturization of samples was performed in *"[…] 4x Lämmli protein sample buffer (Bio-Rad, Hercules, CA, USA, #1610747), diluted with 10 % beta-mercaptoethanol, for 10 min at 95°C"* [1]. 13 µg protein per lane was loaded. *"Gel electrophoresis was performed in XCell SureLock Mini-Cell Electrophoresis Chambers using NOVEX NuPage 4-12 % Bis-Tris Protein Gels, 1,0 mm and MES Running Buffer (20x) in ddH_2O (all ThermoScientific Inc., Waltham, MA, USA)"* [1]. ProSieve Quad Color (Lonza Rockland Inc., Rockland, ME, USA) was used as molecular weight marker. *"For protein blotting, nitrocellulose membranes were soaked into NuPAGEtrade Transfer Buffer (20x) (ThermoScientific Inc, MA, USA). Blotting was performed using a SemiDry Transfer System (peqLab, VWR International, Radnor, DE, USA), for 2 h at constant 0.2 A"* [1]. After blotting, Ponceau S counterstaining of membranes was performed. "*After washing, membranes were incubated overnight at 4 °C with primary antibodies under constant agitation: fibronectin (1:1000 in 0.1 % BSA, abcam) […] and GAPDH (1:1000 in 0.1 % BSA, 14C10, Cell Signaling Technology, Danvers, MA, USA). Membranes were incubated for 2 h at RT with the secondary antibody AlexaFluor488 (1:10.000 in 0.1 % BSA)" [1].* The Amersham Typhoon Biomolecular Imager (Cytiva UK Limited, Buckinghamshire, UK) was used for detection of western blot bands. For further analysis, membranes were frozen at -20°C.

For collagen I alpha detection, the same western blot membranes as for fibronectin detection were used. Frozen membranes were thawed for a few hours before blocking for 45 min with 5 % BSA in 1X PBS. Staining was performed using collagen I alpha antibody (Novus Biologicals; 1:1000 in 0.1 % BSA in 1X PBS) at 4° C overnight under constant agitation. The next day, membranes were washed three times with TPBS for 5 min each, before incubation of secondary antibody AlexaFluor594 (ThermoScientific; 1:10.000 in 0.1 % BSA in 1X PBS). Western blot bands were also detected with the Amersham Typhoon Biomolecular Imager (Cytiva, Marlborough, MA, USA).

2.7 Cytokines measurements

The Multiplex system and the NMI Cytokine Assay Panel 1 and 2 (NMI, Reutlingen, Germany) were used for analysis of cytokines. Assay Panel 1 observed IL-1b, IL-1Ra, IL-12p70. VEGF, IL-13, M-CSF. Assay Panel 2 analyzed IL-4, IL-6, IL-8, IL-10. GM-CSF, INF-gamma, MCP-1, MIP-1-beta, TNF-alpha. For TGF-beta 1-3 the Luminex Performance Human TGF-beta Magnetic Panel FCSTM17-03 (R&D Systems, Minneapolis, MN, USA) was used.

Fibroblasts were seeded into 24-well plates with a density of 5 x 10^4 cells per well. PAM treatment was performed with PAM 1:2, PAM 1:5 and argon as control at 24 h after seeding. The following times and conditions were analyzed:

- MEM culture medium: Detection of cytokines already present in cell culture medium
- Medium from PAM treated fibroblasts without scratch: Collected 4 h, 12 h, 24 h after treatment
- Medium from PAM treated fibroblasts with scratch: Three scratches per well before PAM treatment (*scratch pattern in Figure 4*), collected 4 h, 12 h, 24 h after treatment

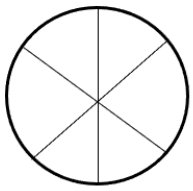

Figure 4. Scratch Pattern used for Cytokine Assay. Scratch was performed using a sterile 100 µl pipette tip before addition of PAM.

We imitated intraoperative injury by performance of scratches which were performed directly before PAM treatment. Scratches were performed using a 100 µl pipette tip by scratching three times through the well: one from top to bottom, one from the upper left

to the lower right and the last one the other way around. The pattern can be seen in Figure 4.

At the respective time points, medium was collected in 96-well plates (Quanterix, Billerica, MA, USA,). Plates were frozen immediately at -80 °C before analysis. Values were normalized to respective control and non-scratch correlate.

2.8 Raman Imaging

For Raman spectroscopic imaging, cells were seeded into 35 mm glass bottom µ-dishes (ibidi GmbH, Gräfelfing, Germany) with 9 x 10^3 cells/cm^2. PAM 1:2 treatment was performed 24 h after seeding, argon served as control. 120 h after treatment, cells were fixed with 4 % PFA for 10 min at RT. Dishes were covered with PBS and stored at 4 °C overnight before measuring.

Single-cell Raman spectra of non-treated and PAM treated cells were acquired utilizing a custom-built Raman microspectrometer (WITec alpha 300 R, Ulm, Germany), equipped with a 532 nm laser (maximum output power 60 mW) [1]. Raman images were obtained at three different positions for fibroblasts (n = 3) at an integration time per spectrum of 0.2 s and a pixel resolution of 1 x 1 µm using a 63x dipping objective (N.A. 1.4; Olympus, Tokyo, Japan). All Raman images were pre-processed by cosmic ray removal, baseline correction (shape algorithm) and normalization (area to 1) and further decomposed into spectral components by true component analysis (TCA) using Project FIVE software (WITec) as described previously [31]. Nuclei, proteins, and lipids were identified as major spectral components and localized in their corresponding intensity distribution in heatmaps resulting in false color-coded Raman images (*Figure 5*). Quantitative image analysis by determining gray value intensities of the spectral heatmaps was performed in ImageJ.

2.8.1 Principal Component Analysis (PCA)

"For in-depth analysis of molecular changes in nuclei, protein or lipid composition, high-intensity pixel representing nuclei, protein and lipid spectra were extracted from the Raman maps and applied for multivariate analysis" [1]. Characterization of spectral features within different data sets by PCA (using The Unscrambler X 10.5, Camo Software AS) was described previously [31]. PCAs were performed to compare nuclei, protein, and lipid information upon PAM treatment. In brief, PCA is an algorithm-based (non-linear iterative partial least square/NIPALS) approach, elaborating vectors – so-called principal components (PCs) – according to spectral similarities and differences. Up to seven PCs were calculated for every PCA, among which PC-1 explains the main variance in spectral information, PC-2 the second most relevant variance and so on. PCs relevant for a discrimination between groups were identified by PCA scores plot. Underlying spectral information was retrieved from the corresponding loadings plots indicating positive peaks dominating in data of positive score ranges and negative peaks for values clustering in negative score ranges, respectively. According to their Raman shift wavenumber, identified loadings peaks could be assigned to a corresponding molecular group, allowing for a sub-structural interpretation based on shifts of the respective spectral signature.

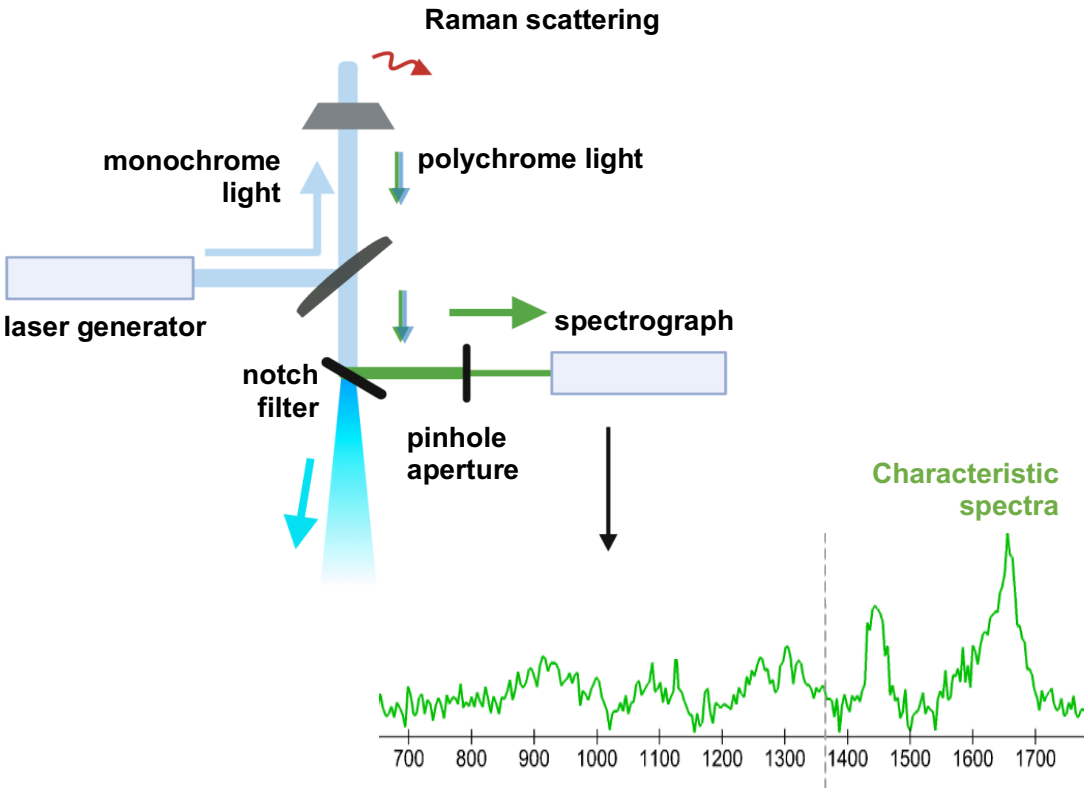

Figure 5. Schematic representation of the Raman microscope. Schematic of a Raman microscope and a resulting characteristic, representative Raman spectrum of a specific biomolecule. The figure was already published in Rasch, M.-L. and Holl, M. *et al.*, *Cell Type-Specific Anti-Adhesion Properties of Peritoneal Cell Treatment with Plasma-Activated Media (PAM)*. Biomedicines **2022**, 10, 927 [1]. Created with BioRender.com.

2.9 Enzyme-linked Immunosorbent Assay (ELISA)

For matrix metalloproteinase (MMP) detection, ELISA assays were performed. Fibroblasts and mesothelial cells were seeded into 6-well plates with a density of 2.5 x 10^5 cells per well. 24 h after seeding, PAM treatment was performed for argon and PAM 1:2 for both mesothelial cells and fibroblasts. Medium was collected after 24 h, 72 h and 120 h and was frozen immediately at -80 °C. For mesothelial cells, MMP levels were only evaluated for 24 h and 72 h. Experiment was performed 24 h after samples of timepoint 120 h were frozen. "*Human ELISA kits for MMP-1 and MMP-2 were both obtained from Thermo Fisher Scientific, Inc. Manufactures protocol was followed, and*

samples were measured at 450 nm using Spark Microplate Reader (Tecan)" [1]. Values were normalized to control.

2.10 Statistical Analysis

Data was analyzed using the SPSS statistics software (IBM Corporation, Armonk, NY, USA). Normal distribution was tested with the Kolmogorov-Smirnov-test. The Mann-Whitney-U-test was applied for calculation of significances of non-normally distributed values, for normal distribution students t-test was applied. P values $\leq$ 0.05 were considered to be statistically significant. Graphics were created by using the GraphPad Prism 9 software (GraphPad Software, San Diego, CA, USA). At least three independent approaches were performed for each experiment.

3. RESULTS

3.1 Definition of PAM dosages and influence on antiproliferation

Analysis of cell-type-specific PAM effects was performed using human peritoneal fibroblasts. The cells were isolated from peritoneal tissue samples obtained within primary caesarean sections. For determination of the therapeutic window, fibroblasts were treated with PAM dosages ranging from 1:1 to 1:10, including PAM only. Cell confluency was monitored using the IncuCyte S3. Confluency was measured 72 h after treatment and values were normalized to the respective control.

Fibroblasts possessed a significantly enhanced reduction of cell confluency after PAM treatment in all groups compared to the control, $p = 0.05$ (*Figure 6A*). Higher PAM concentrations led to lower relative cell confluency than lower concentrations (*Figure 6B*). Fibroblasts treated with PAM concentrations 1:8 and 1:7 reached a similar relative confluency. A comparable cell confluency was also observed between PAM 1:6 and PAM 1:5. Consequently, confluency decreased stronger with PAM than with PAM 1:4. However, treatment with PAM did not completely reduce the fibroblast count.

Based on experiments on mesothelial cells (data obtained by Myriam Holl, member of our working group) the PAM concentrations 1:5 and 1:2 were defined as dosages of interest when compared to the present data on fibroblasts. With the PAM concentration 1:2, a therapeutic window was defined in which the cell type-specific PAM effect mainly affected the proadhesive fibroblasts compared to the mesothelial cells. Besides that, the effect of 1:5 diluted PAM on fibroblasts was further evaluated since relative confluency doubled compared to 1:2 diluted PAM.

Referring to the brightfield images, cells in the argon group almost reached a 100 % confluency compared to the cells treated with PAM 1:5 and PAM 1:2 (*Figure 6A*). Fibroblasts in the PAM 1:2 treatment group notably reduced relative cell confluency and illustrated the antiproliferative effect of PAM on fibroblasts. Confluency of fibroblasts at 72 h after PAM 1:5 treatment illustrated lower antiproliferative effects compared to PAM 1:2.

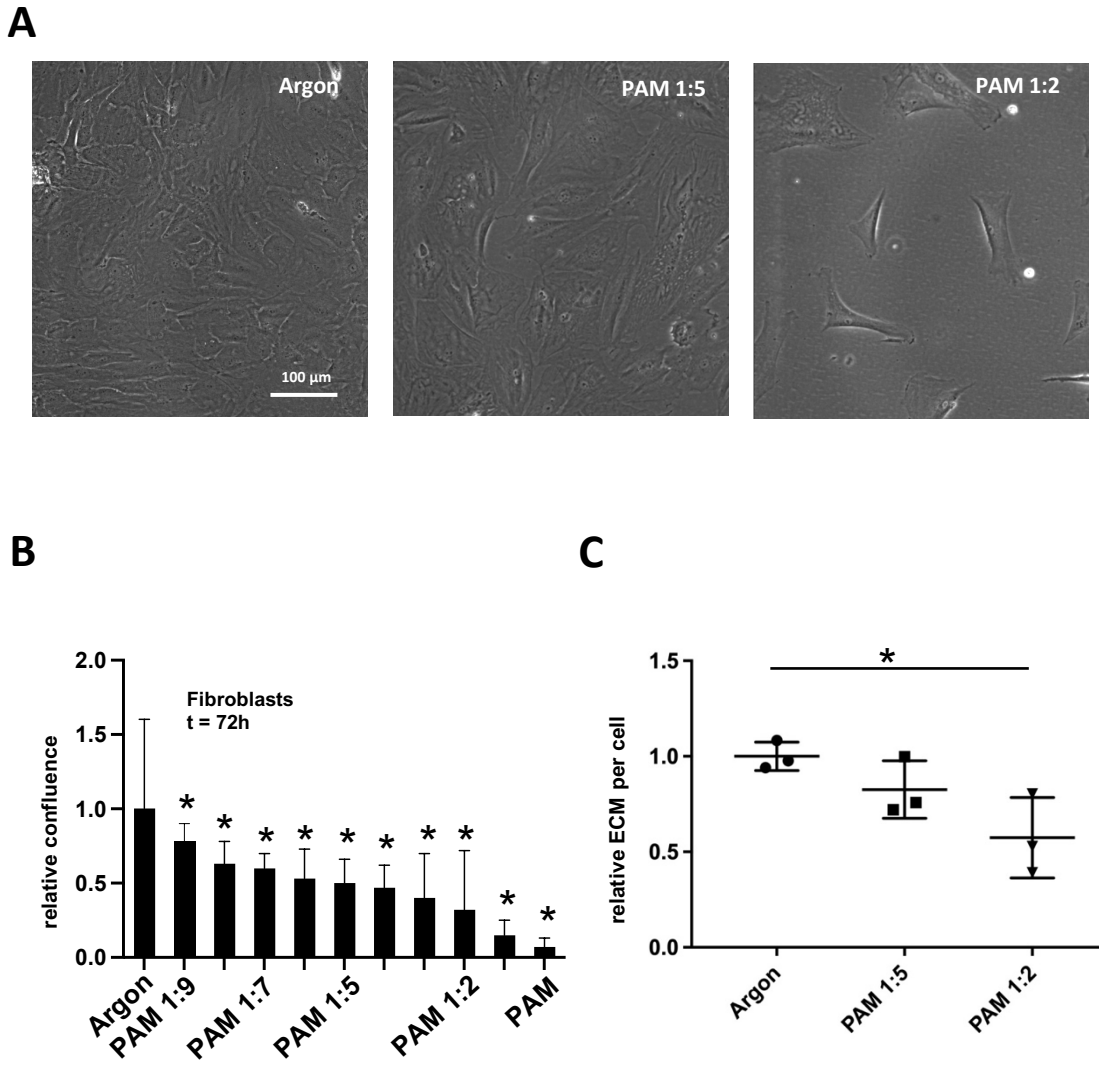

Figure 6. Impact of PAM on cell confluency and ECM synthesis on fibroblasts 72 h after treatment. Relative cell confluency decreased with the intensity of PAM treatment (A). Confluency was determined with the IncuCyte software program and normalized to the control. Lower dilutions led to significantly reduced cell confluency. All PAM treated fibroblasts showed significant decreased relative confluency compared to argon (B). For determination of relative ECM, fibroblasts and the ECM were lyophilized, and weight was normalized to cell count and respective argon mean value. PAM treatment significantly reduced ECM synthesis per cell (C). Stronger treatment led to even more reduced ECM per cell. Significant reduction of relative ECM was observed in PAM 1:2 compared to control. Parts of this figure were already published in Rasch, M.-L. and Holl, M. *et al., Effects of non-invasive physical plasma (NIPP) on the ECM and cells responsible for postoperative intraabdominal adhesions.* Biomedicines, **2022**, 10, 927 [1]. Data are shown as the mean ± SD, n=3, * $p \leq 0.05$.

3.2 Effect of PAM treatment on the extracellular matrix

3.2.1 ECM weight decreases after PAM treatment

The ECM plays an essential part in adhesion formation. Adhesion bands mainly consist of fibronectin and collagen, one of the two main components of the ECM. In the sample preparation for the hydroxyproline (HP) assay for the relative quantification of collagen, fibroblasts and the ECM were collected five days after PAM treatment by use of a cell scraper. Samples were then purified and lyophilized. Weight of the lyophilized ECM was determined before hydrolysis needed for the HP-assay. Measurements were normalized to cell count and the respective control.

Results showed a slight, but not significant decrease in relative ECM production per cell in the PAM 1:5 group compared to the control (Control to PAM 1:5, MD 0.174 ± 0.098 (SEM), p = 0.075) (*Figure 6C*). One patient in the PAM 1:5 treatment group indicated comparable relative ECM values with the mean score of the control group. Values in the control showed a low standard deviation. A significant decrease in relative ECM production per cell was detected in the PAM 1:2 group compared to the argon group (Control to PAM 1:2, MD 0.43 ± 0.13 (SEM), p = 0.015). Mean value approximately halved compared to the control. As in PAM 1:5, one patient's value was notably higher than the one of the other two patients and reached the mean value of PAM 1:5. No significant differences between the two PAM treatment groups could be detected (PAM 1:5 to PAM 1:2, MD 0.25 ± 0.15 (SEM), p = 0.085). Nevertheless, mean value of PAM 1:2 dropped about 0.25 points from mean value of PAM 1:5.

To sum up, fibroblasts significantly decreased their relative ECM production per cell after PAM treatment. PAM 1:2 led to the lowest relative ECM values of all treatment groups. Consequently, stronger PAM treatment efficiently lowers ECM synthesis in fibroblasts.

3.2.2 Effects of PAM treatment on collagen production

3.2.2.1 PAM treatment leads to elevated soluble collagen levels

The Sircol™ Soluble Collagen Assay was performed to evaluate the effect of argon plasma on fibroblasts and their soluble collagen production for the ECM. In this experiment, PAM dilutions 1:2 and 1:5 were examined. Argon served as control. Pepsin-acid digestion of the ECM was performed, followed by the manufacture's Isolation and Concentration Protocol before proceeding to the assay. The measured collagen content was normalized to cell count before normalizing to the respective argon mean value.

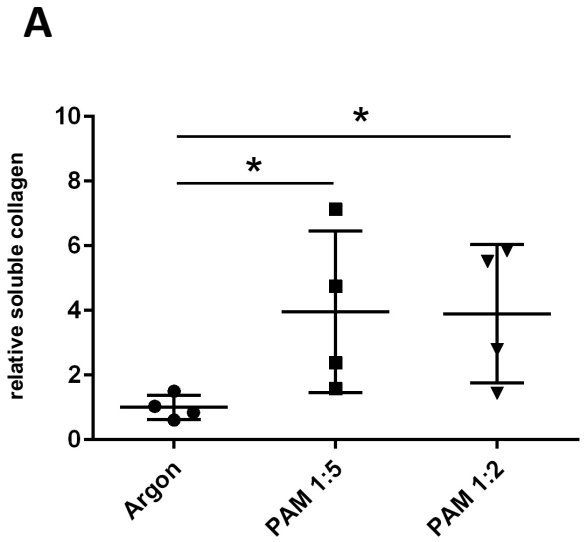

Figure 7. PAM treatment affects soluble collagen levels in fibroblasts. Fibroblasts were evaluated 120 h after PAM treatment performing the Sircol™ Soluble Collagen Assay. Cells and the ECM were digested by pepsin-acid digestion before measurement of soluble collagen. Relative soluble collagen was increasing after treatment in both PAM groups. Data are shown as the mean ± SD, n=4, * $p<0.05$.

Fibroblasts in the argon control group showed approximately four times less soluble collagen per cell than fibroblasts in the PAM treatment groups (*Figure 7*). Values in the control were equally distributed around the mean value and no wide standard deviation could be observed. A significant increase in relative soluble collagen per cell was observed in both PAM groups compared to the control (Control to PAM 1:5, MD 2.96 ± 1.3 (SEM), $p = 0.049$; Control to PAM 1:2, MD 2.89 ± 1.1 (SEM), $p = 0.0036$). Fibroblasts in both PAM groups showed comparable soluble collagen levels per cell to

each other. No significant change in soluble collagen per cell could be detected within the PAM treatment groups (PAM 1:5 to PAM 1:2, MD 0.07 ± 1,6 (SEM), p = 0.48). One patient in group PAM 1:5 showed clearly elevated levels compared to the mean value. Both PAM groups possessed relatively wide standard deviations.

Taken together, PAM treatment leads to a significantly increased relative soluble collagen production per cell in fibroblasts. Both tested PAM concentrations affected the soluble collagen production to a similar extent. Stronger treatment did not have a greater impact on soluble collagen synthesis than weaker PAM.

3.2.2.2 Intracellular collagen content was not modified trough PAM treatment

For evaluating the collagen content in the cell lysates, western blot membranes were restained with the collagen I alpha antibody (Novus Biologicals) and AlexaFluor594 (ThermoScientific). Same membranes as for fibronectin staining were used. For analysis, band densities were corrected to the respective GAPDH and normalized to the respective control using ImageJ software.

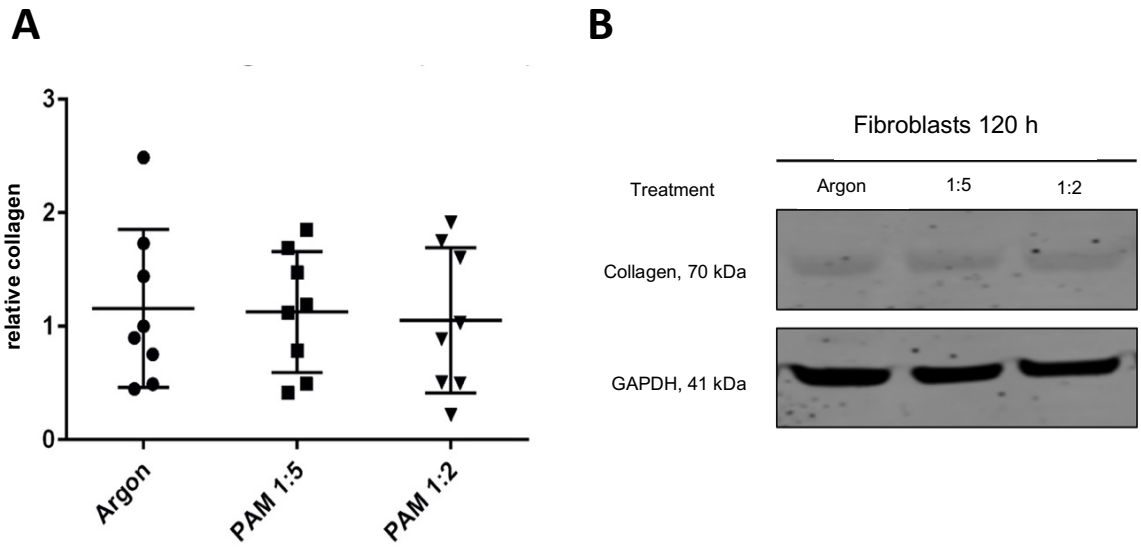

Figure 8. Effect of PAM on intracellular collagen in fibroblasts. Fibroblasts were evaluated 120 h after PAM treatment. Analysis of western blot bands detected no differences between the argon control group and the respective PAM groups (A). For western blot, membranes were stained with collagen I alpha antibody (Novus Biologicals). Intensity of bands were measured by ImageJ software. Bands were shown at 70 kDa (B). Relative collagen at 70 kDa in fibroblasts was not affected by PAM treatment. This figure was already published in Rasch, M.-L. and Holl, M. *et al., Effects of non-invasive physical plasma (NIPP) on the ECM and cells responsible for postoperative intraabdominal adhesions.* Biomedicines, **2022**, 10, 927 [1]. Data are shown as the mean ± SD, n=8, * $p<0.05$.

Bands were only detected at 70 kDa, representing the intracellular collagen. Analysis of intensity of the bands did not show any differences between PAM treated cells and cells in the argon control group (Control to PAM 1:5, MD 0.03 ± 0.13 (SEM), $p = 0.46$; Control to PAM 1:2, MD 0.11 ± 0.33 (SEM), $p = 0.38$) (*Figure 8A and B*). Compared to the respective GAPDH control, all treatment groups possessed considerably lower band intensities. Analysis of the bands using the ImageJ program did not show any significant modifications between the treatment groups PAM 1:2 and PAM 1:5 (PAM 1:5 to PAM 1:2, MD 0.08 ± 0.29 (SEM), $p = 0.4$). Cells treated with PAM 1:2 showed a slight but not significant lower mean intracellular collagen value compared to the argon control. Fibroblasts in the control group and PAM 1:5 treatment group possessed similar relative intracellular collagen levels. A wide value distribution could be detected in every treatment category. One patient in the argon control group showed a clearly elevated relative collagen value compared to the standard deviation bar.

Consequently, the western blot collagen staining indicates that PAM treatment did not alter the intracellular collagen content of fibroblasts. Stronger treatment did not have a greater impact on intracellular collagen levels in fibroblasts than weaker PAM treatment.

3.2.2.3 Total collagen content decreased through PAM treatment

For total collagen detection, immunofluorescence images were analyzed using the ImageJ software and collagen content was semi quantified. In addition, an hydroxyproline assay was performed for quantification of the total collagen content. Fibroblasts underwent treatment with PAM 1:5 and PAM 1:2, argon served as a control. For immunofluorescence semi quantification, cells were stained with collagen I alpha antibody (Novus Biologicals) and AlexaFluor597 (ThermoScientific). Images were taken with a LSM 710 confocal microscope (Carl Zeiss AG), and semi quantification was performed using the ImageJ software.

IF-signal of collagen was mainly detected intracellularly in fibroblasts. As shown earlier in this study, PAM has antiproliferative effects on fibroblasts. IF-staining confirmed this trend by staining the cytoplasmic collagen and therefore accentuating the fibroblasts and the decreasing number of cells after PAM treatment. Especially in the images taken with the 63x objective, the decreased IF-signal intensity can be noticed within PAM treatment. Analysis of IF-intensity of collagen by ImageJ subsequently decreased within PAM treatment and therefore confirmed this trend (*Figure 9A-D*).

Nevertheless, no significant differences could be detected, but stronger PAM treatment such as PAM 1:2 showed lower intensity scores than cells in the PAM 1:5 group or the argon control. Due to the wide standard deviation in the control group, values between the treatment and control groups were not significantly different (Control to PAM 1:5, MD 0.38 ± 0.37 (SEM), $p = 0.17$; Control to PAM 1:2, MD 0.45 ± 0.32 (SEM), $p = 0.11$). No significant modification between treatment groups was detected (PAM 1:5 to PAM 1:2, MD 0.08 ± 0.26 (SEM), $p = 0.39$). PAM dilution 1:5 scored lower intensity values than the control group and slightly higher values compared to cells treated with PAM 1:2. Evaluating the distribution of relative collagen values in the argon control group, relative collagen content per cell of one patient almost exceeded the argon mean value twice. In treatment groups PAM 1:5 and PAM 1:2, values were equally distributed without huge outliers. The results of the IF-collagen analysis led to the assumption that stronger PAM treatment negatively affects the collagen synthesis in fibroblasts. To confirm this thesis, the hydroxyproline assay for quantification of the total collagen amount was performed.

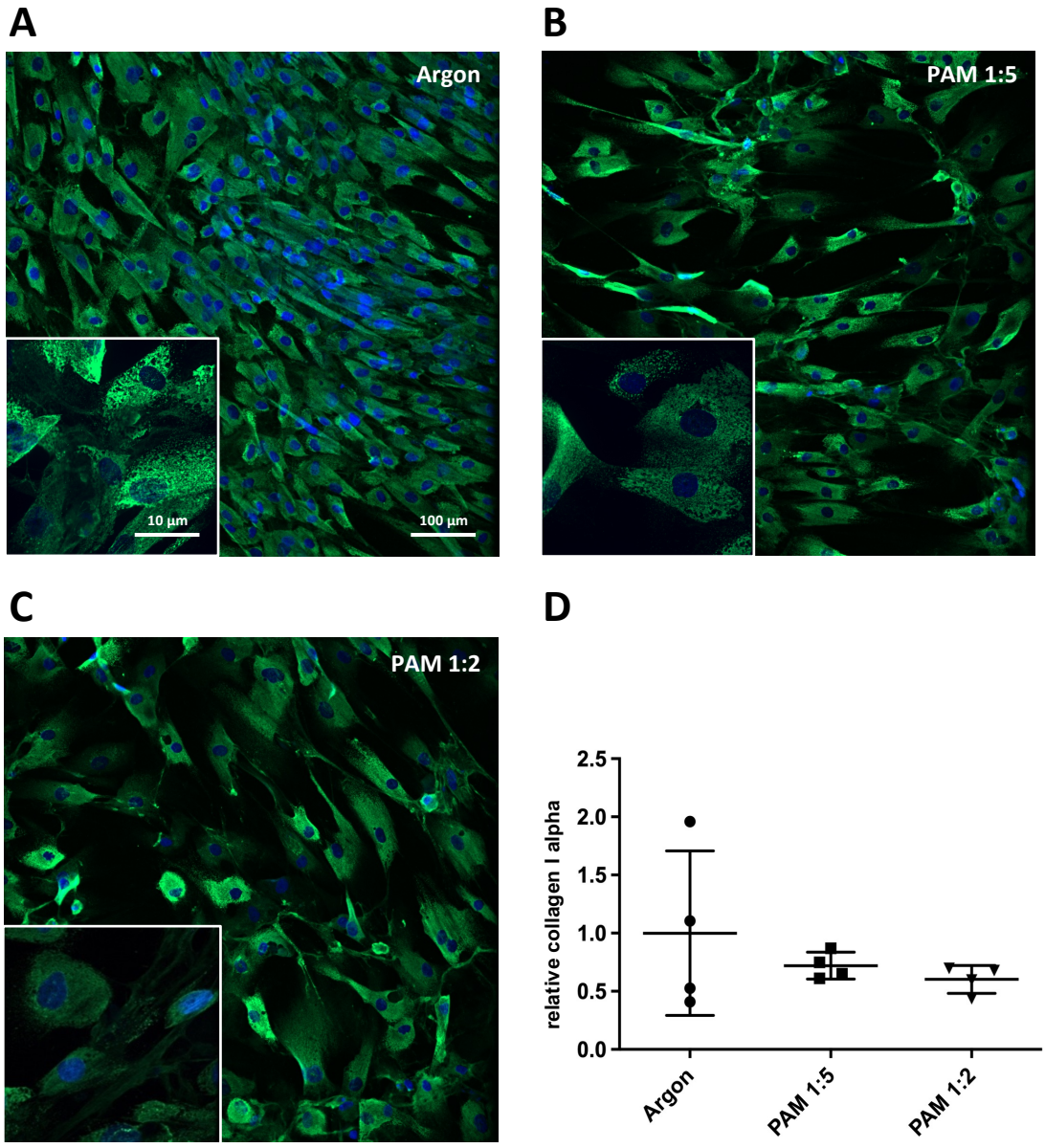

Figure 9. Effect of PAM on collagen expression in fibroblasts. Fibroblasts were evaluated 120 h after PAM treatment. Cells were stained with a collagen I alpha antibody (Novus Biologicals). IF signal decreased within PAM treatment (A-C). Analysis of IF-signal by use ImageJ software showed decreased collagen levels in fibroblasts in PAM treated cells. However, differences were not significant (D). This figure was already published in Rasch, M.-L and Holl, M. *et al., Effects of non-invasive physical plasma (NIPP) on the ECM and cells responsible for postoperative intraabdominal adhesions.* Biomedicines, **2022**, 10, 927 [1]. Data are shown as the mean ± SD, n=4, * $p<0.05$.

For the hydroxyproline assay (Sigma Aldrich), fibroblasts and the synthesized ECM were lyophilized and hydrolyzed using 37 % HCl at 120 h after PAM treatment. Manufactures protocol was followed. Values were obtained from the standard curve and normalized to the respective control.

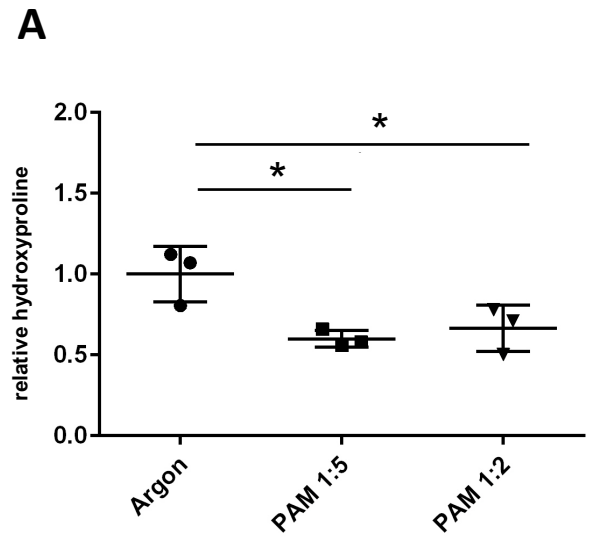

Figure 10. Modification of hydroxyproline in fibroblasts after PAM treatment. Fibroblasts were evaluated 120 h after PAM treatment. For HP analysis, fibroblasts and ECM were lyophilized and then analyzed with an hydroxyproline assay. Relative HP was significantly modified by PAM treatment. No significant modifications between the two PAM groups were detected. Part of this figure were already published in Rasch, M.-L. and Holl, M. *et al., Effects of non-invasive physical plasma (NIPP) on the ECM and cells responsible for postoperative intraabdominal adhesions.* Biomedicines, **2022**, 10, 927 [1]. Data are shown as the mean ± SD, n=3, * $p<0.05$.

Results showed a significant decrease in the relative HP per cell after PAM treatment (*Figure 10*). Fibroblasts in both PAM treatment groups (PAM 1:5 and 1:2) synthesized approximately 30-40 % less relative HP per cell than the cells in the argon control group. Significant decreases could be both observed between argon and PAM 1:5 as well as between argon and treatment group PAM 1:2 (Control to PAM 1:5, MD 0.4 ± 0.1 (SEM), $p = 0.02$; Control to PAM 1:2, MD 0.34 ± 1,3 (SEM), $p = 0.028$). Significant changes between treatment groups PAM 1:2 and PAM 1:5 could not be detected (PAM 1:5 to

PAM 1:2, MD 0.062 ± 0.087 (SEM), p = 0.48). Huge outliners were not detected in neither of the treatment categories. Results of PAM 1:5 showed the smallest standard deviation.

Collagen IF semi quantification has already shown the trend of decreased collagen production in fibroblasts after PAM treatment. With its significant decrease in relative HP synthesis per cell through PAM treatment, the HP assay confirmed this trend.

3.2.3 Effect of PAM on the ECM component fibronectin

3.2.3.1 Fibronectin content decreases through PAM treatment

Relative fibronectin content of cell lysates was determined by western blot. PAM dilutions 1:2 and 1:5 were used for treatment on fibroblasts. Western blot images were taken with the Typhoon Scanner and further analysis was performed through ImageJ software. The density of the bands was corrected to the one of the respective GAPDH and normalized to the respective control.

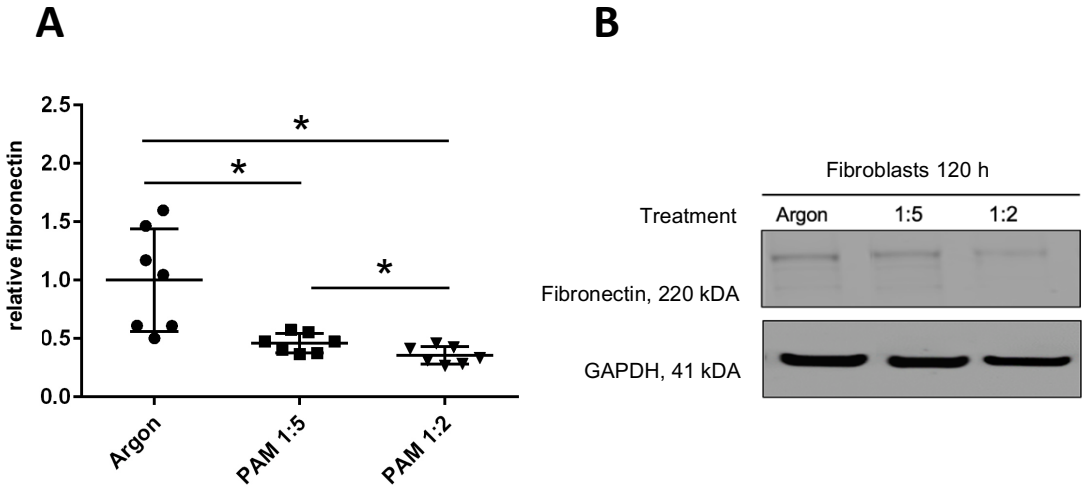

Figure 11. Modification of fibronectin in fibroblasts after PAM treatment (western blot). Fibronectin content was evaluated by western blot at 120 h after PAM treatment. Western blot analysis showed a significant decrease in fibronectin synthesis in both PAM treatment groups (A, B). Parts of this figure were already published in Rasch, M.-L. and Holl, M. *et al., Effects of non-invasive physical plasma (NIPP) on the ECM and cells responsible for postoperative intraabdominal adhesions.* Biomedicines, **2022**, 10, 927 [1]. Data are shown as the mean ± SD, n=7, * $p<0.05$.

Samples from the argon control group showed higher intensities of the western blot bands than cells from PAM treatment groups (*Figure 11B*). Intensity of bands decreased within PAM treatment. Stronger treatment led to weaker western blot signals. Fibroblasts treated with PAM 1:2 showed less intense bands than cells from the PAM 1:5 group. The argon control group presented the most intense western blot signal. Analyzing the bands with ImageJ software, fibroblasts in the PAM 1:2 treatment group showed significant lower fibronectin per cell than cells in the argon control group (Control to PAM 1:2, MD 0.65 ± 0.17 (SEM), p = 0.004) (*Figure 11A*). As in PAM 1:2, fibroblasts in PAM 1:5 possessed significantly lower fibronectin values per cell than the control (Control to PAM 1:5, MD 0.54 ± 0.17 (SEM), p = 0.009). Intensity of bands was also significantly altered after treatment between PAM 1:5 and PAM 1:2 (PAM 1:5 to PAM 1:2, MD 0.11 ± 0.04 (SEM), p = 0.014).

Immunofluorescence staining for fibronectin was performed five days after PAM treatment using the fibronectin antibody from Abcam (1:200). Semi quantification of IF images was performed using the ImageJ software. Numbers were normalized to cell count and the argon mean value.

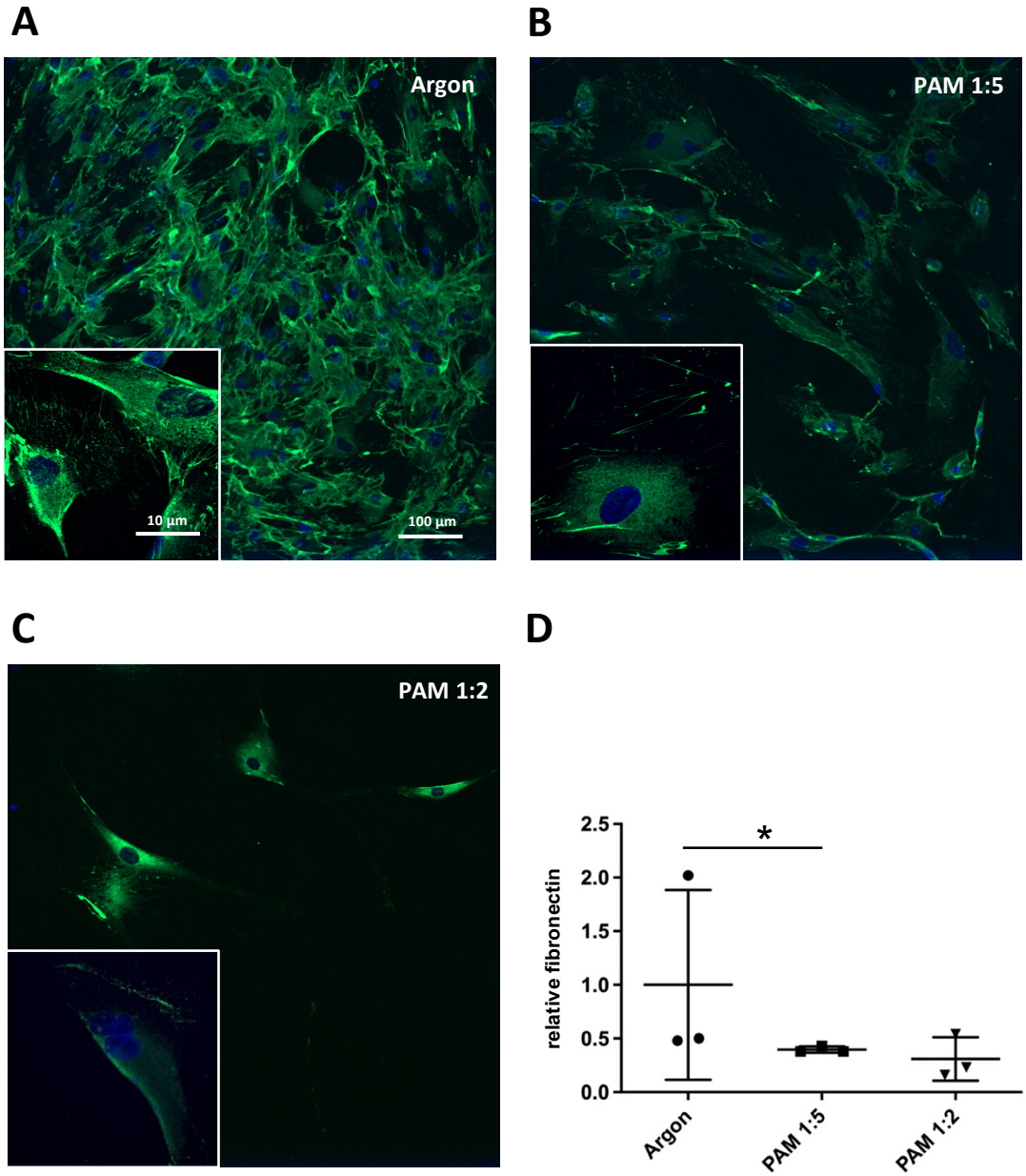

Figure 12. Modification of fibronectin in fibroblasts after PAM treatment (IF). Fibronectin content was evaluated by IF semi quantification at 120 h after PAM treatment by analyzing the IF intensity with ImageJ software. IF intensity decreased after PAM treatment (A-C). PAM significantly lowered relative fibronectin per cell in the PAM 1:5 group compared to the control (D). Fibroblast underwent PAM 1:2 treatment showed lower values than cells in the argon group, but changes were not significant. Parts of this figure were already published in Rasch, M.-L. and Holl, M. *et al., Effects of non-invasive physical plasma (NIPP) on the ECM and cells responsible for postoperative intraabdominal adhesions.* Biomedicines, **2022**, 10, 927 [1]. Data are shown as the mean ± SD, n=3, * $p<0.05$.

Analyzing the IF-staining of fibronectin, fibroblasts in the argon control group grew to the highest confluency and created a strong fibronectin network (*Figure 12A-C*). When being treated with PAM 1:5, cells synthesized less fibronectin and grew to a smaller confluency, again showing the antiproliferative effect of PAM on fibroblasts. Particularly, small fibronectin networks between cells could be observed. When comparing PAM 1:2 and PAM 1:5, no fibronectin networks between cells could be overserved. In both PAM groups, stained fibronectin fibers were mainly detected on an intracellular basis. Intensity of fibronectin staining decreased within PAM treatment. Semi-quantification of IF-signal intensity by ImageJ software showed decreased intensity values per cell in both PAM groups (*Figure 12D*). Fibroblasts in the argon control group showed significant higher relative fibronectin per cell values than cells in the PAM 1:5 group (Control to PAM 1:5, MD 0.6, $p = 0.046$). No significant difference was observed between the control and PAM 1:2 (Control to PAM 1:2, MD 0.7, $p = 0.275$). This may be explained by the wider standard deviation of both groups. Nevertheless, mean value of cells treated with PAM 1:2 decreased compared to cells in the control group. No significant modification between the PAM groups was detected (PAM 1:5 to PAM 1:2, MD 0.09, $p = 0.5$).

Immunofluorescence staining of fibroblasts corresponded to the results of the fibronectin western blot analysis. Results of both methods showed less fibronectin synthesis in PAM treated fibroblasts compared to non-treated cells. Significant reduction in relative fibronectin per cell was only detected between the argon control and PAM 1:5 group in both experiments. Nevertheless, cells who underwent PAM 1:2 treatment presented lower fibronectin values per cell than the argon control group. Taken together, PAM treatment of fibroblasts led to significant decreased fibronectin synthesis per cell. Analysis of western blot corresponded with results of the immunofluorescence staining semi quantification.

3.3 PAM treatment affects cytokine production

Various cytokines participate in the adhesion formation process. Therefore, the most important cytokines involved were examined in this study. Fibroblasts were treated with PAM 1:2, PAM 1:5 and argon as a control. After 24 h, the respective cell culture medium was aspirated and analyzed by a Multiplex Assay System. Cytokine levels of the scratch^{+} group were normalized to the respective scratch^{-} group before normalizing to the respective argon mean value. By this, the effect of the scratch was foregrounded, and an intraperitoneal injury was mimicked. Evaluating the measured cytokines, inter-patient specific differences regarding the measured cytokine levels could be observed.

3.3.1 Some pro inflammatory cytokines indicate decreased levels after PAM

Various pro-inflammatory acting cytokines were assessed in this study.

Analysis of IL-1b showed a decrease in detectable IL-1b per cell when treated with PAM (*Figure 13A*). Stronger PAM treatment led to lower IL-1b values per cell when compared to the argon control group. PAM 1:2 significantly decreased IL-1 levels (Control to PAM 1:2, MD 0.22 ± 0.07 (SEM), p = 0.04). Modifications between the PAM groups as well as between PAM 1:5 and the control were not significant (PAM 1:5 to PAM 1:2, MD 0.13 ± 0.1 (SEM), p = 0.13; Control to PAM 1:5, MD 0.09 ± 0.08 (SEM), p = 0.16).

TNF-alpha levels did not show any significant differences between the different treatment groups (Control to PAM 1:5, MD 0.04 ± 0.05 (SEM), p = 0.27; Control to PAM 1:2, MD 0.05 ± 0.08 (SEM), p = 0.28; PAM 1:5 to PAM 1:2, MD 0.01 ± 0.06 (SEM), p= 0.42) (*Figure 13B*). Only one patient indicated remarkably lower TNF-alpha levels when treated with PAM 1:2 compared to the control. For all other treatment groups and patients, similar values were detected.

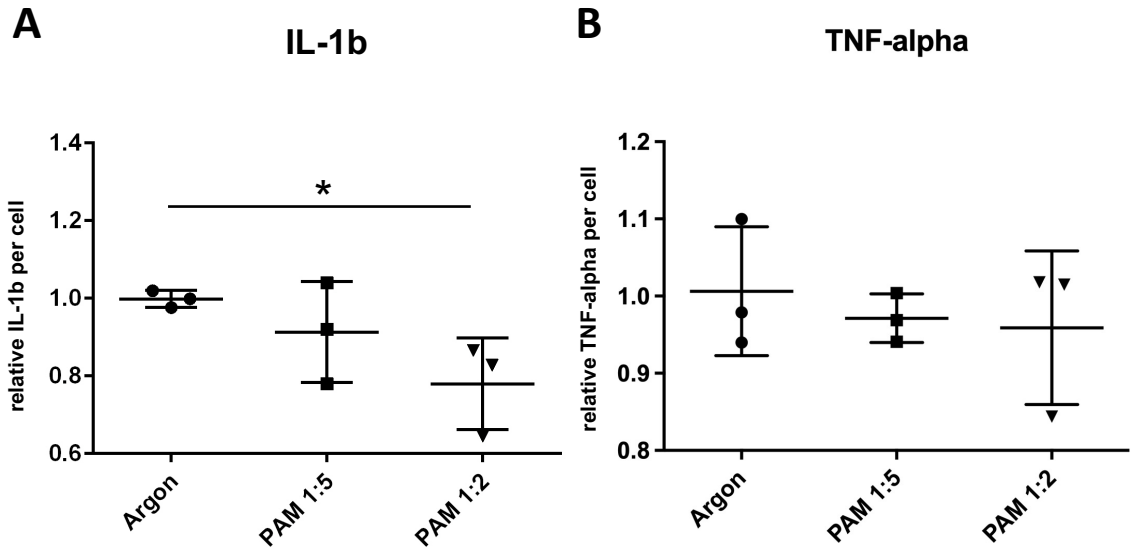

Figure 13. Analysis of pro-inflammatory cytokines IL-1b and TNF-alpha after PAM treatment. Analysis was performed 24 h after PAM treatment of fibroblasts using a Multiplex Assay System. In general, strong PAM treatment led to lower cytokine levels. Significant decreases in cytokine levels were detected in IL-1b in the PAM 1:2 group (A). Analysis of TNF-alpha did not show significantly modified cytokine levels after treatment (B). Parts of this figure were already published in Rasch, M.-L. and Holl, M. *et al., Effects of non-invasive physical plasma (NIPP) on the ECM and cells responsible for postoperative intraabdominal adhesions.* Biomedicines, **2022**, 10, 927 [1]. Data are shown as the mean ± SD, n=3, * $p<0.05$.

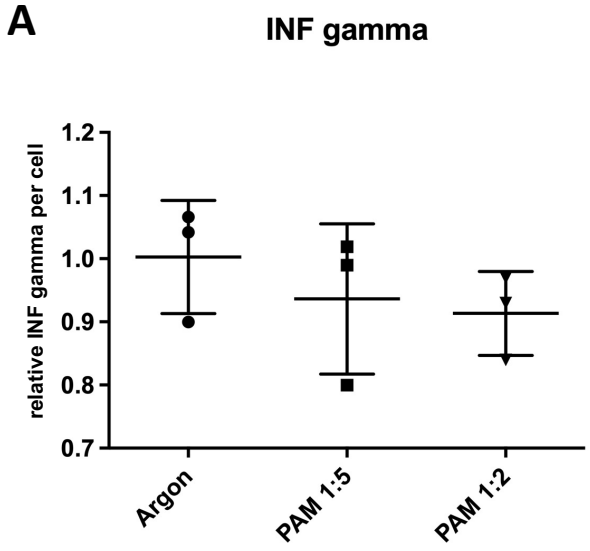

Figure 14. Modification of INF gamma after PAM treatment. Analysis was performed 24 h after PAM treatment of fibroblasts using a Multiplex Assay System. Treatment led to slight but no significantly lowered INF-gamma production in fibroblasts. Data are shown as the mean ± SD, n=3, * $p<0.05$.

In this study, PAM treatment led to slightly lower INF-gamma levels (*Figure 14*). Nevertheless, changes were not significant (Control to PAM 1:5, MD 0.09 ± 0.17 (SEM), $p = 0.24$; Control to PAM 1:2, MD 0.09 ± 0.06 (SEM), $p = 0.12$; PAM 1:5 to PAM 1:2, MD 0.02 ± 0.08 (SEM), $p = 0.39$). Data of one patient were notably lower than the respective mean value in each of the analyzed groups.

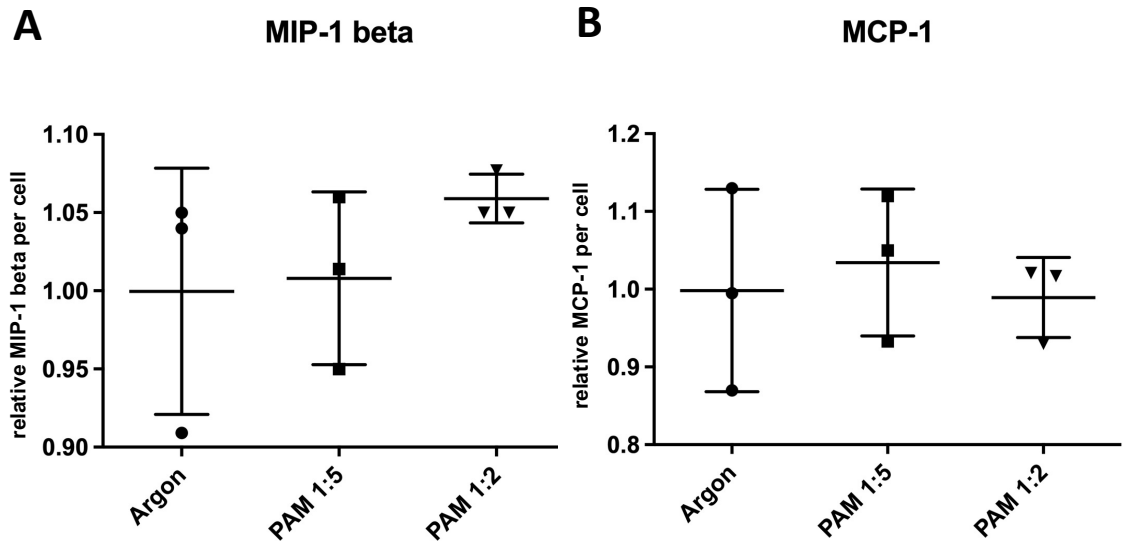

Figure 15. PAM did not affect MIP-1 beta and MCP-1 levels in fibroblasts. Analysis was performed 24 h after PAM treatment of fibroblasts using a Multiplex Assay System. Treatment did not modify the production of either cytokine in fibroblasts (A, B). Data are shown as the mean ± SD, n=3, * $p<0.05$.

For levels of MIP-1-beta, no significant changes were observed even though slightly elevated levels in the PAM 1:2 treatment group could be noticed (Control to PAM 1:2, MD 0.06 ± 0.05 (SEM), p = 0.32; PAM 1:5 to PAM 1:2, MD 0.05 ± 0.03 (SEM), p = 0.1) (*Figure 15A*). Due to wider standard deviations in the control and PAM 1:5 group, changes were not significant (Control to PAM 1:5, MD 0.08 ± 0.06 (SEM), p = 0.44).

The cytokine MCP-1, also called monocyte chemoattractant protein or CCL2, was analyzed as well. Analysis did not show significant modifications between groups (Control to PAM 1:2, MD 0.009 ± 0.08 (SEM), p = 0.46; PAM 1:5 to PAM 1:2, MD 0.05 ± 0.06 (SEM), p = 0.25) (*Figure 15B*). Compared to the control and PAM 1:2, MCP-1 levels were slightly elevated in fibroblasts treated with PAM 1:5 (Control to PAM 1:5, MD 0.04 ± 0.09 (SEM), p = 0.36).

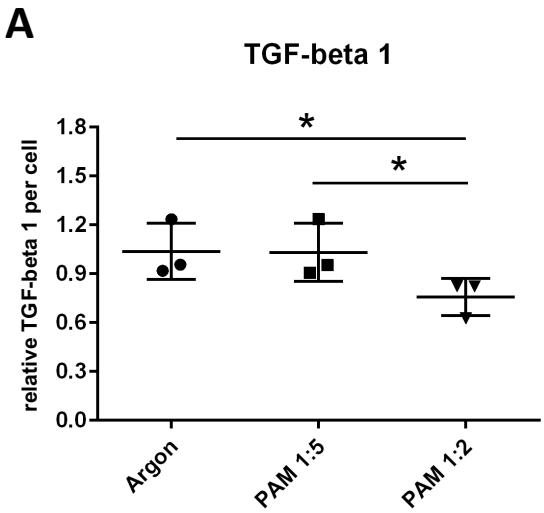

Figure 16. Analysis of TGF-beta 1 after PAM treatment. Analysis was performed 24 h after PAM treatment in fibroblasts using a Multiplex Assay System. Analysis detected significantly decreased TGF-beta 1 levels in PAM 1:2 compared to the control as well as to PAM 1:5. This figure was already published in Rasch, M.-L. and Holl, M. *et al., Effects of non-invasive physical plasma (NIPP) on the ECM and cells responsible for postoperative intraabdominal adhesions.* Biomedicines, **2022**, 10, 927 [1]. Data are shown as the mean ± SD, n=3, * $p<0.05$.

Results of this study showed a significant decrease of relative TGF-beta 1 per cell in den PAM 1:2 group (Control to PAM 1:2, MD 0.28 ± 0.12 (SEM), p = 0.038) (*Figure 16*). No significant difference between the control and PAM 1:5 was detected (Control to PAM 1:5, MD 0.006 ± 0.14 (SEM), p = 0.49). Fibroblasts in both groups synthesized about the same amount of relative TGF-beta 1 per cell. Significant reduction in relative TGF-beta 1 production per cell was also observed in PAM 1:2 compared to cells who underwent PAM 1:5 treatment (PAM 1:5 to PAM 1:2, MD 0.27 ± 0.12 (SEM), p = 0.048). Therefore, stronger PAM treatment led to a significant reduction in TGF-beta 1 levels in fibroblasts.

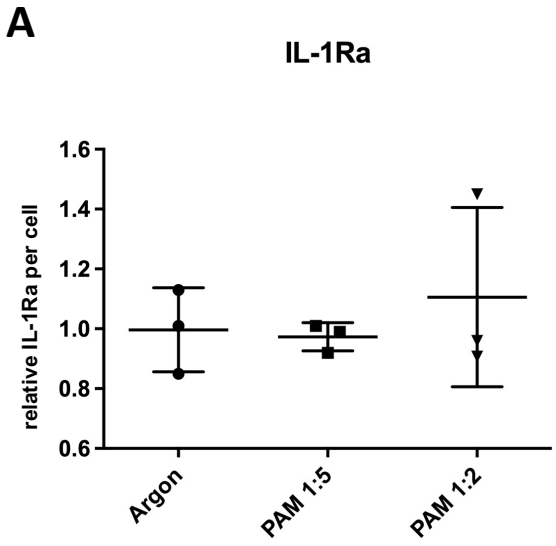

Figure 17. Analysis of IL-1Ra after PAM treatment. Analysis was performed 24 h after PAM treatment in fibroblasts using a Multiplex Assay System. No modification of IL-1Ra levels was detected after treatment. Data are shown as the mean ± SD, n=3, * $p<0.05$.

Il-1Ra is an Interleukin-1 receptor antagonist. No significant impact regarding the IL1-Ra values after PAM treatment on fibroblasts could be detected (Control to PAM 1:5, MD 0.02 ± 0.09 (SEM), p = 0.4; Control to PAM 1:2, MD 0.11 ± 0.19 (SEM), p = 0.3; PAM 1:5 to PAM 1:2, MD 0.12 ± 0.17 (SEM), p = 0.25) (*Figure 17*). One patient in the PAM 1:2 group showed notably higher values than the other patients in this respective treatment group or PAM 1:5 or control group.

To conclude, PAM treatment selectively reduced pro inflammatory acting cytokines like IL-1b or TGF-beta 1. Only stronger treatment led to significant results. PAM treatment did not alter levels of the other examined pro-inflammatory cytokines.

3.3.2 PAM treatment does not change angiogenesis promoting factors

Angiogenesis promoting factors were evaluated in this study as well.

While the mean values did not show any significant changes, the trend of slightly decreased IL-6 levels in fibroblasts after treatment could be detected (Control to PAM 1:5, MD 0.09 ± 0.17 (SEM), p = 0.32; Control to PAM 1:2, MD 0.13 ± 0.17 (SEM), p = 0.24; PAM 1:5 to PAM 1:2, MD 0.04 ± 0.09 (SEM), p = 0.68) (*Figure 18A*). One patient showed remarkably elevated IL-6 levels in the control group which resulted in a wider standard deviation. Compared to results of IL-6, no significant differences between the different treatment groups were detected in IL-8 either (Control to PAM 1:5, MD 0.03 ± 0.14 (SEM), p = 0.41; Control to PAM 1:2, MD 0.14 ± 0.16 (SEM), p = 0.21; PAM 1:5 to PAM 1:2, MD 0.11 ± 0.19 (SEM), p = 0.6) (*Figure 18B*). Regardless the significance, PAM 1:2 treatment tends to lower IL-8 levels in fibroblasts.

As well as for levels of other angiogenesis promoting factors observed in this study, no significant changes in VEGF levels within PAM treatment were noticed (Control to PAM 1:5, MD 0.04 ± 0.05 (SEM), p = 0.27; Control to PAM 1:2, MD 0.07 ± 0.15 (SEM), p = 0.28; PAM 1:5 to PAM 1:2, MD 0.11 ± 0.16 (SEM), p = 0.28) (*Figure 18C*). Noticeably, one patient in the PAM 1:2 group revealed remarkably higher VEGF levels compared to the other patients in the respective treatment group and clearly extended the argon mean value.

To sum up, PAM did not have a significant impact on angiogenesis promoting cytokines synthesized by fibroblasts.

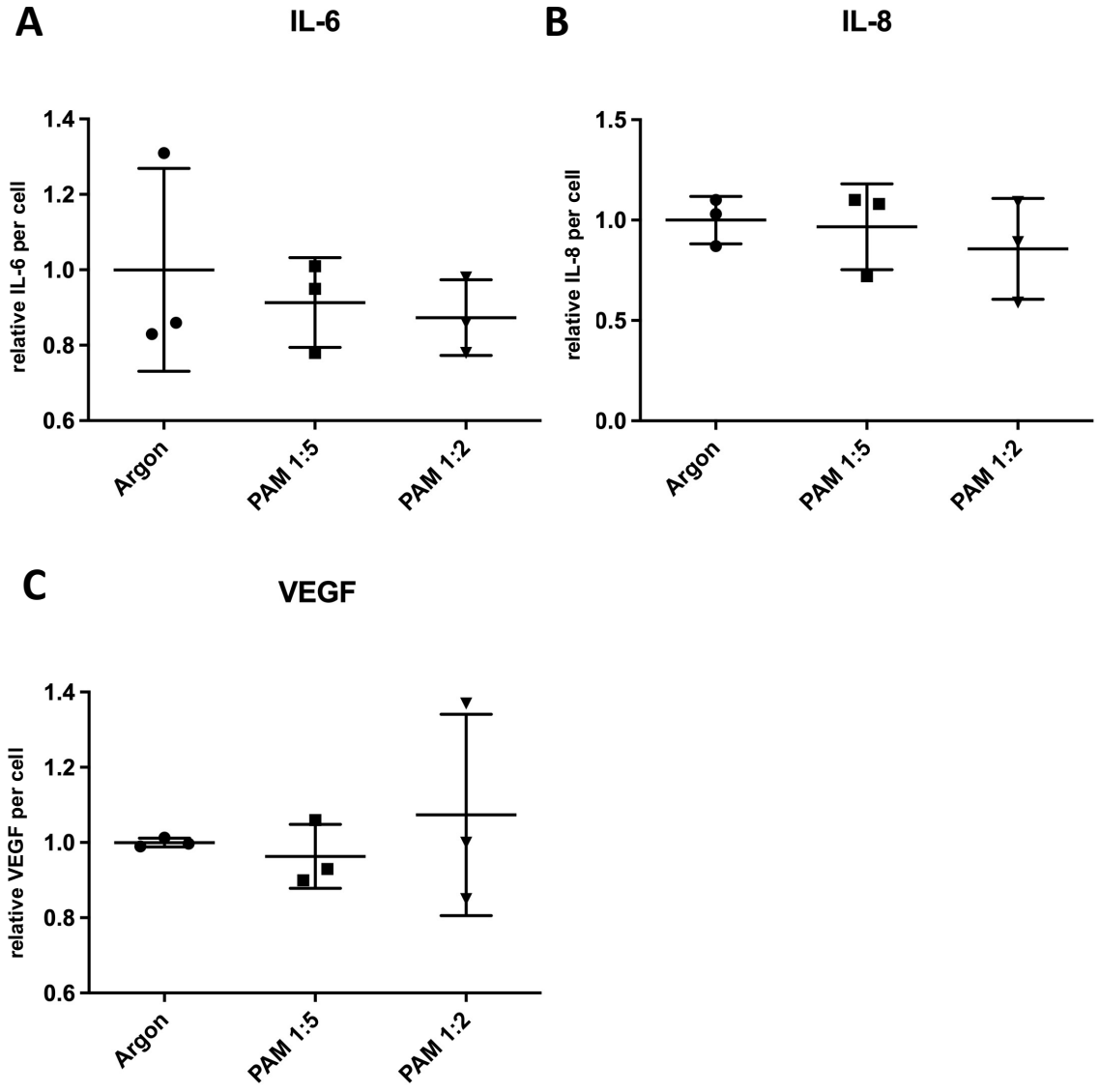

Figure 18. Angiogenesis promoting factors did not significantly change levels after PAM treatment. Analysis was performed using a Multiplex Assay System. IL-6 analysis showed a slight decrease in relative cytokine levels after PAM treatment (A). PAM did not affect cytokine levels of IL-8 (B). Results of VEGF analysis showed a slight increase in cytokine levels in the PAM 1:2 treatment group (C). No significant changes could be detected. Data are shown as the mean ± SD, n=3, * $p<0.05$.

3.3.3 PAM treatment did not impact anti-inflammatory cytokines

Besides pro-inflammatory acting cytokines, the human organism synthesizes cytokines decreasing the inflammation. Therefore, analysis of anti-inflammatory acting cytokines was performed. Analysis did not show any significant changes in IL-4 levels between the argon control and PAM treatment groups (Control to PAM 1:5, MD 0.01 ± 0.11 (SEM), p = 0.47; Control to PAM 1:2, MD 0.03 ± 0.08 (SEM), p = 0.39; PAM 1:5 to PAM 1:2, MD 0.04 ± 0.11 (SEM), p = 0.38) (*Figure 19A*). No trend of modification between PAM treatment groups was observed either. One patient showed remarkably elevated IL-4 levels in the PAM 1:5 group resulting in a wider standard deviation. Looking at IL-10, no significant differences could be observed either (Control to PAM 1:5, MD 0.01 ± 0.02 (SEM), p = 0.32; Control to PAM 1:2, MD 0.04 ± 0.06 (SEM), p = 0.27; PAM 1:5 to PAM 1:2, MD 0.03 ± 0.06 (SEM), p = 0.32) (*Figure 19B*). In the PAM 1:2 group, one patient showed notably higher, and another one remarkably lower IL-10 levels compared to their respective values in the argon control or PAM 1:5 group.

Consequently, results did not reveal an impact of PAM on anti-inflammatory cytokines in fibroblasts.

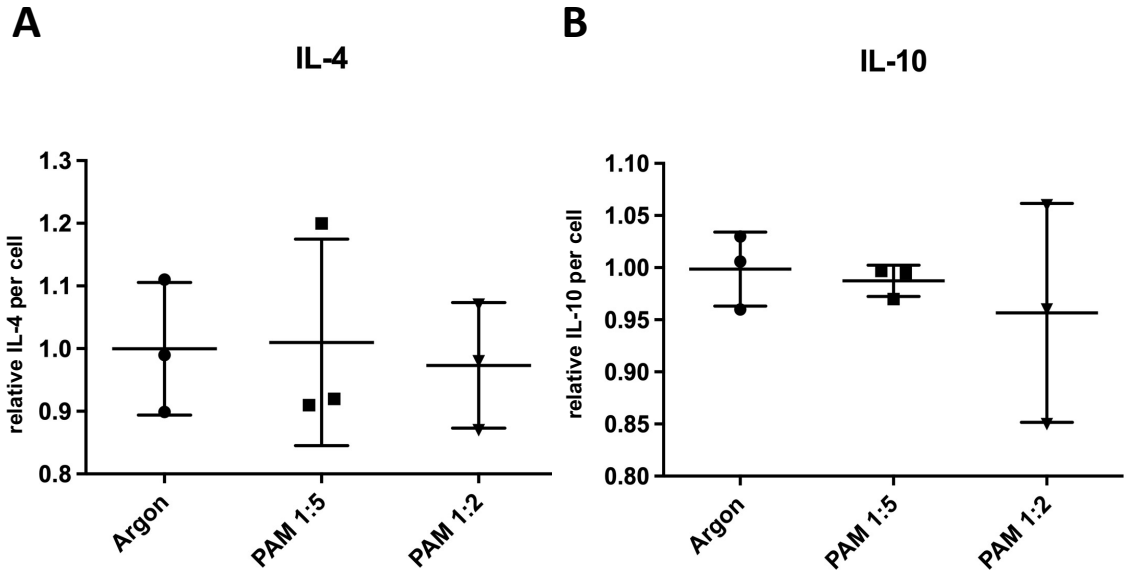

Figure 19. PAM treatment did not change levels of anti-inflammatory acting cytokines. Analysis was performed using a Multiplex Assay System. Analysis of IL-4 as well as IL-10 did not show any significant differences in cytokine levels after PAM treatment. In both groups, the PAM 1:2 group showed slightly reduced values compared to the argon control group. Data are shown as the mean ± SD, n=3, * $p<0.05$.

3.3.4 Some colony stimulating factors change levels after PAM treatment

Macrophages and granulocytes play an important role in adhesion disease as well. Therefore, their growth stimulating factors GM-CSF and M-CSF were analyzed in this study.

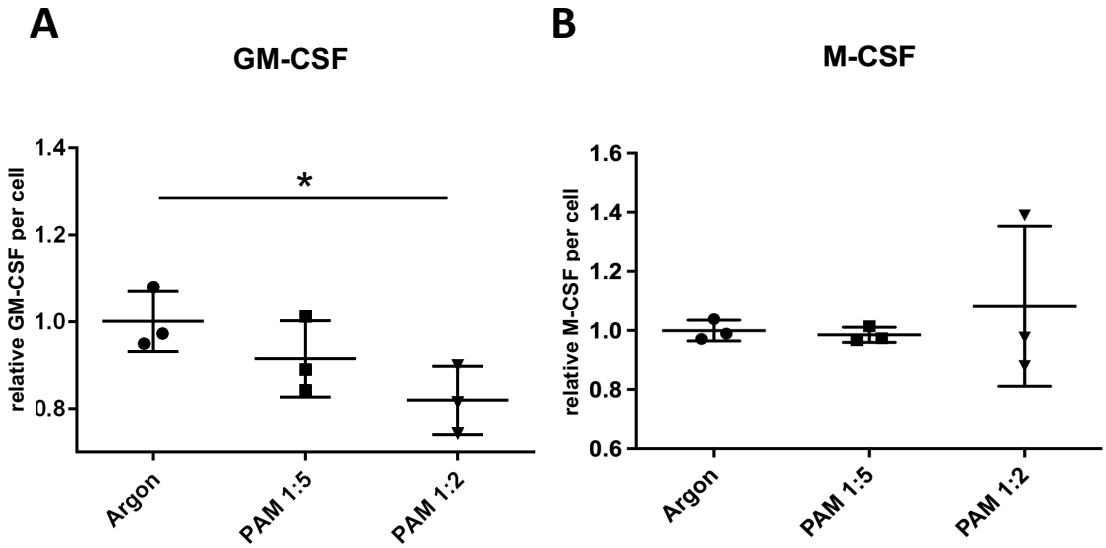

Figure 20. CSF levels were partly altered by PAM treatment. Analysis was performed using a Multiplex Assay System. GM-CSF levels showed reduced values in both PAM treatment groups. PAM 1:2 significantly decreased relative GM-CSF levels in fibroblasts (A). Decreased but no significant changed values could be detected in the PAM 1:5 group. However, PAM treatment did not alter M-CSF levels in fibroblasts (B). Parts of this figure were already published in Rasch, M.-L. and Holl, M. *et al., Effects of non-invasive physical plasma (NIPP) on the ECM and cells responsible for postoperative intraabdominal adhesions.* Biomedicines, **2022**, 10, 927 [1]. Data are shown as the mean ± SD, n=3, * $p<0.05$.

Regarding GM-CSF, significantly decreased values could be observed for PAM 1:2 when tested against the argon control group (Control to PAM 1:2, MD 0.18 ± 0.06 (SEM), p = 0.02) (*Figure 20A*). Even though GM-CSF levels were lower in the PAM 1:5 group than in the control, no significant changes were detected (Control to PAM 1:5, MD 0.09 ± 0.06 (SEM), p = 0.13; PAM 1:5 to PAM 1:2, MD 0.1 ± 0.07 (SEM), p = 0.12). Regarding the growth factor of macrophages (M-CSF), no significant changes were detected (Control to PAM 1:2, MD 0.08 ± 0.16 (SEM), p = 0.33; PAM 1:5 to PAM 1:2, MD 0.09 ± 0.16 (SEM), p = 0.3) (*Figure 20B*). Relative M-CSF levels did not differ between argon or PAM 1:5 (Control to PAM 1:5, MD 0.02 ± 0.03 (SEM), p = 0.3). One patient in the PAM 1:2 group showed remarkably elevated values compared to the other patient of the treatment group. Taken together, PAM treatment decreased GM-CSF levels, but did not have any impact on M-CSF levels.

3.4 Influence of PAM on matrix metalloproteinases 1 and 2

Matrix metalloproteinases (MMP) play an important role in ECM growth and degradation processes. For the measurement of those specific MMPs, fibroblasts and mesothelial cells were treated with PAM 1:2, argon served as control. Cell culture supernatant of fibroblasts was collected at 24 h, 72 h and 120 h after PAM treatment and was frozen right away at -80°C. For mesothelial cells, timepoints 24 h and 72 h post PAM treatment were evaluated. Samples were frozen for a minimum of 24 h before start of the assay. ELISA kits by ThermoScientific were used for analysis. Results were normalized to respective cell count and argon mean.

For fibroblasts, analysis of MMP-1 was done 24 h, 72 h and 120 h post PAM. An inter-patient variance could be observed at each time point and treatment group. No significant change between groups was noticed at any analyzed time points (*Figure 21A*). 24 h post PAM showed no differences between treatment group and control (t24, Control to PAM 1:2, MD 0.1 ± 0.56 (SEM), p = 0.44). Inspecting results at 72 h post PAM, fibroblasts in the PAM 1:2 group presented less relative MMP-1 per cell than cells in the argon control group. Nevertheless, changes in MMP-1 levels were not significant (t72, Control to PAM 1:2, MD 0.43 ± 0.34 (SEM), p = 0.14). Standard deviation of the PAM 1:2 group was notably low compared to the other treatment categories and time points. 120 h after PAM treatment, relative MMP-1 expression did not differ between the control and the treatment group in fibroblasts (t120, Control to PAM 1:2, MD 0.14 ± 0.87 (SEM), p = 0.44). Remarkably wide standard deviations occurred in both treatment groups. Mean value of the PAM group was slightly elevated compared to cells in the control group. To sum up, PAM treatment in fibroblasts modified MMP-1 levels mainly 72 h post treatment.

As in fibroblast's analysis, mesothelial cells did not show any significant changes between argon and PAM 1:2 after 24 h either (t24, Control to PAM 1:2, MD 0.12 ± 0.78 (SEM), p = 0.44) (*Figure 21B*). Values at 24 h presented a huge outlier leading to a wider standard deviation. Results at 72 h after treatment showed a slight but not significant increase in relative MMP-1 per cell in the PAM 1:2 group (t72, Control to PAM 1:2, MD 1,1 ± 0.64 (SEM), p = 0.08).

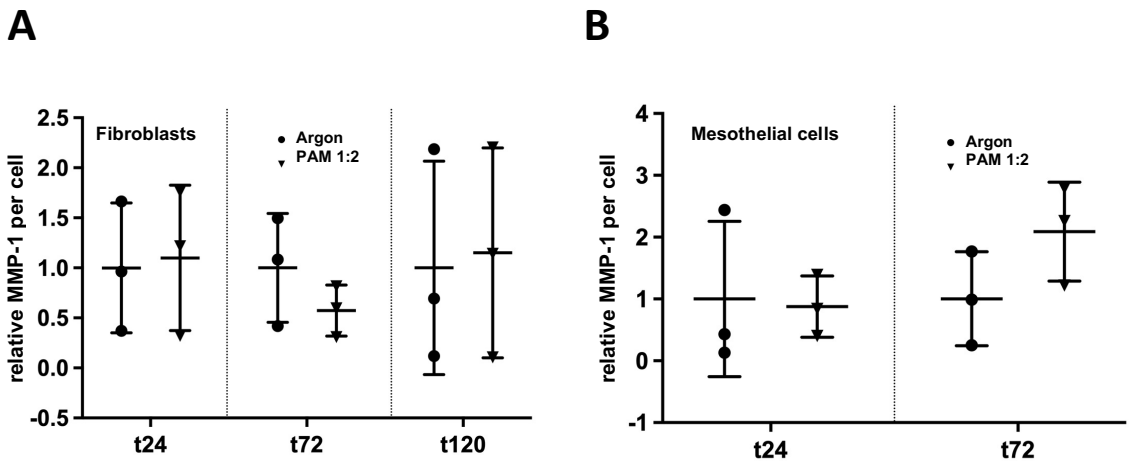

Figure 21. Impact of PAM-treatment on MMP-1 in fibroblasts and mesothelial cells. Both cell types were treated with PAM, analysis was performed 24 h, 72 h and 120 h after treatment performing an ELISA for MMP-1 detection. Fibroblasts (A) and mesothelial cells (B) did not have a significantly altered relative MMP-1 content after treatment. Results slightly differed between cell types after 72 h. Parts of this figure were already published in Rasch, M.-L. and Holl, M. *et al., Effects of non-invasive physical plasma (NIPP) on the ECM and cells responsible for postoperative intraabdominal adhesions.* Biomedicines, **2022**, 10, 927 [1]. Data are shown as the mean ± SD, n=3, * $p<0.05$.

To sum up, passed time after PAM application had a considerable impact on relative MMP-1 synthesis - mainly at 72 h post treatment in both fibroblasts and mesothelial cells. Relative MMP-1 levels were not significantly modified over time in mesothelial cells or fibroblasts for all other timepoints. Slight contrary behaviors between the two cell types could be noticed at 72 h after treatment. Whereas mesothelial cells slightly increased their relative MMP-1 expression after PAM treatment, fibroblasts decreased relative MMP-1 synthesis.

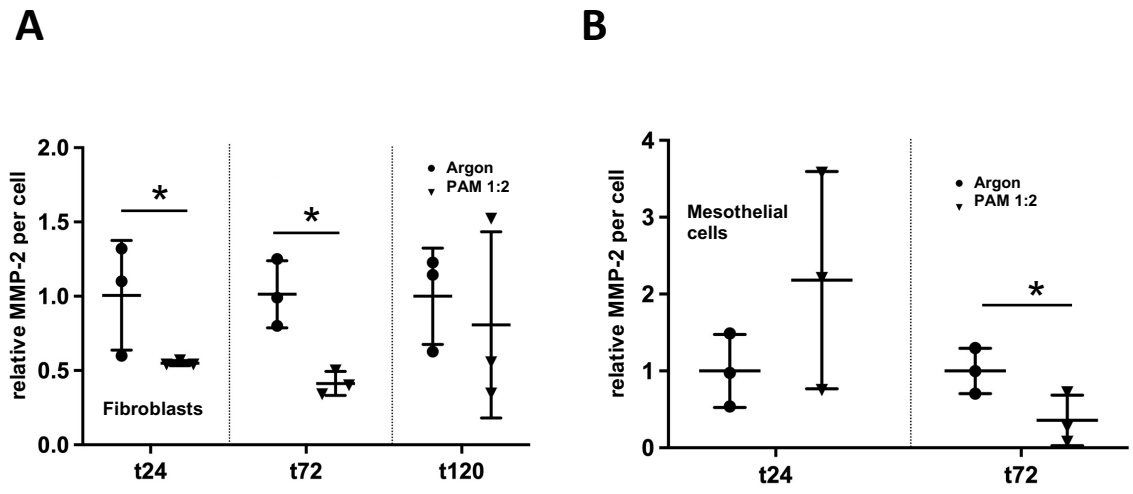

Figure 22. Impact of PAM-treatment on MMP-2 in fibroblasts and mesothelial cells. Both cell types were treated with PAM, analysis was performed 24 h, 72 h and 120 h after treatment performing an ELISA for MMP-2 detection. Relating to MMP-2, fibroblasts significantly decreased relative MMP-2 after treatment after 24 h and 72 h (A). After slightly increasing relative MMP-2 after 24h, mesothelial cells also significantly reduced relative MMP-2 after 72 h (B). Parts of this figure were already published in Rasch, M.-L. and Holl, M. *et al., Effects of non-invasive physical plasma (NIPP) on the ECM and cells responsible for postoperative intraabdominal adhesions.* Biomedicines, **2022**, 10, 927 [1]. Data are shown as the mean ± SD, n=3, * $p<0.05$.

Analysis of relative MMP-2 per cell in fibroblasts 24 h after PAM demonstrated significantly decreased values in the PAM 1:2 treatment group compared to the argon control group (t24, Control to PAM 1:2, MD 0.46 ± 0.21 (SEM), $p = 0.049$) (*Figure 22A*). Relative MMP-2 levels in PAM 1:2 almost halved compared to levels in fibroblasts who underwent argon gas treatment only. One patient in the control group showed remarkably lower values resulting in approximately half of the MMP-2 levels compared to the other patients of the control group. At 72 h post PAM treatment, a significant reduction in relative MMP-2 was achieved in PAM 1:2 (t72, Control to PAM 1:2, MD 0.6 ± 0.14 (SEM), $p = 0.006$). 72 h after PAM treatment, even lower relative MMP-2 per cell compared to values at 24 h post PAM could be detected. As after 24 h post PAM, fibroblasts in the PAM 1:2 group were distributed around the mean value with a low standard deviation. After 120 h, fibroblasts in the argon control group showed slightly higher values than cells in the PAM 1:2 group. Changes were not significant (t120,

Control to PAM 1:2, MD 0.19 ± 0.41 (SEM), p = 0.331). One patient in the PAM 1:2 group possessed remarkably higher relative MMP-2 than the other patients.

As compared to fibroblasts, mesothelial cells showed contrary results 24 h post PAM (*Figure 22B*). Whereas fibroblasts significantly decreased relative MMP-2 per cell, mesothelial cells slightly increased their MMP-2 synthesis. Even though mean value doubled compared to the one of the fibroblasts, no significant changes could be detected due to scattered distribution of values (t24, Control to PAM 1:2, MD 1,2 ± 0.87 (SEM), p = 0.122). After 72 h, mesothelial cells significantly shortened relative MMP-2 production per cell (t72, Control to PAM 1:2, MD 0.64 ± 0.25 (SEM), p = 0.033). Mean value more than halved compared to the control.

In conclusion, PAM treatment led to significantly decreased relative MMP-2 per cell in both cell lines after 72 h. In contrast to increased MMP-2 in mesothelial cells, fibroblasts also possessed significant decreased MMP-2 levels at 24 h post PAM treatment.

3.5 Influence of PAM on cellular components analyzed by Raman microspectroscopy

Raman spectroscopic imaging is a non-invasive method to detect and semi-quantify different molecules like nuclei or specific proteins. Fibroblasts were treated with PAM 1:2, argon served as control. Fibroblasts were cultured five days after PAM treatment before being fixed in 4 % PFA and imaged by marker-independent and contact-free Raman spectroscopy. Identification and comparison of molecular characteristics and cellular components were possible by use of Raman imaging and single spectra extraction.

3.5.1 True Component Analysis (TCA)

Based on the respective fingerprint spectra, Raman imaging and True Component Analysis (TCA) identified and localized the components DNA/nuclei (blue) and proteins (green) (*Figure 23A*). The first identified component was DNA/nuclei and showed peaks at 788 and 1656 cm^{-1} related to O-P-O stretching of DNA/ C_5'-O-P-O-C_3' phosphodiester bands in DNA and T, G, C (ring breathing modes of DNA/RNA bases) (*Figure 23B; Supplementary Table 1*). TCA analysis detected proteins as second component by peaks at 1005, 1088 and 1658 cm^{-1}. Those peaks represent phenylalanine, symmetric PO_2^- stretching of DNA and amide I (protein) (*Figure 23B; Supplementary Table 1*). Further TCA analysis revealed a third component as lipids (*Supplementary Figure 2).*

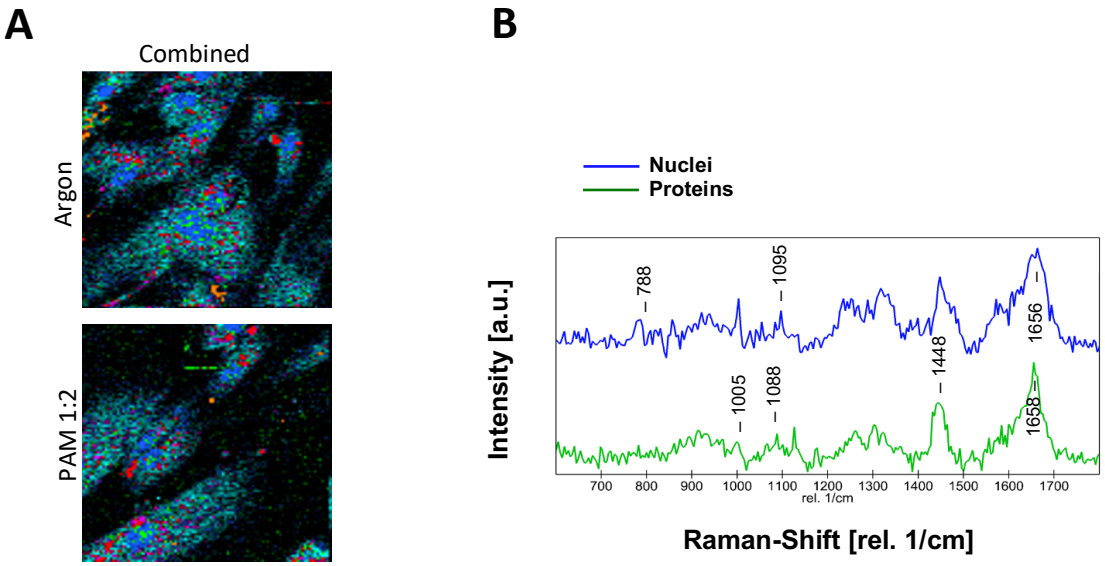

Figure 23. Characteristic spectra of detected molecular structures by Raman imaging. Raman images of fibroblasts. TCA identified nuclei (blue) and proteins (green) (A). The characteristic fingerprint spectra of the respective analyzed components allowed identification of nuclei and protein components (B). Parts of this figure were already published in Rasch, M.-L. and Holl, M. *et al. Effects of non-invasive physical plasma (NIPP) on the ECM and cells responsible for postoperative intraabdominal adhesions.* Biomedicines, **2022**, 10, 927 [1].

3.5.2 Principle Component Analysis (PCA)

For detection of molecular differences between the argon and the PAM treatment group, Principal Component Analysis (PCA) was performed on the extracted single spectra of the nuclei and proteins for each patient (*for PCA of lipids see Supplementary Figure 3).* For the PCA of the nuclei, clustering of both groups could be observed in two of three patients in the PCA scores plot of PC-1 (*Figure 24A-D*). Statistical analysis showed a significant difference in clustering between the argon control group and the PAM 1:2 treatment group in two patients in PC-1 (*Figure 24B and D*). Patient 1 showed negative values in the control group whereas Patient 2 illustrated positive values in this respective group. For the third patient, a significant difference in PC-2 instead of PC-1 could be observed between the respective groups (*Figure 24E and F*). Cells in the argon group indicated negative values whereas the PAM group presented positive ones.

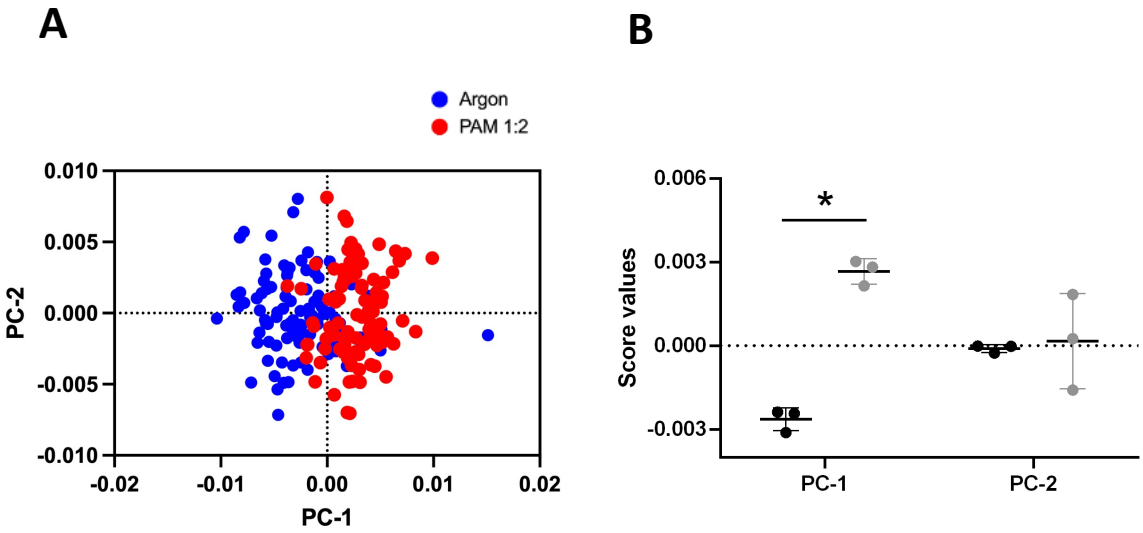

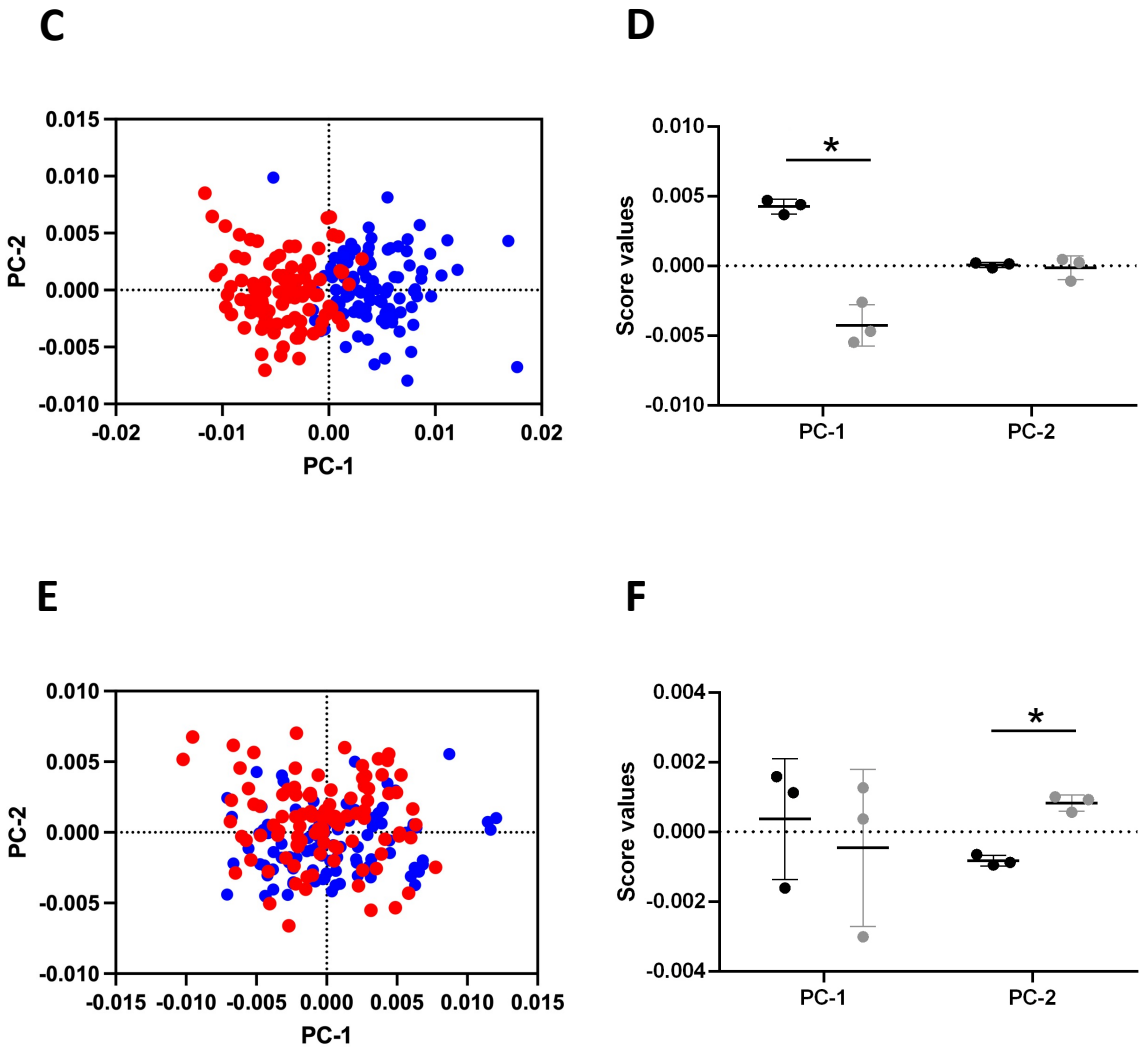

Figure 24. Raman imaging reveals changes in nuclei spectra in fibroblasts. Scores plot of PC-1 vs. PC-2 revealed a trend of clustering between the argon and control group for both patient 1 and 2 (A and C). DNA/nuclei specific average score values indicated significant differences for PC-1 in patient 1 and 2 (B and D). Scores plot of PC-1 vs. PC-2 indicated clustering of groups for 3 (E). DNA/nuclei specific average score values showed significant modifications for PC-2 of patient 3 (F). Data are shown as the mean ± SD, n=3, * $p<0.05$.

As shown in the correlating loadings plot of nuclei-specific PCA, clustering of the groups can be elucidated by peaks at 782 cm^{-1}, 1292 cm^{-1}, 1325 cm^{-1}, 1667 cm^{-1} for patient 1, correlated to changes in DNA, cytosine, CH_3CH_2 wagging mode in purine bases of nucleic acids and C-C stretching bands (*Figure 25A; Supplementary Table 1*). For patient 2, separation of groups can be assigned to peaks at 830 cm^{-1}, 1180 cm^{-1}, 1325 cm^{-1}, 1520 cm^{-1} and 1663 cm^{-1} representing tyrosine, cytosine/guanine, CH_3CH_2 wagging mode in purine bases of nucleic acids, -C=C carotenoid and DNA (*Figure 25C; Supplementary Table 1*). Peaks at 782 cm^{-1}, 826 cm^{-1}, 1071 cm^{-1}, 1239 cm^{-1}, 1259 cm^{-1} and 1508 cm^{-1} in the loadings plot of patient 3 correlated to changes in DNA, O-P-O stretch DNA, symmetric PO_2^- stretching of DNA, amide III, guanine/cytosine (NH_2) and cytosine (*Figure 25E; Supplementary Table 1*).

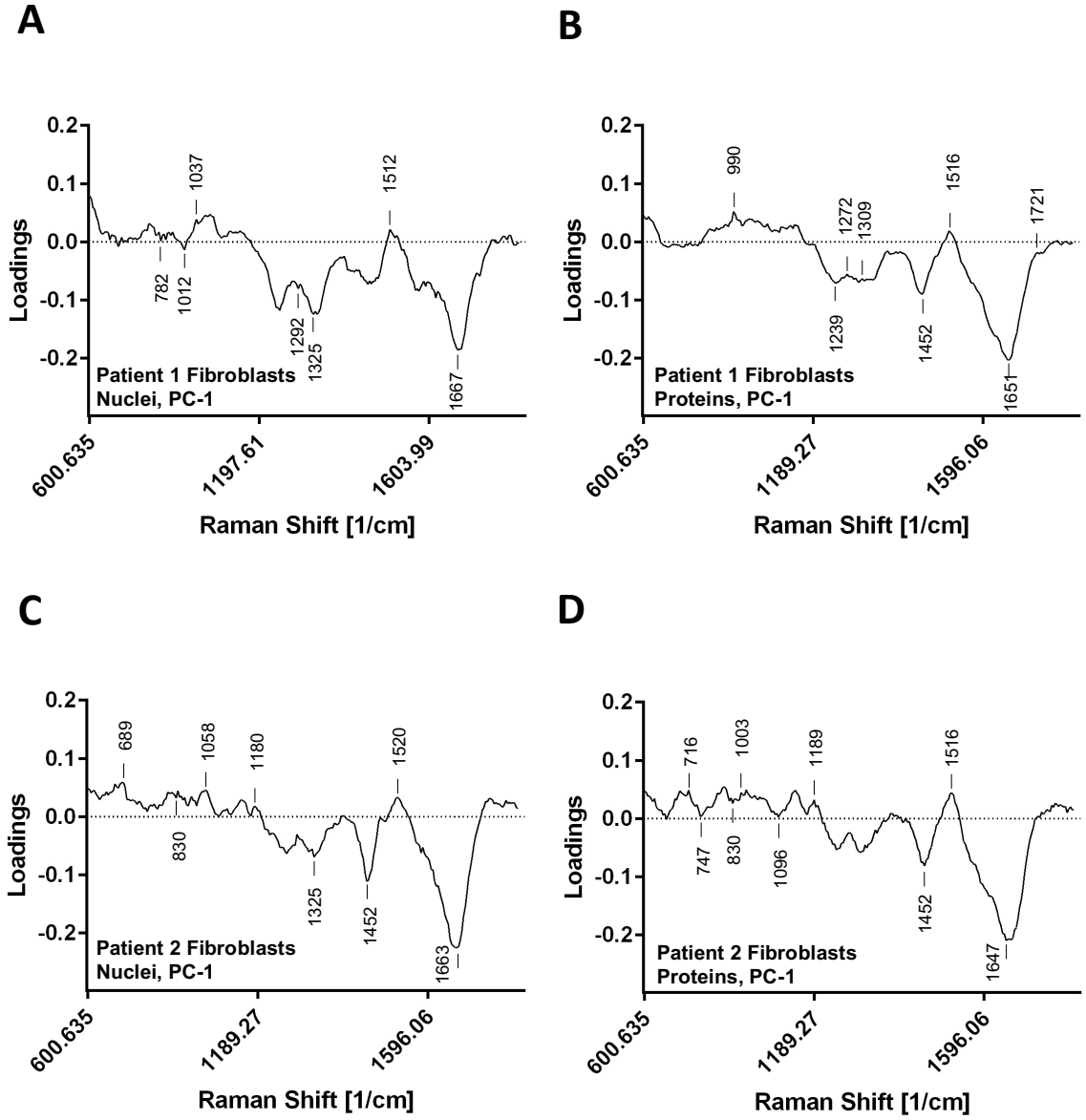

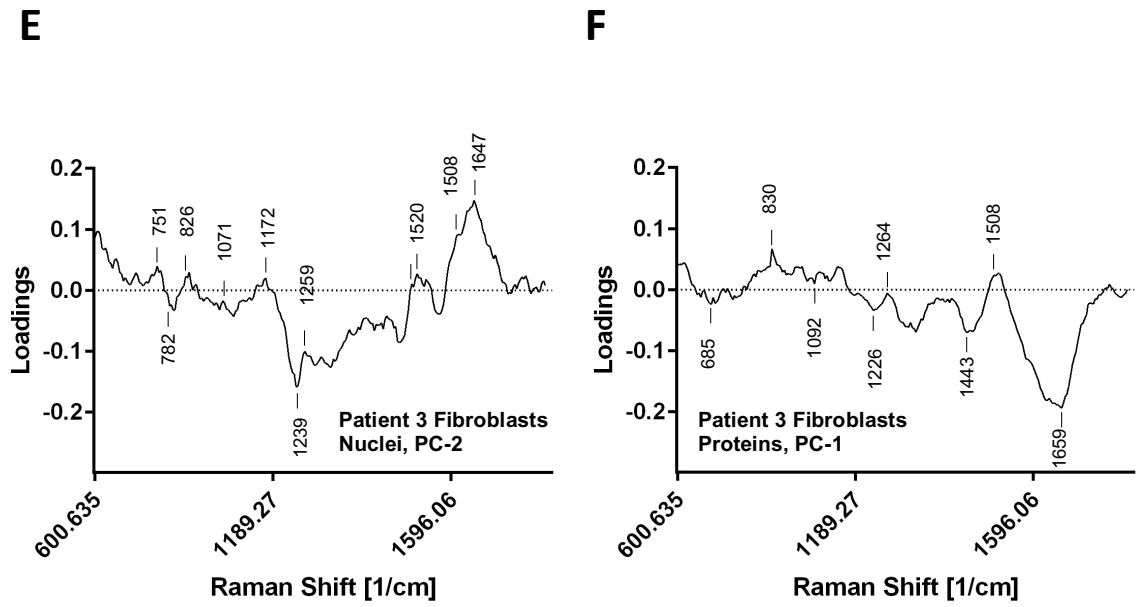

Figure 25. Loadings plots corresponding to specific PCAs of each patient. Corresponding loadings plots of nuclei-specific PCA indicating trend of clustering in PC-1 and of protein-specific PCA explaining trend of separation in PC-1 for patient 1 (A and B). Loadings plots of patient 2 corresponding to nucleic-specific PCA explaining trend of clustering in PC-1 and to protein-specific PCA responsible for trend of clustering in PC-1 (C and D). Corresponding loadings plot of patient 3 of nucleic-specific PCA explaining trend of clustering in PC-2 and of protein-specific PCA explaining trend of separation in PC-1 (E and F).

Similar results could be observed when analyzing the protein spectra. Scores plot of patient 1 revealed the trend of clustering between the different treatment groups. Statistical analysis showed significant differences in both PC-1 and PC-2 (*Figure 26A and B*). Similar findings could be observed after analysis of PC-1 and PC-2 of patient 2 (*Figure 26C and D*). The scores plot showed an even more noticeable trend of clustering of groups. In contrast to the first two patients, an inverse clustering of treatment groups of patient 3 could be observed as argon scored negative values (*Figure 26E and F*). However, separation of groups was only significant in PC-1 (*Figure 26F*).

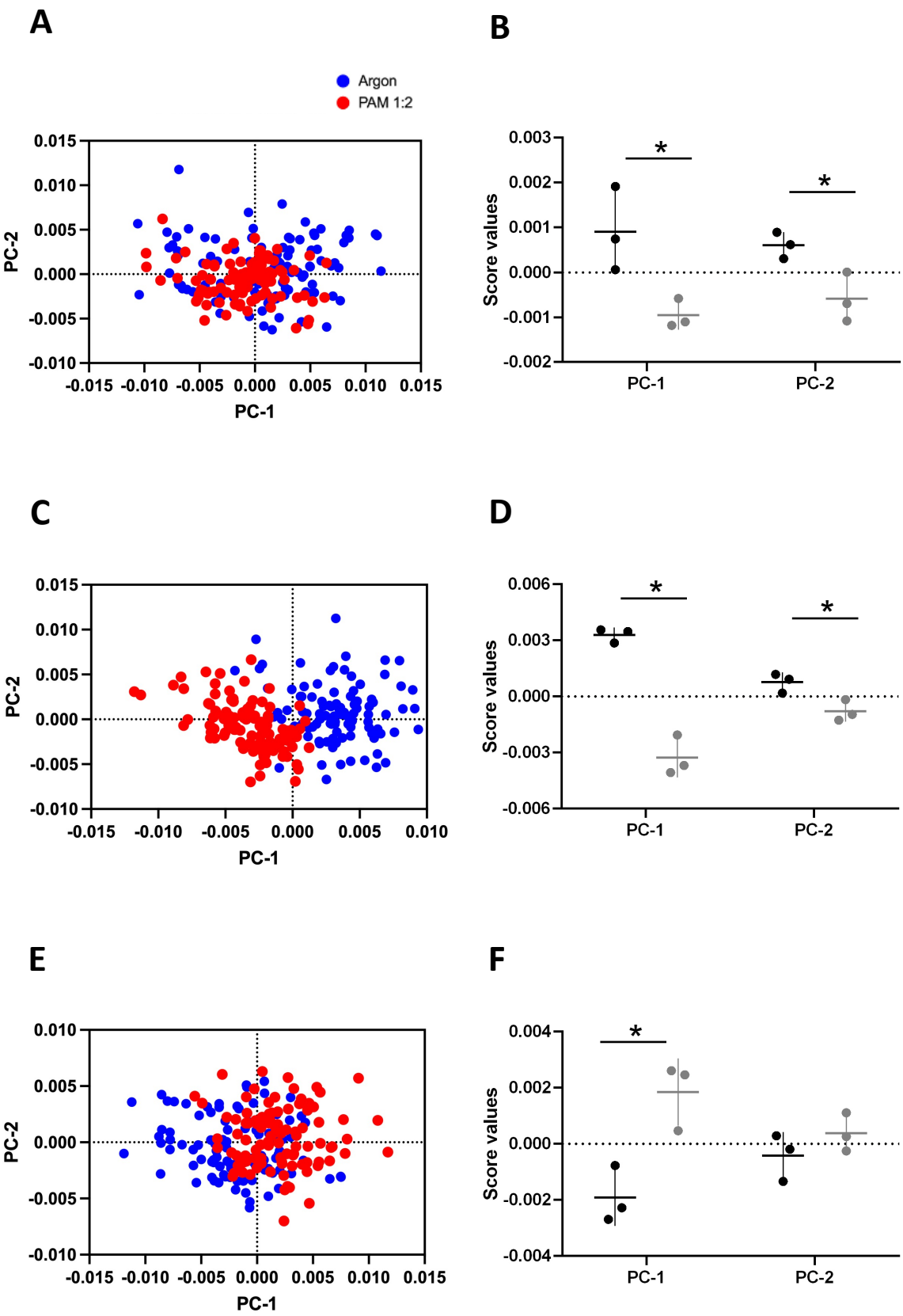
A
Argon
PAM 1:2
PC-2
PC-1
B
Score values
PC-1
PC-2
C
PC-2
PC-1
D
Score values
PC-1
PC-2
E
PC-2
PC-1
F
Score values
PC-1
PC-2

Figure 26. Raman imaging reveals changes in protein spectra in fibroblasts. For both patient 1 and 2, scores plot of PC-1 vs. PC-2 revealed a trend of clustering in the argon and the PAM treatment group (A and C). Protein specific average score values showed significant differences for PC-1 as well as in PC-2 in patient 1 and 2 (B and D). For patient 3, scores plot of PC-1 vs. PC-2 indicated trend of clustering of groups (E). Protein specific average score values showed significant changes in PC-1 of patient 3 (F). Data are shown as the mean ± SD, n=3, * $p<0.05$.

Clustering of groups in patient 1 can be explained by peaks at 1239 cm^{-1}, 1272 cm^{-1}, 1309 cm^{-1}, 1721 cm^{-1} representing amide III, CHα'rocking, CH_3/CH_2 wagging mode of lipid/collagen and C=O (*Figure 25B; Supplementary Table 1*). For patient 2, the loadings plot revealed peaks at 830 cm^{-1}, 1003 cm^{-1}, 1096 cm^{-1}, 1189 cm^{-1} responsible for separation of the argon and PAM treatment group. Peaks are assigned to tyrosine, phenylalanine / C-C skeletal, phosphodioxy (PO_2^- groups) and anti-symmetric phosphate vibrations, explaining the trend of clustering of the groups (*Figure 25D; Supplementary Table 1*). Loadings plot of patient 3 showed peaks at 830 cm^{-1}, 1092 cm^{-1}, 1226 cm^{-1}, 1508 cm^{-1} and 1659 cm^{-1}. Changes in tyrosine, phosphodioxy, anti-symmetric phosphate, cytosine, and amide I (protein) contribute to the trend of separation (*Figure 25F; Supplementary Table 1*).

4. DISCUSSION

Various studies confirmed the effectivity of NIPP in clinical applications. Plasma treatment leads to improved wound healing, has antiproliferative effects and modulates the cell cycle and protein synthesis [23, 30, 35-41]. Plasma activated media and its application has been shown to be as effective as direct plasma treatment [38, 42, 43]. Besides that, studies have shown that NIPP selectively reduces cancer cells [30, 35, 38, 40]. Therefore, NIPP treatment has the potential to serve as a new innovative minimal invasive therapeutical option in different fields of modern medicine. This study aimed to evaluate if PAM has a therapeutical effect on cells responsible for adhesion formation. Since no satisfactory method in the prevention and treatment of postoperative intraperitoneal adhesion is established yet, this study evaluated PAM as a possible application method to prevent the formation of intraperitoneal adhesion [3, 4, 17, 18, 44]. This study reported "*the first application of PAM on human peritoneal tissue*" [1] to anticipate adhesion promoting cell responses. By applying PAM in-vitro, a first proof of concept for the use of PAM as a novel, innovative cell type-specific clinical procedure for the prevention of postoperative or inflammatory intraabdominal adhesions was provided.

Collagen and fibronectin, both particularly synthesized by fibroblasts, play an important part in development of adhesion bands [4]. PAM treatment of fibroblasts reduced cell proliferation and other factors responsible for the adhesion formation process as shown in this study. Other factors contributing to the adhesion formation process like cytokines and matrix metalloproteinases were analyzed as well. Primary isolated cells were exclusively used in this study to display lifelike effects as close as possible. Since fibroblasts were isolated from different patient's peritoneum tissue samples, inter-patient specific differences regarding the results occurred in some extent.

4.1 PAM treatment reduced cell count of fibroblasts

Several studies reported decreased cell proliferation in cancer cells after plasma treatment [36, 45, 46]. In this study, PAM treatment effectively reduced fibroblast cell count. Stronger PAM treatment led to lower cell confluency than weaker treatment. In vivo, this might lead to a lower cell count and therefore fewer active cells in the peritoneal cavity after surgery. On the one hand, less cells would be present and therefore fewer adhesions would be formed. On the other hand, a reduced cell count could be fatal. Injuries require healing processes, induced by cells like fibroblasts and mesothelial cells [4, 5]. By application of strong PAM treatment, physiologically appearing fibroblasts may be reduced to greater extent causing delayed healing processes. Kang and Kim *et al.* investigated non-thermal plasma effects on keloid fibroblasts and compared them to healthy normal fibroblasts [24]. By evaluating the migration potential of the cells, they found that application of non-thermal plasma led to decreased migration of the abnormal keloid fibroblasts but even increased migration of normal fibroblasts. This effect may be found in intraperitoneal fibroblasts as well, but further studies have to be done to distinguish the effect of PAM on cell migration and cell confluency between normal and adhesion fibroblasts. Brun *et al.* exploited the effect of Helium Plasma on human fibroblast-like primary cells. Their results showed increased proliferation and migration of cells after treatment [47]. Reasons for the differences to the results of this present study might be the different choice of gas, origin of cells or concentration of plasma treatment as well as a different kind of plasma application. According to Bourdens *et al.*, dermal fibroblasts were relatively resistant to NIPP mediated cell death, but immediately entered cell cycle arrest and stopped cell proliferation caused by DNA damage [48]. In this study, Raman imaging was performed to detect the impact of PAM treatment on cells in a global context. In addition to the other experiments, Raman imaging was therefore used as a summation method. Analysis of nuclei has shown significant differences between fibroblasts in the control and cells in the plasma treatment group. This finding suggests modifications on a nuclear basis in fibroblasts supporting decreased cell proliferation after treatment. As already stated, further evaluation and comparison of the effect of PAM on peritoneal and adhesion fibroblasts must be done.

PAM treatment was able to induce cell type-specific molecular and cellular responses in treated tissues, leading to preventive anti-adhesive effects. In our publication, selective

PAM effects on fibroblast's gene and cell proliferation were shown. Significant increased double strand breaks in fibroblasts were observed after PAM treatment [1]. Next to DNA damage, cell apoptosis and cycle arrest were detected which were most likely associated with substantial formation of ROS. Reduction of cell confluency therefore might be justified by induction of apoptotic or necrotic effects. However, in this present study it remains unclear whether PAM treatment has a direct cytoreductive effect on fibroblasts or rather reduces fibroblast proliferation, exhibiting a cytostatic effect.

4.2 Extracellular matrix formation was reduced by PAM treatment

Since cells form sufficiently detectable ECM a few days after cultivation, all ECM components were analyzed five days after treatment. Besides examination of the different components after PAM treatment, ECM weight per cell was also assessed. Results showed a significant decrease in the PAM 1:2 group. Adhesion bands mainly consist of ECM components like collagen and fibronectin (*Figure 27A)*. By reducing total ECM expression in fibroblasts, PAM treatment effectively counteracts excessive connective tissue formation (*Figure 27B)*. Consequently, patients with peri- or postoperative PAM treatment would form less adhesion bands after surgery. Complications as well as revision surgeries would then belong to the past in most cases. Raman spectroscopic imaging also demonstrated reduced protein levels after PAM treatment. However, this method was not able to distinguish between intra- and extracellular located proteins. Reduced protein expression can therefore be assigned to either the reduced cell count, to decreased ECM formation, but most likely to both aspects. As ECM weight per cell was decreasing by PAM treatment, the two main components fibronectin and collagen were comprehensively analyzed.

A

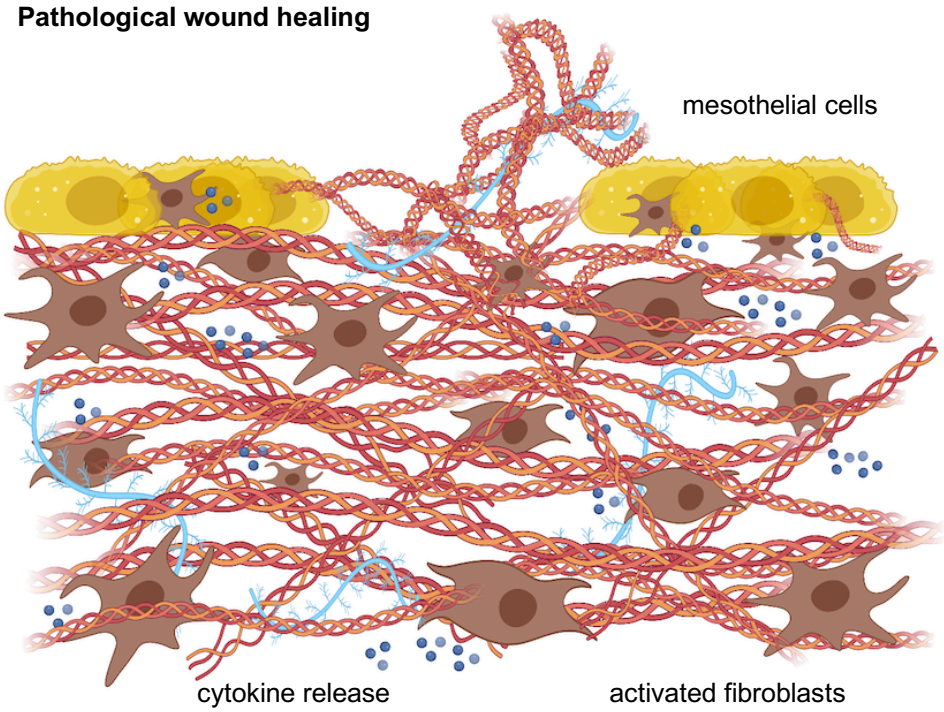
Pathological wound healing
mesothelial cells
cytokine release
activated fibroblasts

B

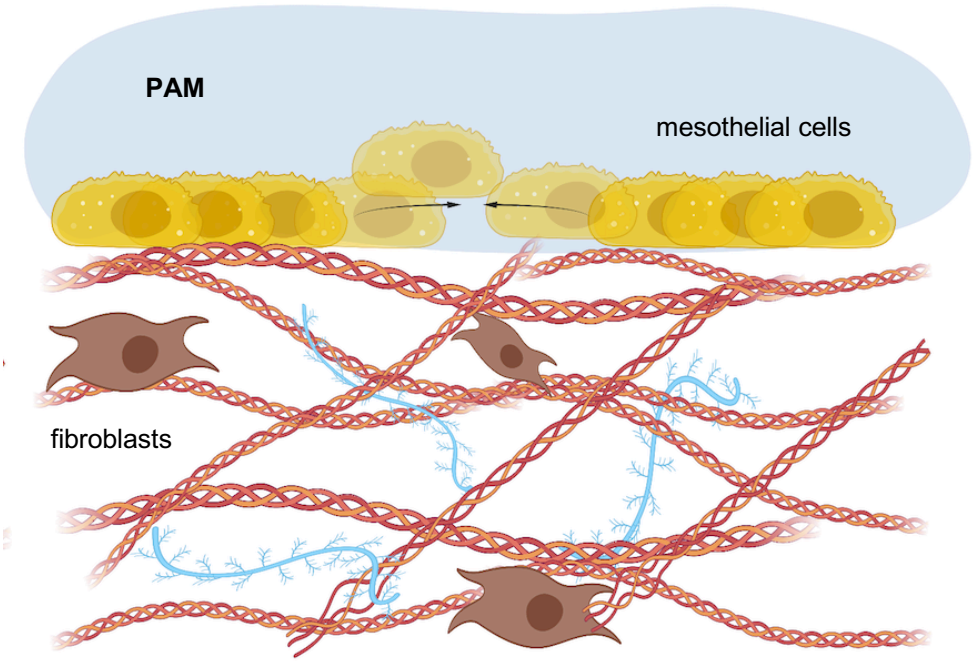
PAM
mesothelial cells
fibroblasts

Figure 27. Predicted impact of PAM treatment on the peritoneal cavity. Without treatment, hyperproliferation of components of the extracellular matrix occur, leading to pathological wound healing and adhesion formation. By treating the peritoneal cavity with PAM, excessive ECM built up can be prevented. This figure was already published in Rasch, M.-L. and Holl, M. *et al., Effects of non-invasive physical plasma (NIPP) on the ECM and cells responsible for postoperative intraabdominal adhesions.* Biomedicines, **2022**, 10, 927 [1]. Created with BioRender.com.

Interestingly, relative soluble collagen content per cell was rising through PAM treatment but relative collagen expression was decreasing. Results of non-invasive Raman spectroscopic imaging confirmed a modification of collagen in fibroblasts after PAM treatment (*see Supplementary Figure 1*). Shi Xingmin *et al.* confirmed the finding of decreased collagen production in fibroblasts after stronger plasma treatment [49]. In contrast to the results concerning the total or soluble collagen expression, the intracellular collagen content in fibroblasts did not differ between the different treatment groups. Therefore, processes which lead to the reduced total collagen expression occur in the extracellular environment.

In the process of collagen deposition several enzymes are involved, such as endopeptidases and matrix metalloproteinases. PAM may interfere with the mechanism of transforming soluble collagen into an insoluble state and therefore be responsible for the contrary results. As an explanatory approach, the process of the formation of collagen fibrils might be disturbed. By cleaving the N and C terminus, several endopeptidases transform the pro-collagen into collagen which can then be arranged into collagen fibrils [50]. When those enzymes would be inhibited through PAM species like reactive oxygen species, higher elevated soluble collagen levels but lower total collagen levels would be detected. Another explanatory approach might be the modification of matrix metalloproteinases after PAM treatment. In this study we examined MMP-1 and MMP-2 levels in fibroblasts and mesothelial cells. MMP-1 belongs to the collagenase family and cleaves collagen-I, II and III [51, 52]. According to several studies, MMP levels were shown to be significantly elevated in adhesion fibroblasts [4, 53]. No modification of MMP-1 levels in fibroblasts was observed at 24 h or 120 h after PAM treatment. At 72 h, MMP-1 levels notably but not significantly decreased after PAM treatment. This finding

might contribute to reduced collagen degradation and might be an explanatory approach of elevated soluble collagen values measured in this study. On the other hand, the decrease in MMP-1 was small and not significant whereas soluble collagen showed a clearly significant increase. It remains unclear whether the discrepancy might be explained by the MMP-1 theory alone. Furthermore, it should be evaluated whether in vitro injured fibroblasts will also show decreased MMP-1 values after PAM treatment as normal fibroblasts did in this study. In contrast to slightly decreasing levels in fibroblasts, MMP-1 levels in mesothelial cells were notably rising 72 h after treatment. This finding may contribute to improved cell migration of the cells into the wound after intraoperative PAM treatment. Studies have shown the importance of MMP-1 as well as of MMP-2 in the cell migration process of several cells [54]. The combination of decreased MMP-1 levels in fibroblasts and increased levels in mesothelial cells leads to the assumption of an improved and physiological wound healing process without excessive collagen band formation after application of PAM treatment. Besides its impact on cell migration, MMP-2 (gelatinase-1) is also responsible for cleaving fibronectin, collagen IV and elastin [55]. Additionally, an increase in MMP-2 also leads to promoted angiogenesis [56]. Even though gelatinase-1 is involved in the ECM degradation, elevated levels can somehow be found in adhesions [55]. By cleaving collagen IV, part of the basement membrane, fibrosis and adhesion formation are promoted [57]. Some studies even imply a role of MMP-2 levels as adhesion marker [58]. As fibroblasts are mainly responsible for collagen synthesis, the findings of significantly reduced MMP-2 levels after treatment indicate less adhesion formation. Cleavage of the basement membrane of fibroblasts is minimized, reducing fibroblast migration, and the risk of fibrosis shortened.

As stated, the discrepancy between lowered total collagen amounts and enhanced soluble collagen levels, may be explained by changed MMP levels. Furthermore, expression of other enzymes which were not evaluated in this study may contribute to this finding. On one hand, slightly reduced MMP-1 levels in fibroblasts 72 h after treatment may lead to less collagen cleaving and therefore elevated soluble collagen levels. On the other hand, inhibition of MMP-2 may result in less collagen IV depletion and therefore to a reduced total collagen expression. Also, endopeptidases activity might be restrained due to plasma treatment and therefore total collagen formation may be limited.

Fibronectin is another major component of the ECM and therefore another important part of adhesion bands. Despite decreased collagen formation, analysis has shown a significant decrease in relative fibronectin production per cell after PAM treatment. No significant differences between the various PAM dosages could be detected. Following PAM treatment *in vivo*, fibroblasts in the intraperitoneal cavity therefore might not form sufficiently stable adhesion bands and the risk of development of intestinal bowel obstruction or chronic pain conditions could be minimized. It has been shown that fibronectin and its polymerization are essential for ECM stability and composition [11, 59-61]. By reducing fibronectin expression, amounts of newly formed ECM will decrease as the matrix becomes unstable. Therefore, adhesion bands would lack stability as well and its formation and maintenance will be reduced. Besides that, already formed fibronectin networks require continuous fibronectin synthesis to impede their degradation [62]. Since PAM inhibits fibronectin expression, the network will not be maintained or further built-up. Moreover, fibronectin is also required for attachment of additional cells [62]. Cells like fibroblasts will not be able to sufficiently attach to the fibronectin network and therefore synthesis of further ECM components will be diminished.

4.3 Cytokine levels were differently altered by PAM treatment

Various cytokines have been shown to be involved in the adhesion formation process. Especially TGF-beta possesses pro-adhesiogenic properties [4, 63, 64]. PAM treatment effectively reduced TGF-beta-1 levels in fibroblasts. The cytokine is acting in a pro-adhesiogenic manner by elevating collagen synthesis, stimulating ECM formation and angiogenesis [4, 5, 9, 63]. Furthermore, elevated levels of the cytokine were detected in adhesion tissue [4, 64]. Analysis 24 h after PAM treatment showed a significant decrease in relative TGF-beta per cell as a response to cellular stress and damage in fibroblasts. Hereby, PAM affects another mechanism related to elevated postoperative collagen synthesis. By performing a scratch on the fibroblast monolayer before PAM treatment, peritoneal injury was mimicked. Therefore, the significant decrease in TGF-beta-1 implies an even more meaningful impact on PAM as an option for the avoidance of postoperative adhesion formation. Kang and Kim *et al.* found that plasma treatment decreased collagen production in keloid fibroblasts by a reduction of TGF-beta but had no effect on normal fibroblasts [24]. Elevated TGF-beta led to increased collagen synthesis in keloid fibroblasts. By only affecting the abnormal fibroblasts in the skin, intraperitoneal PAM treatment might have the same effect on peritoneal fibroblasts. By that, excessive collagen deposition by modified injured fibroblasts could be decreased as well and the normal fibroblasts could contribute to the physiological wound healing process. The experimental design and the findings of the present study correlate to the results of Kang and Kim *et al*. In contrast, healthy fibroblasts reacted with increased TGF-beta synthesis, improving wound healing processes, as shown in Arndt *et al.* [65]. This again shows that a precise distinction between plasma effects on healthy and on adhesion associated fibroblasts is essential.

Besides TGF-beta-1, several other cytokines are involved in the adhesion formation process. Right after a peritoneal injury, elevated levels of IL-1 and TNF-alpha can be found around the injury [4, 66]. Strong PAM 1:2 treatment effectively reduced subtype IL-1b levels after a stimulated injury through scratch application. Since IL-1 acts as a pro inflammatory cytokine and is especially synthesized by injured cells, PAM treatment might effectively reduce overshooting immune reactions and adhesion formation. Various studies confirmed that collagen synthesis is modified through IL-1b but are discordant whether it lowers or rises the amount of collagen [67-71]. In addition, IL-1b

might stimulate the epithelial-mesenchymal-transition (EMT) of mesothelial cells into fibroblasts [4, 72]. By reducing IL-1b levels through stronger PAM, the treatment may lead to a reduced inflammatory environment. EMT of mesothelial cells could be inhibited as well. Therefore, less fibroblasts and transformed mesothelial cells would be present in the peritoneal cavity after surgery leading to less adhesion formation.

Several other cytokines being measured in this study did not show any changes in their respective levels after PAM treatment. Besides IL-1b, other pro-inflammatory acting cytokines were evaluated. TNF-alpha or INF-gamma were not significantly altered by plasma application but showed the trend of a slight decrease after treatment. Both cytokines can be found in elevated levels in the peritoneal fluid of patients with adhesion formation [4, 73, 74]. The present study only evaluated fibroblast levels up to 24 h after plasma treatment, therefore evaluation of cytokine levels over a prolonged period may show even more significant changes in PAM 1:2 treatment group.

Macrophages and granulocytes are also present in the abdominal cavity after surgical procedures. Higher levels lead to increased inflammatory responses and therefore to elevated adhesion formation [4, 75]. This study investigated their growth stimulating factors, GM-CSF for both macrophages and granulocytes and M-CSF for macrophages only. Plasma treatment significantly decreased GM-CSF but not M-CSF. This finding is leading to the assumption of a lowered macrophage and granulocyte count in the peritoneal cavity after plasma treatment. Since GM-CSF both influences macrophage and granulocyte differentiation beside its pro-inflammatory properties [76, 77], the non-plasma responding behavior of M-CSF is negligible when relating to the anti-adhesiogenic effects of the treatment.

Since angiogenesis is an essential factor in the establishment of adhesions, angiogenesis promoting factors such as IL-8 and VEGF were inspected. Neither of them presented changed levels after plasma treatment. Various studies reported elevated levels of VEGF in patients with postoperative intraabdominal adhesions [4]. By demonstrating reduced adhesion formation after anti-VEGF therapy, the importance of this cytokine in the adhesion formation process was accentuated [78-80]. IL-8 has one of the greatest pro-angiogenetic effects on endothelial cells which can also be found in tumor diseases [81, 82]. Besides that, IL-8 acts as a chemokine, attracting even more pro-inflammatory cells

of the innate immune system, such as neutrophils and macrophages [5]. Unfortunately, plasma treatment did not alter levels of any examined angiogenesis promoting factor in this study. Nonetheless, plasma application effectively reduced important ECM components such as collagen and fibronectin. Without these two most important adhesiogenic components, angiogenesis only plays a subordinate part in the adhesion formation process.

4.4 Conclusion and clinical significance

In the present study, PAM was applicated on human peritoneal tissue to study the prevention of pro-adhesive cell responses. Significant decreases of several components being involved in the adhesion formation process were found after PAM treatment. ECM components like collagen and fibronectin were significantly reduced after treatment. These findings may predict that the application of PAM is an effective method in the prevention of postoperative intraabdominal adhesions. PAM may be applicated intraperitoneally at the end of surgery before skin suture to minimize complications provoked by adhesion bands. Up to date, no sufficient methods in preventing the adhesion formation after surgery is available yet. In conclusion, PAM could be routinely incorporated into surgical procedures across the board for effective adhesion prophylaxis.

5. SUMMARY

Postoperative intraabdominal adhesions remain a serious problem in many surgical specialties responsible for a variety of serious and partly even life-threatening clinical disorders. Several approaches in prevention and treatment have been made but with no clear clinical benefits. Administration of plasma activated media (PAM) represents a promising treatment option. In this study, the effect of PAM on cells and components responsible for increased adhesion formation was evaluated. Two main components of the extracellular matrix (ECM) – collagen and fibronectin – are mainly synthesized by fibroblasts and represent two main parts in adhesion formation. By PAM treatment of primarily isolated fibroblasts, antiproliferative effects and modification of the above-mentioned ECM components were detected. Significant decreased hydroxyproline after PAM treatment indicated a reduced collagen synthesis. Fibronectin was also significantly reduced after treatment. Playing part in the ECM transformation and degradation process, type 1 and 2 matrix metalloproteinases (MMP) were examined as well. Changes were detected in both MMP-1 and MMP-2 after PAM treatment. Modifications in proteins as well as in lipids and the DNA of fibroblasts were observed by contactless and marker independent Raman microspectroscopy.

Various pro- as well as anti-inflammatory cytokines modulate adhesiogenesis. PAM treatment efficiently reduced extracellular TGF-beta levels - a cytokine with pro-inflammatory and pro-adhesiogenic properties.

The interaction of anti-proliferative properties, decreased expression of essential ECM-components and the reduction of pro-inflammatory cytokines might enable a targeted anti-adhesiogenic intraoperative tissue treatment. In conclusion, PAM outlines a promising method for prevention and treatment of postoperative intraabdominal adhesions and other inflammatory diseases.

ZUSAMMENFASSUNG

Intraabdominelle postoperative Adhäsionen stellen weiterhin ein großes Problem in den chirurgischen Fächern der Medizin dar, da sie für eine große Anzahl an ernstzunehmenden und teils auch lebensbedrohlichen Erkrankungen verantwortlich sind. Die bisher verfügbaren Ansätze zur Prävention und Behandlung haben keinen klinisch durchschlagenden Erfolg gebracht. Der Einsatz von Plasma-aktivierten Medien (PAM) stellt hierbei eine vielversprechende Methode dar. In dieser Arbeit wurde der Effekt von PAM auf Zellen und zelluläre Faktoren untersucht, welche für die Entstehung von Adhäsionen verantwortlich sind. Zwei Hauptkomponenten extrazellulärer Matrix (ECM) – Fibronektin und Kollagen – werden insbesondere von Fibroblasten synthetisiert und stellen zwei Hauptbestandteile in der Adhäsionsentstehung dar. PAM-Behandlung von primär-isolierten Fibroblasten führte zu anti-proliferativen Effekten und Änderung der Expression o.g. ECM-Faktoren. Durch die Detektion einer signifikanten Verringerung von Hydroxyprolin durch PAM, konnte auf eine verminderte Kollagen-Synthese rückgeschlossen werden. Auch Fibronektin wurde nach PAM-Behandlung signifikant vermindert nachgewiesen. Typ 1 und 2 Matrixmetalloproteinasen (MMP) spielen eine wichtige Rolle bei der Umwandlung und dem Abbau von ECM und wurden durch die PAM-Behandlung signifikant in ihrer Funktion beeinflusst. Durch kontaktlose und Marker-unabhängige Raman-Mikrospektroskopie wurden Veränderungen von Proteinen als auch von Lipiden und der DNA in Fibroblasten detektiert.

Pro- und antiinflammatorische Zytokine spielen eine wesentliche regulatorische Rolle in der Adhäsiogenese. PAM-Behandlung reduzierte die extrazellulären Level von TGF-beta, ein Zytokin mit sowohl proinflammatorischen als auch pro-adhäsiogenen Eigenschaften.

Das Zusammenspiel von antiproliferativen Eigenschaften, der verminderten Expression von essenziellen ECM-Bestandteilen und der Reduktion pro-inflammatorischer Zytokine könnte eine zielgerichtete anti-adhäsiogene intraoperative Gewebebehandlung ermöglichen. Zusammengefasst stellt die Behandlung mit PAM daher eine aussichtsreiche Methode zur Prävention und Behandlung von postoperativen Adhäsionen und anderen inflammatorischen Erkrankungen dar.

6. REFERENCES

1. *Holl, M.; *Rasch, M.-L.; Becker, L.; Keller, A.-L.; Schulze-Rhonhoff, L.; Ruoff, F.; Templin, M.; Keller, S.; Neis, F.; Keßler, F.; Andress, J.; Bachmann, C.; Krämer, B.; Schenke-Layland, K.; Brucker, S.Y.; Marzi, J.; Weiss, M., *Cell Type-Specific Anti-Adhesion Properties of Peritoneal Cell Treatment with Plasma-Activated Media (PAM).* Biomedicines, 2022. **10**.
2. Ellis, H., B.J. Moran, J.N. Thompson, M.C. Parker, M.S. Wilson, D. Menzies, A. McGuire, A.M. Lower, R.J. Hawthorn, F. O'Brien, S. Buchan, and A.M. Crowe, *Adhesion-related hospital readmissions after abdominal and pelvic surgery: a retrospective cohort study.* Lancet, 1999. **353**(9163): p. 1476-80.
3. Practice Committee of American Society for Reproductive Medicine in collaboration with Society of Reproductive, S., *Pathogenesis, consequences, and control of peritoneal adhesions in gynecologic surgery: a committee opinion.* Fertil Steril, 2013. **99**(6): p. 1550-5.
4. Beyene, R.T., S.L. Kavalukas, and A. Barbul, *Intra-abdominal adhesions: Anatomy, physiology, pathophysiology, and treatment.* Curr Probl Surg, 2015. **52**(7): p. 271-319.
5. Cheong, Y.C., S.M. Laird, T.C. Li, J.B. Shelton, W.L. Ledger, and I.D. Cooke, *Peritoneal healing and adhesion formation/reformation.* Hum Reprod Update, 2001. **7**(6): p. 556-66.
6. van Baal, J.O.A.M., K.K. Van de Vijver, R. Nieuwland, C.J.F. van Noorden, W.J. van Driel, A. Sturk, G.G. Kenter, L.G. Rikkert, and C.A.R. Lok, *The histophysiology and pathophysiology of the peritoneum.* Tissue and Cell, 2017. **49**(1): p. 95-105.
7. Ritsu, M., K. Kawakami, E. Kanno, H. Tanno, K. Ishii, Y. Imai, R. Maruyama, and M. Tachi, *Critical role of tumor necrosis factor-α in the early process of wound healing in skin.* Journal of Dermatology & Dermatologic Surgery, 2017. **21**(1): p. 14-19.
8. Mori, H., M. Sawairi, M. Nakagawa, N. Itoh, K. Wada, and T. Tamaya, *Expression of interleukin-1 (IL-1) beta messenger ribonucleic acid (mRNA) and IL-1 receptor antagonist mRNA in peritoneal macrophages from patients with endometriosis.* Fertil Steril, 1992. **57**(3): p. 535-42.
9. Ambler, D.R., A.M. Golden, J.S. Gell, G.M. Saed, D.J. Carey, and M.P. Diamond, *Microarray expression profiling in adhesion and normal peritoneal tissues.* Fertil Steril, 2012. **97**(5): p. 1158-64 e1-4.
10. diZerega, G.S. and J.D. Campeau, *Peritoneal repair and post-surgical adhesion formation.* Hum Reprod Update, 2001. **7**(6): p. 547-55.
11. Lenselink, E.A., *Role of fibronectin in normal wound healing.* Int Wound J, 2015. **12**(3): p. 313-6.
12. Gelse, K., *Collagens—structure, function, and biosynthesis.* Advanced Drug Delivery Reviews, 2003. **55**(12): p. 1531-1546.
13. Xu, S., H. Xu, W. Wang, S. Li, H. Li, T. Li, W. Zhang, X. Yu, and L. Liu, *The role of collagen in cancer: from bench to bedside.* Journal of Translational Medicine, 2019. **17**(1).
14. Cissell, D.D., J.M. Link, J.C. Hu, and K.A. Athanasiou, *A Modified Hydroxyproline Assay Based on Hydrochloric Acid in Ehrlich's Solution*

Accurately Measures Tissue Collagen Content. Tissue Engineering Part C: Methods, 2017. **23**(4): p. 243-250.
15. Caley, M.P., V.L. Martins, and E.A. O'Toole, *Metalloproteinases and Wound Healing.* Adv Wound Care (New Rochelle), 2015. **4**(4): p. 225-234.
16. Rajab, T.K., K.O. Kimonis, E. Ali, A.C. Offodile, 2nd, M. Brady, and R. Bleday, *Practical implications of postoperative adhesions for preoperative consent and operative technique.* Int J Surg, 2013. **11**(9): p. 753-6.
17. De Wilde, R.L., *Postoperative abdominal adhesions and their prevention in gynaecological surgery. Expert consensus position.* Gynecol Surg, 2007. **4**: p. 161–168.
18. Liakakos, T., N. Thomakos, P.M. Fine, C. Dervenis, and R.L. Young, *Peritoneal adhesions: etiology, pathophysiology, and clinical significance. Recent advances in prevention and management.* Dig Surg, 2001. **18**(4): p. 260-73.
19. Souza, L.B.d., J.I.d.S. Silva, L. Bagne, A.T. Pereira, M.A.d. Oliveira, B.B. Lopes, M.E.C.d. Amaral, A.A. de Aro, M.A.M. Esquisatto, G.M.T.d. Santos, and T.A.M.d. Andrade, *Argon Atmospheric Plasma Treatment Promotes Burn Healing by Stimulating Inflammation and Controlling the Redox State.* Inflammation, 2020. **43**(6): p. 2357-2371.
20. Heinlin, J., G. Isbary, W. Stolz, G. Morfill, M. Landthaler, T. Shimizu, B. Steffes, T. Nosenko, J.L. Zimmermann, and S. Karrer, *Plasma applications in medicine with a special focus on dermatology.* Journal of the European Academy of Dermatology and Venereology, 2011. **25**(1): p. 1-11.
21. Nehra, V., A. Kumar, and H.K. Dwivedi, *Atmospheric Non-Thermal Plasma Sources.* International Journal of Engineering, 2008. **2**(1): p. 53-68.
22. Yan, D., J.H. Sherman, and M. Keidar, *Cold atmospheric plasma, a novel promising anti-cancer treatment modality.* Oncotarget, 2017. **8**(9): p. 15977-15995.
23. Kim, S.J. and T.H. Chung, *Cold atmospheric plasma jet-generated RONS and their selective effects on normal and carcinoma cells.* Sci Rep, 2016. **6**: p. 20332.
24. Kang, S.U., Y.S. Kim, Y.E. Kim, J.K. Park, Y.S. Lee, H.Y. Kang, J.W. Jang, J.B. Ryeo, Y. Lee, Y.S. Shin, and C.H. Kim, *Opposite effects of non-thermal plasma on cell migration and collagen production in keloid and normal fibroblasts.* PLoS One, 2017. **12**(11): p. e0187978.
25. Arndt, S., M. Landthaler, J.L. Zimmermann, P. Unger, E. Wacker, T. Shimizu, Y.F. Li, G.E. Morfill, A.K. Bosserhoff, and S. Karrer, *Effects of cold atmospheric plasma (CAP) on ss-defensins, inflammatory cytokines, and apoptosis-related molecules in keratinocytes in vitro and in vivo.* PLoS One, 2015. **10**(3): p. e0120041.
26. Gan, L., J. Jiang, J.W. Duan, X.J.Z. Wu, S. Zhang, X.R. Duan, J.Q. Song, and H.X. Chen, *Cold atmospheric plasma applications in dermatology: A systematic review.* J Biophotonics, 2021. **14**(3): p. e202000415.
27. Weltmann, K.D., Kindel, E., Brandenburg, R., Meyer, C., Bussiahn, R., Wilke, C., and von Woedtke, T., *Atmospheric Pressure Plasma Jet for Medical Therapy: Plasma Parameters and Risk Estimation.* Contrib. Plasma Phys, 2009. **49**(No.9): p. 631 – 640.
28. Weiss, M., J. Barz, M. Ackermann, R. Utz, A. Ghoul, K.D. Weltmann, M.B. Stope, D. Wallwiener, K. Schenke-Layland, C. Oehr, S. Brucker, and P. Loskill, *Dose-Dependent Tissue-Level Characterization of a Medical Atmospheric*

Pressure Argon Plasma Jet. ACS Appl Mater Interfaces, 2019. **11**(22): p. 19841-19853.
29. Gay-Mimbrera, J., M.C. Garcia, B. Isla-Tejera, A. Rodero-Serrano, A.V. Garcia-Nieto, and J. Ruano, *Clinical and Biological Principles of Cold Atmospheric Plasma Application in Skin Cancer.* Adv Ther, 2016. **33**(6): p. 894-909.
30. Utsumi, F., H. Kajiyama, K. Nakamura, H. Tanaka, M. Hori, and F. Kikkawa, *Selective cytotoxicity of indirect nonequilibrium atmospheric pressure plasma against ovarian clear-cell carcinoma.* Springerplus, 2014. **3**: p. 398.
31. Holl, M., L. Becker, A.L. Keller, N. Feuerer, J. Marzi, D.A. Carvajal Berrio, P. Jakubowski, F. Neis, J. Pauluschke-Frohlich, S.Y. Brucker, K. Schenke-Layland, B. Kramer, and M. Weiss, *Laparoscopic Peritoneal Wash Cytology-Derived Primary Human Mesothelial Cells for In Vitro Cell Culture and Simulation of Human Peritoneum.* Biomedicines, 2021. **9**(2).
32. Capella-Monsonís, H., J.Q. Coentro, V. Graceffa, Z. Wu, and D.I. Zeugolis, *An experimental toolbox for characterization of mammalian collagen type I in biological specimens.* Nature Protocols, 2018. **13**(3): p. 507-529.
33. Keller, S., A. Liedek, D. Shendi, M. Bach, G.E.M. Tovar, P.J. Kluger, and A. Southan, *Eclectic characterisation of chemically modified cell-derived matrices obtained by metabolic glycoengineering and re-assessment of commonly used methods.* RSC Advances, 2020. **10**(58): p. 35273-35286.
34. Keller, S., K. Wörgötter, A. Liedek, P.J. Kluger, M. Bach, G.E.M. Tovar, and A. Southan, *Azide-Functional Extracellular Matrix Coatings as a Bioactive Platform for Bioconjugation.* ACS Applied Materials & Interfaces, 2020. **12**(24): p. 26868-26879.
35. Weiss, M., D. Gumbel, N. Gelbrich, L.O. Brandenburg, R. Mandelkow, U. Zimmermann, P. Ziegler, M. Burchardt, and M.B. Stope, *Inhibition of Cell Growth of the Prostate Cancer Cell Model LNCaP by Cold Atmospheric Plasma.* In Vivo, 2015. **29**(5): p. 611-6.
36. Schneider, C., S. Arndt, J.L. Zimmermann, Y. Li, S. Karrer, and A.K. Bosserhoff, *Cold atmospheric plasma treatment inhibits growth in colorectal cancer cells.* Biol Chem, 2018. **400**(1): p. 111-122.
37. Partecke, L.I., K. Evert, J. Haugk, F. Doering, L. Normann, S. Diedrich, F.U. Weiss, M. Evert, N.O. Huebner, C. Guenther, C.D. Heidecke, A. Kramer, R. Bussiahn, K.D. Weltmann, O. Pati, C. Bender, and W. von Bernstorff, *Tissue tolerable plasma (TTP) induces apoptosis in pancreatic cancer cells in vitro and in vivo.* BMC Cancer, 2012. **12**: p. 473.
38. Koensgen, D., I. Besic, D. Gumbel, A. Kaul, M. Weiss, K. Diesing, A. Kramer, S. Bekeschus, A. Mustea, and M.B. Stope, *Cold Atmospheric Plasma (CAP) and CAP-Stimulated Cell Culture Media Suppress Ovarian Cancer Cell Growth - A Putative Treatment Option in Ovarian Cancer Therapy.* Anticancer Res, 2017. **37**(12): p. 6739-6744.
39. Haertel, B., K. Wende, T. von Woedtke, K.D. Weltmann, and U. Lindequist, *Non-thermal atmospheric-pressure plasma can influence cell adhesion molecules on HaCaT-keratinocytes.* Exp Dermatol, 2011. **20**(3): p. 282-4.
40. Arndt, S., E. Wacker, Y.F. Li, T. Shimizu, H.M. Thomas, G.E. Morfill, S. Karrer, J.L. Zimmermann, and A.K. Bosserhoff, *Cold atmospheric plasma, a new strategy to induce senescence in melanoma cells.* Exp Dermatol, 2013. **22**(4): p. 284-9.

41. Xu, D., X. Luo, Y. Xu, Q. Cui, Y. Yang, D. Liu, H. Chen, and M.G. Kong, *The effects of cold atmospheric plasma on cell adhesion, differentiation, migration, apoptosis and drug sensitivity of multiple myeloma.* Biochem Biophys Res Commun, 2016. **473**(4): p. 1125-1132.
42. Tanaka, H. and M. Hori, *Medical applications of non-thermal atmospheric pressure plasma.* J Clin Biochem Nutr, 2017. **60**(1): p. 29-32.
43. Mohades, S., N. Barekzi, and M. Laroussi, *Efficacy of Low Temperature Plasma against SCaBER Cancer Cells.* Plasma Processes and Polymers, 2014. **11**(12): p. 1150-1155.
44. Brochhausen, C., V.H. Schmitt, C.N. Planck, T.K. Rajab, D. Hollemann, C. Tapprich, B. Kramer, C. Wallwiener, H. Hierlemann, R. Zehbe, H. Planck, and C.J. Kirkpatrick, *Current strategies and future perspectives for intraperitoneal adhesion prevention.* J Gastrointest Surg, 2012. **16**(6): p. 1256-74.
45. Lee, S., H. Lee, H. Bae, E.H. Choi, and S.J. Kim, *Epigenetic silencing of miR-19a-3p by cold atmospheric plasma contributes to proliferation inhibition of the MCF-7 breast cancer cell.* Sci Rep, 2016. **6**: p. 30005.
46. Xu, S., Y. Wang, Y. Que, C. Ma, S. Cai, H. Wang, X. Yang, C. Yang, C. Cheng, G. Zhao, and Y. Hu, *Cold atmospheric plasmaactivated Ringer's solution inhibits the proliferation of osteosarcoma cells through the mitochondrial apoptosis pathway.* Oncol Rep, 2020. **43**(5): p. 1683-1691.
47. Brun, P., S. Pathak, I. Castagliuolo, G. Palu, P. Brun, M. Zuin, R. Cavazzana, and E. Martines, *Helium generated cold plasma finely regulates activation of human fibroblast-like primary cells.* PLoS One, 2014. **9**(8): p. e104397.
48. Bourdens, M., Y. Jeanson, M. Taurand, N. Juin, A. Carriere, F. Clement, L. Casteilla, A.L. Bulteau, and V. Planat-Benard, *Short exposure to cold atmospheric plasma induces senescence in human skin fibroblasts and adipose mesenchymal stromal cells.* Sci Rep, 2019. **9**(1): p. 8671.
49. Shi, X., J. Cai, G. Xu, H. Ren, S. Chen, Z. Chang, J. Liu, C. Huang, G. Zhang, and X. Wu, *Effect of Cold Plasma on Cell Viability and Collagen Synthesis in Cultured Murine Fibroblasts.* Plasma Science and Technology, 2016. **18**(4): p. 353-359.
50. Kadler, K.E., D.F. Holmes, J.A. Trotter, and J.A. Chapman, *Collagen fibril formation.* Biochem J, 1996. **316 (Pt 1)**: p. 1-11.
51. Kerkela, E. and U. Saarialho-Kere, *Matrix metalloproteinases in tumor progression: focus on basal and squamous cell skin cancer.* Exp Dermatol, 2003. **12**(2): p. 109-25.
52. Ziober, B., *Type I collagen degradation by invasive oral squamous cell carcinoma.* Oral Oncology, 2000. **36**(4): p. 365-372.
53. Saed, G.M., W. Zhang, and M.P. Diamond, *Molecular characterization of fibroblasts isolated from human peritoneum and adhesions.* Fertil Steril, 2001. **75**(4): p. 763-8.
54. Vu, T.H. and Z. Werb, *Matrix metalloproteinases: effectors of development and normal physiology.* Genes Dev, 2000. **14**(17): p. 2123-33.
55. Junga, A., M. Pilmane, Z. Abola, and O. Volrats, *Tumor necrosis factor alpha, protein gene product 9.5, matrix metalloproteinase-2 and tissue inhibitor of metalloproteinase-2 presence in congenital intra-abdominal adhesions in children under one year of age.* Arch Med Sci, 2021. **17**(1): p. 92-99.

56. Stetler-Stevenson, W.G., *Matrix metalloproteinases in angiogenesis: a moving target for therapeutic intervention.* J Clin Invest, 1999. **103**(9): p. 1237-41.
57. Horejs, C.M., J.P. St-Pierre, J.R.M. Ojala, J.A.M. Steele, P.B. da Silva, A. Rynne-Vidal, S.A. Maynard, C.S. Hansel, C. Rodriguez-Fernandez, M.M. Mazo, A.Y.F. You, A.J. Wang, T. von Erlach, K. Tryggvason, M. Lopez-Cabrera, and M.M. Stevens, *Preventing tissue fibrosis by local biomaterials interfacing of specific cryptic extracellular matrix information.* Nat Commun, 2017. **8**: p. 15509.
58. Christodoulidis, G., I. Tsilioni, M.E. Spyridakis, T. Kiropoulos, S. Oikonomidi, G. Koukoulis, and K. Tepetes, *Matrix metaloproteinase-2 and -9 serum levels as potential markers of intraperitoneal adhesions.* J Invest Surg, 2013. **26**(3): p. 134-40.
59. Sottile, J. and D.C. Hocking, *Fibronectin polymerization regulates the composition and stability of extracellular matrix fibrils and cell-matrix adhesions.* Mol Biol Cell, 2002. **13**(10): p. 3546-59.
60. Donaldson, D.J. and J.T. Mahan, *Fibrinogen and fibronectin as substrates for epidermal cell migration during wound closure.* J Cell Sci, 1983. **62**: p. 117-27.
61. Mao, Y. and J.E. Schwarzbauer, *Fibronectin fibrillogenesis, a cell-mediated matrix assembly process.* Matrix Biol, 2005. **24**(6): p. 389-99.
62. Theocharis, A.D., S.S. Skandalis, C. Gialeli, and N.K. Karamanos, *Extracellular matrix structure.* Advanced Drug Delivery Reviews, 2016. **97**: p. 4-27.
63. Roberts, A.B., M.B. Sporn, R.K. Assoian, J.M. Smith, N.S. Roche, L.M. Wakefield, U.I. Heine, L.A. Liotta, V. Falanga, J.H. Kehrl, *Transforming growth factor type beta: rapid induction of fibrosis and angiogenesis in vivo and stimulation of collagen formation in vitro.* Proc Natl Acad Sci U S A, 1986. **83**(12): p. 4167-71.
64. Holmdahl, L., K. Kotseos, M. Bergstrom, P. Falk, M.L. Ivarsson, and N. Chegini, *Overproduction of transforming growth factor-beta1 (TGF-beta1) is associated with adhesion formation and peritoneal fibrinolytic impairment.* Surgery, 2001. **129**(5): p. 626-32.
65. Arndt, S., P. Unger, E. Wacker, T. Shimizu, J. Heinlin, Y.F. Li, H.M. Thomas, G.E. Morfill, J.L. Zimmermann, A.K. Bosserhoff, and S. Karrer, *Cold atmospheric plasma (CAP) changes gene expression of key molecules of the wound healing machinery and improves wound healing in vitro and in vivo.* PLoS One, 2013. **8**(11): p. e79325.
66. Chazaud, B., *Macrophages: supportive cells for tissue repair and regeneration.* Immunobiology, 2014. **219**(3): p. 172-8.
67. Postlethwaite, A.E., R. Raghow, G.P. Stricklin, H. Poppleton, J.M. Seyer, and A.H. Kang, *Modulation of fibroblast functions by interleukin 1: increased steady-state accumulation of type I procollagen messenger RNAs and stimulation of other functions but not chemotaxis by human recombinant interleukin 1 alpha and beta.* J Cell Biol, 1988. **106**(2): p. 311-8.
68. Kahari, V.M., J. Heino, and E. Vuorio, *Interleukin-1 increases collagen production and mRNA levels in cultured skin fibroblasts.* Biochim Biophys Acta, 1987. **929**(2): p. 142-7.
69. Xiao, H., A.M. Ji, Z.L. Li, X.D. Song, D. Su, and A.H. Chen, *Interleukin-1beta inhibits collagen synthesis and promotes its decomposition in cultured cardiac fibroblasts.* Sheng Li Xue Bao, 2008. **60**(3): p. 355-61.

70. Bhatnagar, R., H. Penfornis, A. Mauviel, G. Loyau, J. Saklatvala, and J.P. Pujol, *Interleukin-1 inhibits the synthesis of collagen by fibroblasts.* Biochem Int, 1986. **13**(4): p. 709-20.
71. Borthwick, L.A., *The IL-1 cytokine family and its role in inflammation and fibrosis in the lung.* Semin Immunopathol, 2016. **38**(4): p. 517-34.
72. Masola, V., A. Carraro, S. Granata, L. Signorini, G. Bellin, P. Violi, A. Lupo, U. Tedeschi, M. Onisto, G. Gambaro, and G. Zaza, *In vitro effects of interleukin (IL)-1 beta inhibition on the epithelial-to-mesenchymal transition (EMT) of renal tubular and hepatic stellate cells.* J Transl Med, 2019. **17**(1): p. 12.
73. Kaidi, A.A., T. Gurchumelidze, M. Nazzal, P. Figert, C. Vanterpool, and Y. Silva, *Tumor necrosis factor-alpha: a marker for peritoneal adhesion formation.* J Surg Res, 1995. **58**(5): p. 516-8.
74. Kosaka, H., T. Yoshimoto, T. Yoshimoto, J. Fujimoto, and K. Nakanishi, *Interferon-gamma is a therapeutic target molecule for prevention of postoperative adhesion formation.* Nat Med, 2008. **14**(4): p. 437-41.
75. Vural, B., N.Z. Canturk, N. Esen, S. Solakoglu, Z. Canturk, G. Kirkali, and C. Sokmensuer, *The role of neutrophils in the formation of peritoneal adhesions.* Hum Reprod, 1999. **14**(1): p. 49-54.
76. Hamilton, J.A., *GM-CSF in inflammation.* Journal of Experimental Medicine, 2020. **217**(1).
77. Becher, B., S. Tugues, and M. Greter, *GM-CSF: From Growth Factor to Central Mediator of Tissue Inflammation.* Immunity, 2016. **45**(5): p. 963-973.
78. Ignjatovic, D., K. Aasland, M. Pettersen, S. Sund, Y. Chen, M. Spasojevic, and J.M. Nesgaard, *Intra-abdominal administration of bevacizumab diminishes intra-peritoneal adhesions.* Am J Surg, 2010. **200**(2): p. 270-5.
79. Saltzman, A.K., T.A. Olson, D. Mohanraj, L.F. Carson, and S. Ramakrishnan, *Prevention of postoperative adhesions by an antibody to vascular permeability factor/vascular endothelial growth factor in a murine model.* Am J Obstet Gynecol, 1996. **174**(5): p. 1502-6.
80. Carmeliet, P., *Mechanisms of angiogenesis and arteriogenesis.* Nat Med, 2000. **6**(4): p. 389-95.
81. Srivastava, S.K., A. Bhardwaj, S. Arora, N. Tyagi, A.P. Singh, J.E. Carter, J.G. Scammell, Ø. Fodstad, and S. Singh, *Interleukin-8 is a key mediator of FKBP51-induced melanoma growth, angiogenesis and metastasis.* British Journal of Cancer, 2015. **112**(11): p. 1772-1781.
82. Aalinkeel, R., B. Nair, C.K. Chen, S.D. Mahajan, J.L. Reynolds, H. Zhang, H. Sun, D.E. Sykes, K.C. Chadha, S.G. Turowski, K.D. Bothwell, M. Seshadri, C. Cheng, and S.A. Schwartz, *Nanotherapy silencing the interleukin-8 gene produces regression of prostate cancer by inhibition of angiogenesis.* Immunology, 2016. **148**(4): p. 387-406.
83. Movasaghi, Z., S. Rehman, and I.U. Rehman, *Raman Spectroscopy of Biological Tissues.* Applied Spectroscopy Reviews, 2007. **42**(5): p. 493-541.
84. Frank, C.J., R.L. McCreery, and D.C.B. Redd, *Raman Spectroscopy of Normal and Diseased Human Breast Tissues.* Analytical Chemistry, 2002. **67**(5): p. 777-783.
85. Meister, K., D.A. Schmidt, E. Brundermann, and M. Havenith, *Confocal Raman microspectroscopy as an analytical tool to assess the mitochondrial status in human spermatozoa.* Analyst, 2010. **135**(6): p. 1370-4.

86. Gargotti, M., E. Efeoglu, H.J. Byrne, and A. Casey, *Raman spectroscopy detects biochemical changes due to different cell culture environments in live cells in vitro.* Analytical and Bioanalytical Chemistry, 2018. **410**(28): p. 7537-7550.
87. Tang, P., W. Cheng, X. He, Q. Zhang, J. Zhong, X. Lu, S. Liu, and L. Zhong, *Raman spectrum spectral imaging revealing the molecular mechanism of Berberine-induced Jurkat cell apoptosis and the receptor-mediated Berberine delivery system.* Biomedical Optics Express, 2019. **10**(4).
88. Zhu, G., X. Zhu, Q. Fan, and X. Wan, *Raman spectra of amino acids and their aqueous solutions.* Spectrochimica Acta Part A: Molecular and Biomolecular Spectroscopy, 2011. **78**(3): p. 1187-1195.
89. Marzi, J., E.M. Brauchle, K. Schenke-Layland, and M.W. Rolle, *Non-invasive functional molecular phenotyping of human smooth muscle cells utilized in cardiovascular tissue engineering.* Acta Biomaterialia, 2019. **89**: p. 193-205.
90. Ho, Y.-S., Y. Chen, J. Dai, X. Zhou, Y. Liu, W. Zhang, and G. Peng, *Raman Spectroscopy Analysis of the Biochemical Characteristics of Molecules Associated with the Malignant Transformation of Gastric Mucosa.* PLoS ONE, 2014. **9**(4).
91. Chan, J.W., D.S. Taylor, T. Zwerdling, S.M. Lane, K. Ihara, and T. Huser, *Micro-Raman Spectroscopy Detects Individual Neoplastic and Normal Hematopoietic Cells.* Biophysical Journal, 2006. **90**(2): p. 648-656.
92. Jyothi Lakshmi, R., V.B. Kartha, C. Murali Krishna, R.S. JG, G. Ullas, and P. Uma Devi, *Tissue Raman spectroscopy for the study of radiation damage: brain irradiation of mice.* Radiat Res, 2002. **157**(2): p. 175-82.
93. Ruiz-Chica, A.J., M.A. Medina, F. Sánchez-Jiménez, and F.J. Ramírez, *Characterization by Raman spectroscopy of conformational changes on guanine–cytosine and adenine–thymine oligonucleotides induced by aminooxy analogues of spermidine.* Journal of Raman Spectroscopy, 2004. **35**(2): p. 93-100.
94. Stone, N., C. Kendall, J. Smith, P. Crow, and H. Barr, *Raman spectroscopy for identification of epithelial cancers.* Faraday Discussions, 2004. **126**.
95. Notingher, I., C. Green, C. Dyer, E. Perkins, N. Hopkins, C. Lindsay, and L.L. Hench, *Discrimination between ricin and sulphur mustard toxicity in vitro using Raman spectroscopy.* Journal of The Royal Society Interface, 2004. **1**(1): p. 79-90.
96. Okotrub, K.A., N.V. Surovtsev, V.F. Semeshin, and L.V. Omelyanchuk, *Raman spectroscopy for DNA quantification in cell nucleus.* Cytometry Part A, 2015. **87**(1): p. 68-73.

*Authors contributed equally to this work.

7. ERKLÄRUNG ZUM EIGENANTEIL

Die Arbeit wurde am Department für Frauengesundheit der Universität Tübingen und am NMI Naturwissenschaftlich Medizinisches Institut in Reutlingen unter der Betreuung von Herrn Prof. Dr. med. Martin Weiss und Herrn Prof. Dr. med. Bernhard Krämer (Doktorvater) durchgeführt.

Die Konzeption der Studie erfolgte durch Herrn Prof. Dr. med. Martin Weiss und mich selbst. Sämtliche Versuche wurden nach Einarbeitung durch Labormitglieder (Anna-Lena Keller, Felix Ruoff, Laura Schultze-Rhonhof, Dr. rer. nat. Silke Keller) eigenständig an die Fragestellung adaptiert und durchgeführt. Bei der Auswertung der Ergebnisse des Raman-Imagings wurde ich unterstützt durch Frau Dr. rer. nat. Julia Marzi und Herrn Lucas Becker. Die Auswertung der Multiplex-Assays wurde nach Probenvorbereitung und -behandlung durch mich von der Arbeitsgruppe von Herrn Dr. rer. nat. Jens Göpfert durchgeführt.

Die statistische Auswertung erfolgte eigenständig nach Rücksprache mit Prof. Dr. med. Martin Weiss durch mich.

Ich versichere, das Manuskript selbstständig verfasst zu haben und keine weiteren als die von mir angegebenen Quellen verwendet zu haben.

Die wörtlich übernommenen Textpassagen aus der Originalpublikation wurden von mir selbst verfasst. Sämtliche übernommenen und / oder modifizierten Abbildungen wurden ebenfalls von mir selbst unter der Aufsicht von Prof. Dr. med. Martin Weiss entworfen.

Tübingen, den 30.05.2022

Marie-Lena Rasch

8. VERÖFFENTLICHUNGEN

*Rasch, M.-L. and *Holl, M. *et al*., *Cell type-specific anti-adhesion properties of peritoneal cell treatment with plasma-activated media (PAM*). Biomedicines **2022,** 10, 927. https://doi.org/10.3390/ biomedicines10040927

*Authors contributed equally to this work.

APPENIDX

Supplementary Data

Raman spectroscopic imaging detecting collagen spectra

Since the extracted collagen spectra was too weak to uniquely match the collagen reference spectra and for further PCA, semi quantification of the Raman images of the collagen spectra was performed. As seen in Supplementary Figure 1, collagen expression in fibroblasts was reduced through PAM treatment. However, the change was not significant. Raman images of the collagen spectra (green) revealed decreased collagen signals (*Supplementary Figure 1*) in two of three patients.

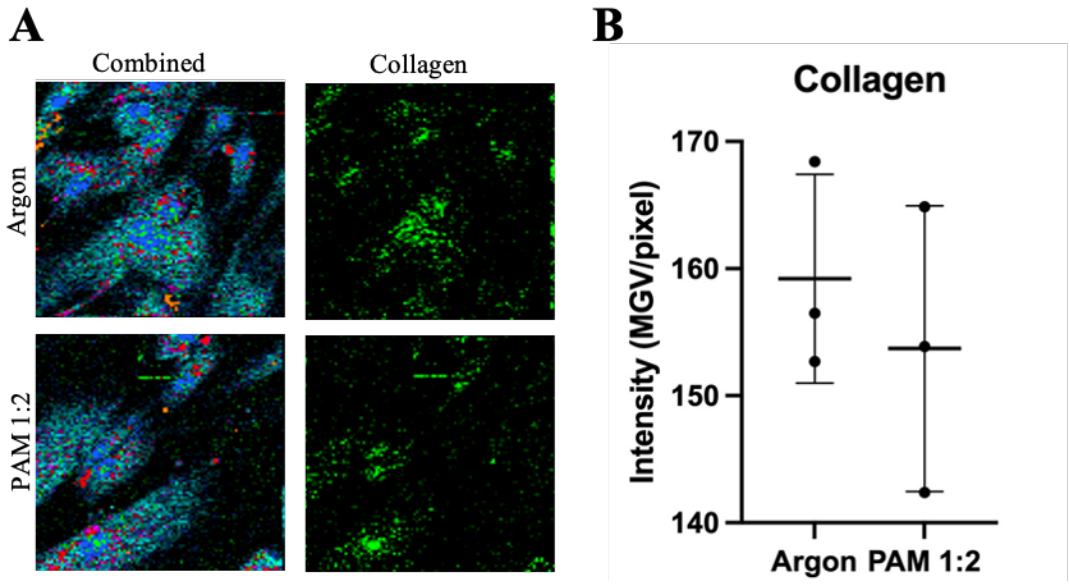

Supplementary Figure 1. Extracted collagen spectra. TCA revealed a spectrum partially related to a collagen reference spectrum. Semi quantification of the intensity of pixels was performed. Analysis revealed a slight but not significant modification in collagen after PAM treatment.

Raman spectroscopic imaging detecting lipid spectra in fibroblasts

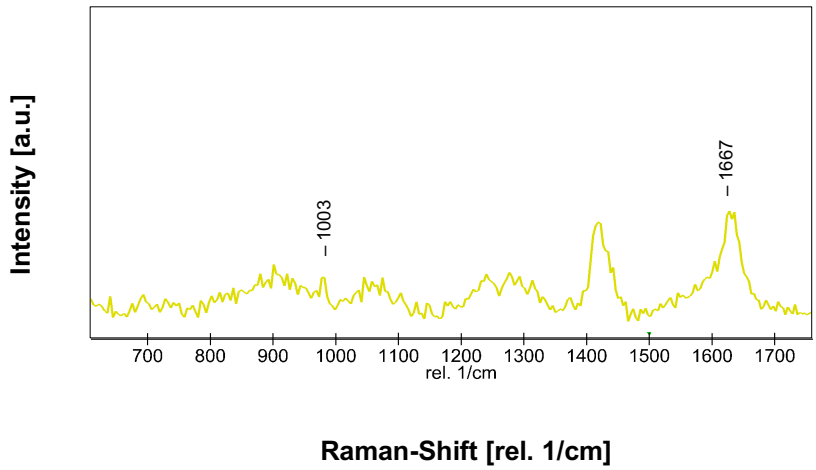

Supplementary Figure 2. Fingerprint spectrum of lipids. TCA identified the characteristic spectrum of lipids. Peaks at 1003 and 1667 cm^{-1} are related to lipids representing phenylalanine/C-C skeletal and C-C stretching band [*Supplementary Table 1*]. Parts of this figure were already published in Rasch, M.-L. and Holl, M. *et al., Effects of non-invasive physical plasma (NIPP) on the ECM and cells responsible for postoperative intraabdominal adhesions.* Biomedicines, **2022**, 10, 927 [1].

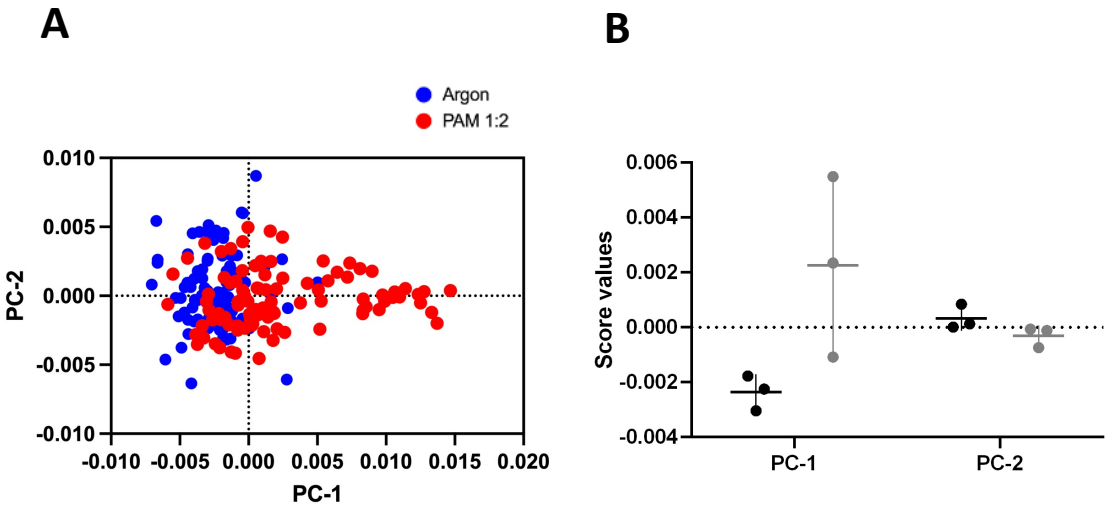

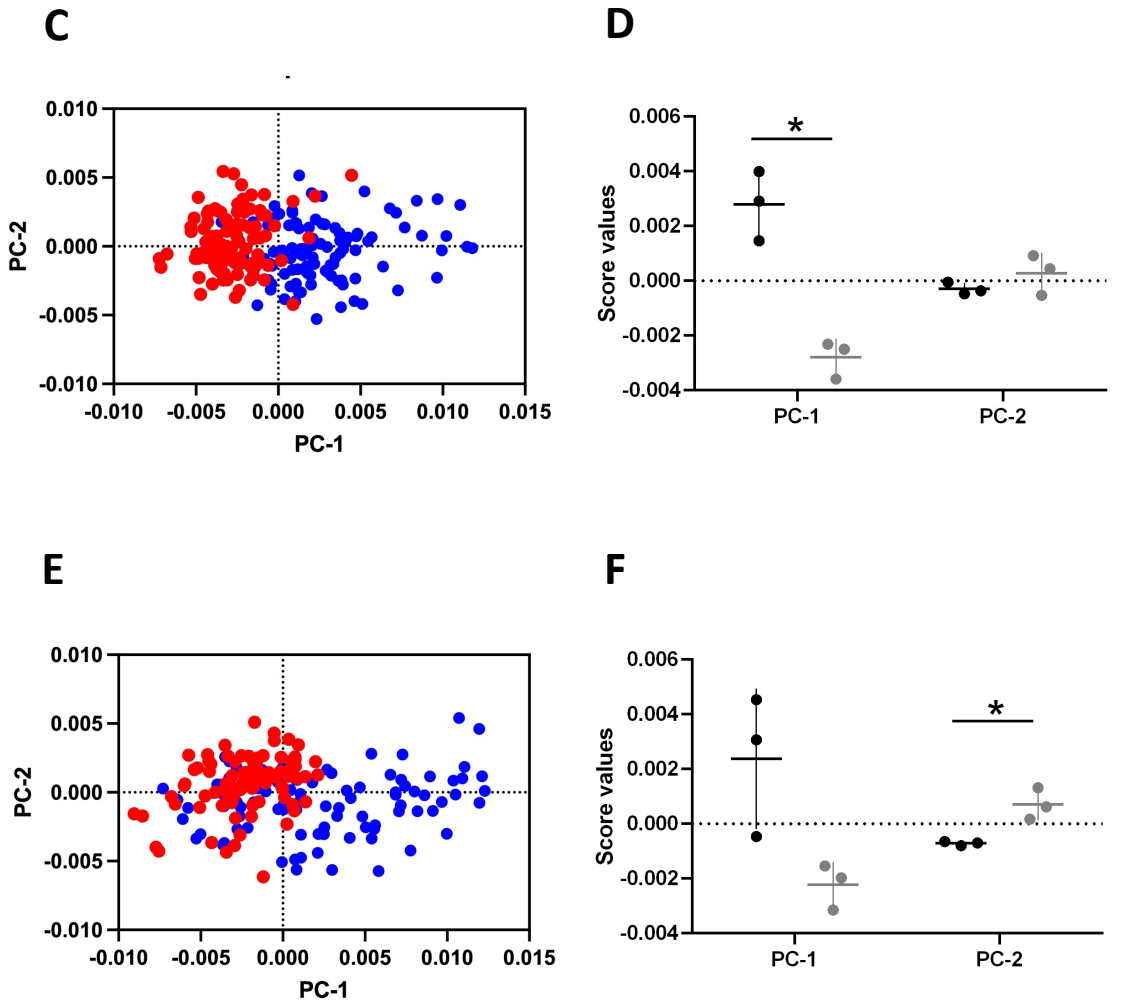

Supplementary Figure 3. **Raman imaging reveals changes in lipid spectra in fibroblasts**. Lipid-specific scores plot of PC-1 vs. PC-2 revealed a slight trend of clustering between groups for patient 1 (*A*). Lipids specific average score values indicated no significant differences in either PC-1 or PC-2 (*B)*. Scores plot of PC-1 vs. PC-2 indicated clustering of groups for both patient 2 and 3 (*C and E*). Lipids specific average score values revealed significant modifications for PC-1 of patient 2 (*D*). For patient 3, significant differences between groups were detected in the lipids-specific average score values of PC-2 (*F*). Data are shown as the mean ± SD, n=3, * $p<0.05$.

Supplementary Table 1. Raman peaks and their molecular assignments after identification by PCAs.

Peaks	Assignment	Reference
693	Nucleotide conformation	[83]
710	n (C-S) trans (amino acid methionine)	[83]
728	C-C stretching proline (collagen assignment)	[83, 84]
751	mitochondria	[85]
782	DNA	[83]
788	O-P-O stretching of DNA/C_5'-O-P-O-C_3' phosphodiester bands in DNA	[83]
810	Phosphodiester (Z-Marker) DNA	[83, 86]
826	O-P-O stretch DNA	[83]
830	Tyrosine	[83]
1003	Phenylalanine, C-C skeletal	[83, 87]
1005	Phenylalanine	[88]
1008	Phenylalanine / Proteoglycans	[83, 89]
1066	Proline (collagen assignment)	[83, 84]

1070-90	Symmetric PO_2^- stretching of DNA	[83]
1092	Phosphodioxy	[83]
1093	Symmetric PO_2^- stretching vibration of the DNA backbone	[83, 90, 91]
1096	Phosphodioxy (PO_2^-) groups	[83]
1113	Amide III (proteins) / C-C in lipids, fatty acids	[83, 92]
1153	Carbohydrates	[83]
1180	Cytosine, Guanine	[93]
1182	Cytosine, Guanine, Adenine	[83, 94]
1185-300	Anti-symmetric phosphate	[83]
1239	Amide III	[83]
1259	Guanine, cytosine (NH_2)	[93]
1272	CH α'rocking	[83]
1292	Cytosine	[83]
1309	CH_3CH_2 wagging mode of lipid/collagen	[83]
1325-30	CH_3CH_2 wagging mode in purine bases of nucleic acids	[83]

1454	CH_2 stretching / CH_3 deformation	[83]
1506/08/10	Cytosine	[83]
1520	-C=C - carotenoid	[83, 86, 89, 95]
1655-80	T, G, C (ring breathing modes of DNA/RNA bases); Amide I (protein)	[83]
1661	Amide I	[83, 94]
1663	DNA	[96]
1667	Protein band / C-C stretch	[83, 90, 95]
1716-41	C=O	[83]

DANKSAGUNG

An dieser Stelle möchte ich mich bei allen bedanken, die zum guten Gelingen dieser Arbeit beigetragen haben.

Zunächst möchte ich Prof. Dr. med. Martin Weiss für die herausragende Betreuung während der gesamten Zeit danken. Hervorzuheben sind insbesondere das stets offene Ohr für jegliche Fragen meinerseits, die unzähligen Ideen für die experimentelle Visualisierung sowie den großen Ehrgeiz, der auch mal zur Beantwortung von Mails zu sehr später Stunde, aber insbesondere zum guten Gelingen meiner Dissertation geführt hat.

Zudem möchte ich mich bei Laura Schultze-Rhonhof und Anna-Lena Keller für die großartige Einarbeitung in die Laborwelt bedanken. Auch Myriam Holl als Co-Autorin, Labor-Nachbarin und Kaffepausenpartnerin gilt ein besonderer Dank.

Ein großer Dank gilt auch Dr. med. Linus Kloker, der mir bei allgemeinen Labor- und insbesondere statistischen Fragestellungen rund um die Uhr mit Rat und Tat zur Seite stand.

In diesem Zuge möchte ich auch Prof. Dr. med. Bernhard Krämer als meinem Doktorvater danken.

Ein besonderer Dank gilt neben meinen engsten Freunden auch meiner Familie und insbesondere meinen Eltern, die mich in meinem Vorhaben und dieser Arbeit immer unterstützt und ermutigt haben.

Zuletzt möchte ich mich bei der Deutschen Forschungsgemeinschaft bedanken, die mich und meine Arbeit durch eine Förderung im Rahmen des GRK 2543 unterstützt haben.